Characterization of the Dynamic Response of Continuous Systems Discretized Using Finite Element Methods

by

Sandra Rugonyi

Nuclear Engineer, Balseiro Institute, Argentina (1995)
Master of Science in Mechanical Engineering, M.I.T. (1999)

Submitted to the Department of Mechanical Engineering
in partial fulfillment of the requirements for the degree of

Doctor of Philosophy in Mechanical Engineering

at the

MASSACHUSETTS INSTITUTE OF TECHNOLOGY

June 2001

Author .....
Department of Mechanical Engineering
May 25, 2001

Certified by .....
Klaus-Jürgen Bathe
Professor of Mechanical Engineeing
Thesis Supervisor

Accepted by .....
Ain Ants Sonin
Chairman, Graduate Committee

Characterization of the Dynamic Response of Continuous Systems Discretized Using Finite Element Methods

by

Sandra Rugonyi

Submitted to the Department of Mechanical Engineering
on May 25, 2001, in partial fulfillment of the
requirements for the degree of
Doctor of Philosophy in Mechanical Engineering

Abstract

Nonlinear dynamic physical systems exhibit a rich variety of behaviors. In many cases, the system response is unstable, and the behavior may become unpredictable. Since an unstable or unpredictable response is usually undesirable in engineering practice, the stability characterization of a system's behavior becomes essential.

In this work, a numerical procedure to characterize the dynamic stability of continuous solid media, discretized using finite element methods, is proposed. The procedure is based on the calculation of the maximum Lyapunov characteristic exponent (LCE), which provides information about the *asymptotic* stability of the system response. The LCE is a measure of the average divergence or convergence of nearby trajectories in the system phase space, and a positive LCE indicates that the system asymptotic behavior is chaotic, or, in other words, asymptotically dynamically unstable. In addition, a *local* temporal stability indicator is proposed to reveal the presence of local dynamic instabilities in the response. Using the local stability indicator, dynamic instabilities can be captured shortly after they occur in a numerical calculation. The indicator can be obtained from the successive approximations of the response LCE calculated at each discretized time step. Both procedures can also be applied to fluid-structure interaction problems in which the analysis focuses on the behavior of the structural part.

The response of illustrative structural systems and fluid flow-structure interaction systems, in which the fluid is modeled using the Navier-Stokes equations, was calculated. The systems considered present both stable and unstable behaviors, and their LCEs and local stability indicators were computed using the proposed procedures. The stability of the complex behaviors exhibited by the problems considered was properly captured by both approaches, confirming the validity of the procedures proposed in this work.

Thesis Supervisor: Klaus-Jürgen Bathe
Title: Professor of Mechanical Engineeing

Acknowledgments

Now that I have finished my graduate work at MIT, my mind goes back in time and I cannot regret the decision to come here. My memory is full of enriching experiences. I remember moments of intense joy, and extremely stressful situations. This is the life at MIT, full of contrasts. Needless to say that I could not have come so far if it were not for all the people that, in one way or another, were near me.

I would like to take this time to thank all the people that made this possible. I am sure I will not include absolutely everyone in this acknowledgement, since otherwise the list will be extensive, but at least let me mention the people that had most influenced my life during this four years.

First of all I would like to express my deepest gratitude to Prof. Klaus-Jürgen Bathe, my thesis advisor, who guided me through the world of research and could always find the way to challenge me. I truly enjoyed our fruitful discussions during the development of this research work, and I am grateful for his constant support and encouragement. I would also want to thank the members of my Thesis Committee, Prof. Carlos E. S. Cesnik and Prof. Ahmed F. Ghoniem, for their suggestions and encouragement during the development of my thesis.

I am very grateful to Prof. Eduardo Dvorkin for giving me the opportunity, when I was an inexperienced engineer, to explore the world of finite element methods and for encouraging me to continue my studies at MIT. His advice and wise guidance during my "first steps" are invaluable to me.

This research has been partially supported by the Rocca Fellowship for which I am very grateful.

I would also like to thank the people of the Finite Element Research Group at MIT (my office-mates) Suvranu De, Nagi El-Abassi, Anca Ferent, Dena Hendriana, Jean-François Hiller, Phill-Seung Lee, Daniel Pantuso, Juan Pablo Pontaza, Denise Poy and Ami Salomon for their encouragement and support, and for providing a friendly atmosphere in the "lab". We spent many afternoons discussing academic problems and sharing experiences that enriched me beyond expectations. In addition, I am

thankful to the researchers of ADINA R & D for their help and support with the use of ADINA. I would also like to thank Leslie Regan, from the Mechanical Engineering Department, for her patience, help and constant support, and for having always a big smile.

During this four years, the constant support of my friends, who always found the way to give me strength during difficult moments and with whom I shared many exciting experiences of my life, was invaluable. A big *thank you* to Emma Sánchez, Galit Toledo, Rita Toscano, Miguel Marioni and Debra Blanchard: without you I could not have made it.

I would like to express my gratitude to my parents, whose support and encouragement mean the most to me.

Finally, my utmost gratitude goes to Mauro, my husband and best friend, for his love and encouragement and for always showing me the light at the end of the tunnel and giving meaning to my life.

Contents

1 Introduction **10**

2 Discrete dynamical systems **16**

2.1 Nonlinear dynamic equations 16

2.2 Dynamic responses of nonlinear systems 19

2.2.1 Steady-state behavior 19

2.2.2 Periodic solutions 20

2.2.3 Chaotic behavior 20

2.3 Stability of motions: Lyapunov stability 21

2.4 Lyapunov characteristic exponents 24

2.4.1 Definition and properties of Lyapunov characteristic exponents 24

2.4.2 Numerical calculation of the maximum Lyapunov characteristic exponent 31

3 Governing equations of continuous media **34**

3.1 Kinematics of continuous media 35

3.1.1 Lagrangian formulation 35

3.1.2 Eulerian formulation 36

3.1.3 Arbitrary Lagrangian-Eulerian formulation 37

3.2 Conservation equations 38

3.2.1 Mass conservation 39

3.2.2 Momentum conservation 39

3.3 Equations of motion 40

3.3.1 Structural equations 40
3.3.2 Fluid flow equations 42
3.3.3 Fluid flow-structural interface conditions 44

4 Finite element formulation **45**
4.1 Structural equations 46
4.2 Fluid flow discretization 47
4.3 Fluid flow-structural interaction problems 52

5 Lyapunov characteristic exponents of continuous systems **61**
5.1 Structural problems 64
5.2 Fluid problems 77
5.3 Fluid-structure interaction problems 79
5.4 Local stability 80

6 Numerical examples **82**
6.1 Discrete nondimensional equation of motion: the Duffing equation . . 82
6.2 Structural systems 92
6.2.1 Analysis of steady-state behavior 92
6.2.2 Buckled beam analysis 95
6.2.3 Beam subjected to nonlinear boundary condition 98
6.3 Fluid-structure interaction 101
6.3.1 Collapsible channel 102
6.3.2 Modified collapsible channel model 106

7 Conclusions and future work **114**

A Exponential divergence of trajectories in phase space **118**

List of Figures

2-1 Graphical representation of the different types of stability of a motion, according to Lyapunov. 23

2-2 Graphical representation of the evolution of perturbations in all directions in a two-dimensional phase space. The vectors $\mathbf{e}_1$ and $\mathbf{e}_2$ change directions as the value of t increases. However, we are concerned with the basis vectors associated with $t \to \infty$. 27

3-1 Reference, spatial and mesh configurations. 36

4-1 9/3 element. 50

4-2 General fluid-structure interaction problem. 53

5-1 Numerical calculation of norm of the perturbation for the harmonic oscillator equation. The time step used in all three cases is $\Delta t = 0.3$. a) $\omega = 1$, b) $\omega = 100$, c) $\omega = 5000$. 72

6-1 Sketch of the potential function of the Duffing equation without forcing and when all the parameters are positive numbers. 84

6-2 Sketch of the phase portrait for the Duffing equation without forcing. The black dots correspond to stable fixed points for the system, whereas the white dot (at the plot origin) corresponds to the unstable fixed point. 85

6-3 Different behaviors exhibit by the Duffing equation and the values of the LCEs associated with them. a) Steady-state response. b) Oscillatory behavior. c) Chaotic response. 88

6-4 Values of $ln(d)$ as a function of time for two responses of the Duffing equation. a) Oscillatory behavior. b) Chaotic response. 89
6-5 Values of k_n obtained when the Duffing equation presents the chaotic behavior considered above, and for different values of the time step used to discretize the equations in time. 90
6-6 Comparison of the values of k_n obtained for the chaotic response of the Duffing equation considered above, using the method proposed by Benettin et al. and the proposed procedure. 91
6-7 Cantilever beam used in the analysis of the perturbation evolution of a steady-state behavior. 92
6-8 LCE calculation of a steady-state solution of the cantilever beam. Oscillation of the values of k_n are typical when using the proposed procedure (since the norm of the perturbation is calculated using only displacements). 94
6-9 Buckled beam problem considered. 96
6-10 Mid-point displacement of buckled beam problem and LCE calculation. 97
6-11 Fourier spectrum of the buckled beam response obtained for the mid-point displacement. 97
6-12 Plot of $ln(d)$ as a function of time for the buckled beam problem. Note that the local stability of the system is captured by this graph, without explicitly calculating the system LCE (which defines only the system long-term stability). 99
6-13 Convergence analysis for the LCE value obtained in the case of the buckled beam. 100
6-14 Beam subject to nonlinear boundary conditions. Sketch of system considered. 100
6-15 Displacement of the end of the beam with an attached cubic spring (the "free-end") as a function of time; and the calculated values of k_n, which give the response LCE in the limit for time going to infinity. . 102

6-16 Fourier spectrum of the response obtained for the beam with an attached cubic spring, shown in Figure 6-15. 103
6-17 Calculated $ln(d)$ as a function of time, for the beam problem with nonlinear boundary conditions. 104
6-18 Collapsible channel problem considered. 106
6-19 Mid-point displacement of the collapsible segment for the collapsible channel problem depicted in figure 6-18, and the calculated LCE. . . 107
6-20 Plot of the $ln(d)$ as a function of time for the collapsible channel problem. 108
6-21 Power spectrum of the mid-point collapsible segment displacement obtained for the channel problem. 109
6-22 Modified collapsible channel problem considered. A parabolic velocity profile, constant in time, is imposed at the tube inlet. The linear truss of constant $k = \frac{EA}{L}$, acts over one point of the membrane when it reaches a vertical displacement of 0.009m or more inside the channel, and it does not interfere with the fluid flow inside the channel. 110
6-23 Collapsible segment mid-point displacement for the channel problem depicted in Figure 6-22, together with the calculated values of k_n. . . 111
6-24 Power spectrum of the mid-point collapsible segment displcement obtained for the modified channel problem. 112
6-25 Plot of $ln(d)$ as a function of time for the modified channel problem. . 113

A-1 Natural logarithm of the distance between two trajectories that were originally very close to each other. The trajectories were calculated using the Duffing equation and for the value of parameters analyzed in Chapter 6 that result in a chaotic behavior. 120

Chapter 1

Introduction

The complexity and large variety of behaviors that nonlinear systems can exhibit have fascinated researchers for centuries. For many systems, even weak nonlinearities cannot be neglected since they significantly affect the long-term system response. Furthermore, analytical solutions are usually difficult or impossible to obtain, and consequently, techniques have been developed to approximate either the system response in time or its asymptotic behavior (usually when weak nonlinearities are present). Unfortunately, all these analytical techniques, although very useful, are only applicable to a relatively small number of systems due to the intrinsic complexities of them.

The availability of computers made possible the numerical calculation of the response of systems that were impossible or extremely difficult to solve by other means, and therefore it opened a broad spectrum of new possibilities. Furthermore, as the speed and storage capacity of computers increases, the calculation of more complex and larger systems becomes feasible. Numerical methods constitute nowadays an essential tool in the analysis and understanding of the behavior of systems, with applications in almost all areas of engineering and science.

Since the early inception of the analysis of mechanical systems, it was recognized that nonlinear systems, as opposed to their linear counterparts, exhibit a large variety of behaviors. It was then also acknowledged that the characterization of the system's response stability, not only of equilibrium points but also of motions, was important.

Thus, mathematical tools, such as perturbation methods, were developed to assess the stability of system behaviors. When using perturbation methods the system response is slightly perturbed and the evolution of the perturbations as a function of time solved (or approximated). Generally, if the perturbations decay as a function of time, the system dynamic behavior analyzed is stable, whereas if the perturbation grows in time, the response is unstable. Due to the complexity of the calculations involved, analytical techniques were limited to the study of relatively simple systems. Therefore, for the stability characterization of system's responses, computers are invaluable tools for researchers and engineers in the study of large and complex systems. The objective of this work is to use numerical methods to characterize the stability of the dynamic response of continuous systems.

Let us begin with a brief description of what has been done in the area in the past. By the end of the 19th century, mathematicians had noticed that certain dynamical systems present *irregular* solutions. For those irregular solutions, small perturbations in the initial conditions lead to large differences in the system response at a later time, making prediction impossible. Nevertheless, it was believed and generally accepted that using powerful enough computers any deterministic system (i.e. a system that has no random inputs or parameters, and which is governed by a known equation of motion) could eventually be solved and its response predicted.

In the second half of the 20th century, Lorenz was computing trajectories of a very simple deterministic system he had developed with the aim of studying and predicting the weather. To his surprise, he found that for certain values of the parameters of his equations, *irregular* solutions exist [18]. The name *chaotic behavior*, to define the response of such trajectories, was then employed to describe this type of motions.

A chaotic behavior is characterized by a non-periodic response and sensitivity to initial conditions. Nearby trajectories in phase space (the space of displacements and velocities in a classical mechanical system) diverge exponentially fast (on average) from each other, and the response becomes unpredictable.

Since the work of Lorenz, many researchers have studied the chaotic behavior of numerous low-order discrete equations of motion and maps. Furthermore, techniques

were developed to characterize a chaotic response by assessing how fast nearby trajectories in phase space diverge from each other. Such measures include the Lyapunov characteristic exponents of a system response and the Kolmogorov entropy (which can be calculated by knowing the Lyapunov characteristic exponents). Even though the concept of Lyapunov characteristic exponent was developed in 1892 by A. M. Lyapunov, the basis for its numerical calculation was only given in 1976 by Benettin et al. [4] [3].

In engineering practice, turbulence, a chaotic behavior of fluids, was known since long ago, and researchers have characterized and calculated it by means of statistical variables. It was also recognized that the exact system behavior is unpredictable in the presence of turbulence, since it is impossible to exactly trace the trajectory of a particle, no matter how much we try to avoid errors in the calculation. Although the dynamic behavior of a turbulent flow is unstable and unpredictable, its mixing characteristics are usually desired in engineering systems, for example to dissipate heat in a more efficient way.

However, the recognition that the response of solid mechanics problems as well as electrical systems can become chaotic was more surprising and somewhat unexpected. Especially surprising was the fact that nonlinear systems of equations with only a few degrees of freedom, obtained from Newton laws of motion, could exhibit a chaotic response. In contrast to fluid systems, in structural mechanics an unstable behavior is usually not desirable and hence the chaotic behavior unacceptable. Thus, the characterization of the dynamic stability of structural engineering systems becomes important.

Chaotic responses have been observed in diverse dynamical continuous systems, including buckled beams and arcs with periodic excitations, electro-mechanical systems, systems subject to nonlinear boundary conditions such as contact, pipes conveying fluid and fluid flow over plates, to mention just a few [24].

Previous works on the chaotic behavior of continuous systems include experimental investigations and the use of reduction methods, see for example [25] [27] [16] [6] [32]. In the case of experimental investigations, the procedure employed consists of

recording some of the system variables as a function of time. Then, the time histories are analyzed using Fourier and correlation analyses and finally numerical techniques are applied (see for example [38]) to obtain an approximation of the response Lyapunov characteristic exponent. This approach, although powerful, is not available for every system since the costs of it might be unaffordable. In the case of reduction techniques, it is assumed that the system response is accurately described by considering the response of only a few system modes. The continuous equations that describe the system behavior are then reduced to a system of a few coupled discrete nonlinear equations, that can be analyzed using the available techniques for the analysis of discrete systems of equations. However, the amount of modes needed to accurately represent the system behavior is not always evident. Even worse, when strong nonlinearities are present, the linearized modes are no longer accurate to describe the system behavior, and nonlinear modes, which can be very difficult to obtain, should be employed. Therefore, reduction methods also present intrinsic limitations. A more general procedure to assess the local stability and calculate the Lyapunov characteristic exponent of a continuous system response is therefore needed.

It is important to emphasize here the main differences between systems of equations obtained by discretizing a continuous system and discrete equations of motion. The objective of this discussion is to explain why the numerical techniques developed to calculate the LCE of discrete systems could not be employed in the calculation of the LCE of continuous systems. The first difference is that when discretizing a continuous medium using finite element methods, a large number of discrete equations is obtained. Another immediate difference is that the continuous problem boundary conditions have to be satisfied at all times. However, the most important difference is that distinct time scales are present in the continuum discretized equations. Usually the time step chosen to discretize the equations (when using an unconditionally stable time integration scheme) does not accurately capture the smaller time scales involved in the equations. From the discussion of Chapter 5, it becomes clear that the algorithm to calculate the LCE of discrete systems, describe in Chapter 2, is no longer applicable in the calculation the LCE of continuous systems, and a new procedure

needs to be developed.

In this work, a numerically efficient procedure to calculate the Lyapunov characteristic exponent of structural and fluid-structure interaction continuous systems is proposed. In the procedure presented here the continuous equations of motion are first discretized using the finite element method, and then the Lyapunov characteristic exponent of the system response is calculated, considering all the system discretized modes. As far as we know, this is the first work in which the Lyapunov characteristic exponent of continuous systems, discretized using finite element methods, is calculated by perturbing all the discretized modes (or degrees of freedom).

In many situations, it is not important to know the *exact* value of the Lyapunov characteristic exponent, which is a measure of the *asymptotic* divergence of trajectories in phase space, but rather to know whether the dynamic response of the system is unstable at any time. In such situations, the characterization of the response *local* stability becomes very important and desirable. A local stability indicator, which can be obtained from successive approximations of the value of the Lyapunov characteristic exponent, is proposed to assess the local stability of the system response considered. These approximations are calculated at each time step in the LCE procedure proposed, and therefore the local stability indicator can be thought of as a by-product of the Lyapunov characteristic exponent calculation.

The thesis is organized as follows. In Chapter 2 a brief review of the theory of discrete nonlinear dynamic systems is given, which includes the definition of the Lyapunov characteristic exponent and its numerical calculation. Chapter 3 is devoted to the continuum governing equations of solid media and fluid flows that are used in this work, as well as the conditions that must be satisfied at a fluid-structure interface when solving fluid-structure interaction problems. Chapter 4 describes the finite element discretization of those governing equations and the implementation of the fluid-structure interaction procedure employed. In Chapter 5, a numerically efficient algorithm to calculate the Lyapunov characteristic exponent of structural problem and of fluid-flows with structural interactions and a local stability indicator are proposed. Subsequently, in Chapter 6, numerical examples are presented and the

Lyapunov characteristic exponents calculated using the proposed algorithm. Finally, in Chapter 7 the conclusions of this work are given and future research in the analysis and characterization of the dynamic behavior of continuous systems is suggested.

Chapter 2

Discrete dynamical systems

Nonlinear dynamic systems can exhibit a large variety of dynamic responses, some of which are stable, and some unstable and unpredictable. Since instabilities in the system response are usually undesirable, it is not only important to calculate the response of the system but also to characterize its stability.

The objective of this work is to find numerical algorithms to characterize the stability of the dynamic behavior of nonlinear equations of motion, and to obtain information about the system response predictability.

In the following, a short introduction to some relevant aspects of nonlinear theory, needed for the development of this work, is given. For a more detailed explanation of the techniques available to study nonlinear systems and their responses, see for instance [37] [28] [8] [1].

2.1 Nonlinear dynamic equations

Consider the following system of discrete nonlinear non-dimensional ordinary differential equations,

$$\dot{\mathbf{x}} = \mathbf{f}(\mathbf{x}) \tag{2.1}$$

with initial conditions

$$\mathbf{x}(t_0) = \mathbf{x}_0 \tag{2.2}$$

where $\mathbf{x} \in \Re^n$ is the vector of state variables for the system, the dot indicates differentiation with respect to time, $\mathbf{f}$ is assumed to be a smooth vector valued function of $\mathbf{x}$ defined on some subset $U \subseteq \Re^n$ such that $\mathbf{f} : U \to \Re^n$, $\mathbf{x}_0 \in U$ and t_0 is the initial time. The system defined by equations (2.1) is called *autonomous* since the function $\mathbf{f}(\mathbf{x})$ does not depend explicitly on time.

When the function $\mathbf{f}$ is also a function of time, $\mathbf{f} = \mathbf{f}(\mathbf{x}, t)$, the system of equations is called *non-autonomous*. However, a non-autonomous system can be converted into an *autonomous* one. Assuming that $\mathbf{x} \in \Re^n$, by performing a change of variables of the form $x_{n+1} = t$, equation (2.1) becomes,

$$\begin{aligned} \dot{\mathbf{x}} &= \mathbf{f}(\mathbf{x},\ x_{n+1}) \\ \dot{x}_{n+1} &= 1 \end{aligned} \tag{2.3}$$

In this way, the time t is included as an additional state variable, and hence, all the techniques employed in the analysis of autonomous systems are also applicable to the non-autonomous ones.

The vector field $\mathbf{f}$ generates a *flow* $\phi_t : U \to \Re^n$, where $\phi_t = \phi(\mathbf{x}, t)$ is a smooth function defined for all $\mathbf{x} \in U$, and t in some interval $(a, b) \in \Re$. The flow ϕ_t satisfies,

$$\frac{d}{d\,t}\left(\phi(\mathbf{x}, t)\right)_{t=\tau} = \mathbf{f}(\phi(\mathbf{x}, \tau)) \tag{2.4}$$

Therefore, ϕ_t represents all possible solutions of equation (2.1) for all $\mathbf{x} \in U$.

In addition, $\phi(\mathbf{x}_0, \cdot) : (a, b) \to \Re^n$ defines a *solution curve* or *trajectory* of the system of equations (2.1) with initial conditions (2.2) [8]. The solution is also denoted by $\mathbf{x}_r(t)$ for simplicity later in this work.

Let us define here, following [8], some sets defined in an Euclidean space (although they can in general be defined in other spaces) that would be useful for the discussions below. A set S_o is *open* if for each point $\mathbf{x} \in S_o$ there is a real number $\varepsilon > 0$ such that if the distance between two points $\mathbf{x}$ and $\mathbf{y}$ is less than ε, then $\mathbf{y} \in S_o$. A set S_c is *closed*, if it contains all its limit points (or "boundary" points). A closed

and bounded set is a *compact* set. A p-dimensional manifold $M \subset \Re^n$ $(p < n)$ of a dynamical system is a set such that for each $\mathbf{x}$ belonging to the manifold there is a neighborhood S_m of $\mathbf{x}$ for which there is a smooth invertible mapping $\phi : \Re^p \rightarrow S_m$.

The solution of equations (2.1) and (2.2) is unique, at least locally, if the *existence and uniqueness theorem* [8] is satisfied:

Theorem 1: Let $U \subset \Re^n$ be an open subset of the real Euclidean space, let $\mathbf{f}$ be a continuously differentiable (C^1) function in U and let $\mathbf{x}_0 \in U$; then, there is some constant $c > 0$ and a *unique* solution $\phi(\mathbf{x}_0, t)$ on some time interval $(-c, c)$, which satisfies equation (2.1) with initial conditions (2.2). $\diamond$

Of course the theorem applies to all systems of equations that satisfy the theorem conditions, and therefore unique solutions exist *regardless* of the dynamic stability of the system (i.e. it is applicable to responses such as steady-state solutions, periodic or quasi periodic solutions, chaotic behavior, etc.).

Theorem 1 is only *local* on time [1] since it can only guarantee the existence and uniqueness of solutions in some finite time interval $(-c, c)$. The theorem becomes *global*, and thus solutions exist for *all* times, if $\mathbf{x}$ is defined on a compact manifold M [8].

Theorem 2: Equation (2.1), with $\mathbf{x} \in M$, and $\mathbf{f}$ a continuously differentiable (C^1) function, has solution curves defined for all $t \in \Re$. $\diamond$

Therefore, flows on spheres or tori, for example, are defined for all values of time, since the trajectories cannot escape from the mentioned manifolds.

In this work only *deterministic systems*, that is to say systems that contain no stochastic terms or inputs and whose equations of motions are known, will be considered. In addition, only systems that satisfy the conditions of Theorem 1 and therefore have a unique solution, $\phi(\mathbf{x}_0, t) = \mathbf{x}_r(t)$, called the *reference solution*, will be discussed.

The space of state variables $\mathbf{x} \in \Re^n$ of the system defined by equation (2.1) is

[1] It is possible to find examples of equations defined in $\Re^n$ for which solutions exist for all values of t, but in general it is not possible to show the global existence in such cases without specifically investigating the particular system.

called the system *phase space*. Phase portraits, wich are plots of the trajectories in the phase space, are often used to analyze the response of nonlinear systems. The existence of unique solutions for the system of equations considered implies that trajectories never intersect in phase space.

An *invariant set* S for a flow ϕ_t is a subset $S \subset \Re^n$ such that $\phi(\mathbf{x}, t) \in S$ for all $t \in \Re$. In addition, a closed invariant set $A \subset \Re^n$ is called an *attracting set* if there is some neighborhood A' of A such that $\phi(\mathbf{x}, t) \in A'$ for all $t \geq 0$ and $\phi(\mathbf{x}, t) \to A$ as $t \to \infty$ for all $\mathbf{x} \in A'$. The subset of all points in which the system initial conditions can lie so that the trajectories are attracted to the attracting set A is called the *domain of attraction* or *basin of attraction* of A. Thus, all trajectories starting in the domain of attraction of an attracting set are "captured" by the set. These concepts will be used in relation with the stability of motions and the chaotic behavior of systems. In this context, the attracting set of a chaotic system, observed numerically, will be called a *strange attractor*, although in theory there is some distinction between an attractor and an attracting set [2] (see [8] for a detailed discussion).

Given a nonlinear system of equations with specified initial conditions, our problem is to find the reference solution and to determine its stability.

2.2 Dynamic responses of nonlinear systems

The solution of nonlinear equations of the form (2.1) with initial conditions (2.2) can present a rich variety of behaviors. Some of them are somewhat surprising and can only occur for nonlinear systems. Some of the behaviors that were observed in physical systems are mentioned below.

2.2.1 Steady-state behavior

A steady-state response can take place for both linear or nonlinear systems, and it is obtained when $\dot{\mathbf{x}} = \mathbf{0}$ in equation (2.1). Thus, a steady-state response is obtained when the system reaches a state that does not depend on time, and therefore $\mathbf{x}$ is

[2] An attractor can be defined as an attracting set that contains a dense orbit.

a constant vector, also known as a fixed or equilibrium point of equations (2.1). In a dynamic solution, a (stable) steady-state response is obtained for large values of time, for dissipative systems, or when the initial conditions coincide with the system fixed point, for conservative systems.

2.2.2 Periodic solutions

Periodic solutions can be obtained for both linear and nonlinear systems. For conservative systems (which can be linear or nonlinear), the amplitude of oscillations depends on the system initial conditions.

For nonlinear equations self-excited oscillations, also called limit cycles, can occur [37]. A limit cycle is an isolated closed orbit in phase space, which can occur even without imposing an external periodic forcing to the governing equations of motion. In other words, a limit cycle is a periodic solution, and neighboring trajectories are either attracted or repelled by the limit cycle (depending on the stability of it). In addition, for initial conditions lying in the basin of attraction of a limit cycle, the amplitude of the resulting self-excited oscillations does not depend on the system initial conditions.

2.2.3 Chaotic behavior

Among the different behaviors that a nonlinear system can exhibit, the chaotic response is one of the most intriguing ones. The most impressive characteristic is that an *non-periodic* random-like response (the chaotic response) can be obtained from a completely deterministic system, for which all the inputs are known. This is in contrast with the usual meaning of random system, in which a random response is observed because it is impossible to identify and control all the inputs to the system in an experimental setup.

A chaotic response is characterized by its sensitivity to initial conditions that results in an unpredictable behavior. Nearby trajectories in phase space diverge from each other exponentially fast. Therefore, two trajectories, which are initially infinites-

imally close to each other, are separated after a relatively short time, associated with the *prediction time* of the system.

However, even when a chaotic response is observed, in the long-term, the trajectories occupy only a certain closed subset of the phase space, an attracting set called the *strange attractor*. All trajectories that originate close enough to this subset, in its domain of attraction, are attracted to it, in a similar way as trajectories that are close to a limit cycle are attracted to it. It can happen, for example, that for certain initial conditions a nonlinear system is completely regular, and for instance the trajectories approach a fixed point (steady-state) as time evolves; whereas for other initial conditions the system behavior becomes chaotic. In addition, it is also possible to have a system with different chaotic attractors. Therefore, we refer to a *chaotic response* of a system and *not* a chaotic system.

2.3 Stability of motions: Lyapunov stability

The concept of stability in physics can be applied to both *equilibrium* positions and *motions*. In the first case, we consider solutions of equation (2.1) such that $\dot{\mathbf{x}} = \mathbf{0}$, and therefore $\mathbf{f}(\mathbf{x}) = \mathbf{0}$. The zeroes of $\mathbf{f}(\mathbf{x})$ are called the system *equilibrium positions* or *fixed points*. If the equilibrium is perturbed and the system returns (after certain time) to the same equilibrium position, the equilibrium is said to be asymptotically stable, and stable (or neutrally stable) [8] if the perturbed trajectory remains sufficiently close to the fixed point for all times.

In this work, we are concerned about the *stability of motions*. Therefore, we want to investigate what happens when a system that is not in an equilibrium position is perturbed. To characterize the stability of motions, the concept of Lyapunov stability can be used [10].

Considering equations (2.1) and (2.2), we now assume that the reference solution, $\mathbf{x}_r(t)$, which describes the system dynamic behavior, is slightly perturbed at time t, that is to say,

$$\mathbf{x}(t) = \mathbf{x}_r(t) + \mathbf{y}(t) \tag{2.5}$$

where $\mathbf{x}$ is now the perturbed vector of state variables and $\mathbf{y}$ is the perturbation vector, which is such that $\|\mathbf{y}\| << \|\mathbf{x}_r\|$. The equation that describes the evolution of the perturbation is given by

$$\dot{\mathbf{y}} = \mathbf{f}(\mathbf{x}_r + \mathbf{y}) - \mathbf{f}(\mathbf{x}_r) \tag{2.6}$$

The stability of the reference trajectory can now be established by looking at the stability of the equilibrium point $\mathbf{y} = \mathbf{0}$ of equation (2.6). Considering an initial perturbation $\mathbf{y}_0$ at time t_0^*, the *Lyapunov stability* is defined as follows [10],

- The equilibrium is said to be *stable* if given two real numbers, ε, δ, for each $\varepsilon > 0$ there exists a $\delta > 0$ such that if $\|\mathbf{y}_0\| < \delta$ then $\|\mathbf{y}(t)\| < \varepsilon$ for $t > t_0^*$.

- The equilibrium is said to be *quasi-asymptotically stable* if there exists a $\delta > 0$ such that if $\|\mathbf{y}_0\| < \delta$ then $\lim_{t\to\infty} \|\mathbf{y}(t)\| = 0$.

- The equilibrium is said to be *asymptotically stable* if it is both stable and quasi-asymptotically stable.

- The equilibrium ($\mathbf{y} = \mathbf{0}$), and therefore the motion considered, is *unstable* if it is not stable.

These concepts apply to the stability of a motion, and therefore it is possible to consider stable or unstable trajectories in phase space. For example, a trajectory that ends in a fixed point (i.e. a steady state solution) or in a limit cycle is stable, since trajectories that are initially close to each other converge to the fixed point or limit cycle orbit. However, a chaotic trajectory is unstable since nearby trajectories diverge from each other. A graphical representation of the different types of stability, according to Lyapunov, is shown in Figure 2-1.

Note that in the definition of quasi-asymptotic stability, the system is not necessarily stable at all times (it is only required for it to be stable for large times).

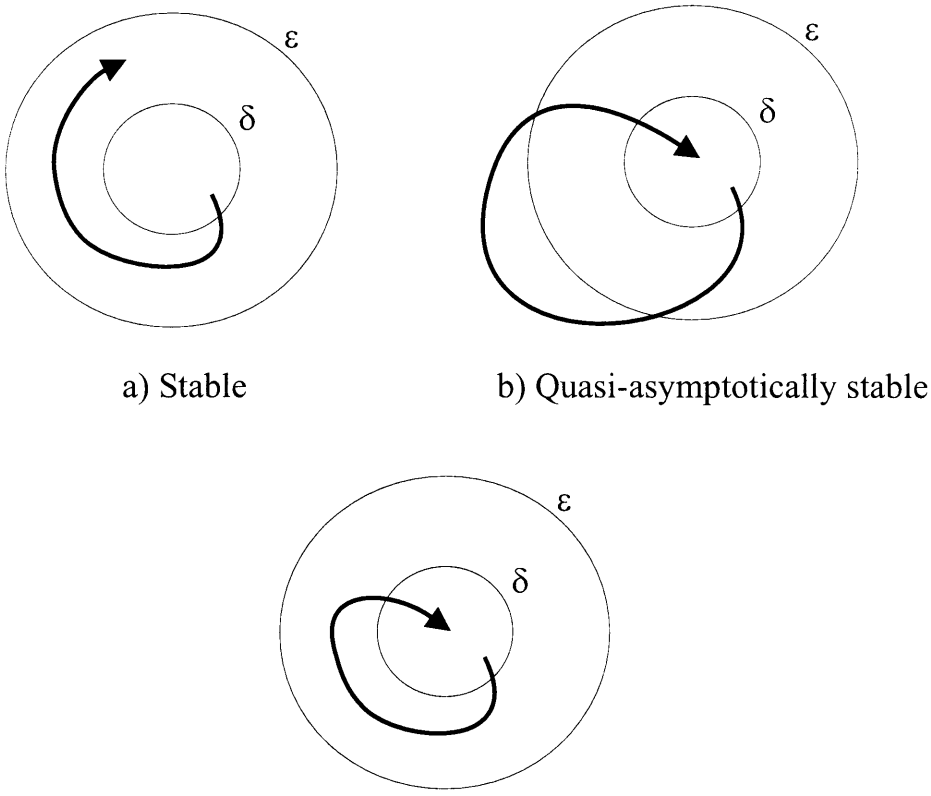

Figure 2-1: Graphical representation of the different types of stability of a motion, according to Lyapunov.

2.4 Lyapunov characteristic exponents

The Lyapunov characteristic exponents are used to characterize a system dynamic behavior, especially in the case in which a chaotic response is obtained. In this section, the definition and properties of Lyapunov characteristic exponents are considered, and the numerical calculation of the maximum Lyapunov characteristic exponent of order one briefly discussed (for discrete systems of equations of the form of equation (2.1)).

2.4.1 Definition and properties of Lyapunov characteristic exponents

Consider the case of a nonlinear system of equations of the form (2.1), for which the function $\mathbf{f}$ generates a differentiable flow ϕ_t defined on a differentiable manifold, M. We are interested in the asymptotic behavior (as $t \to \infty$) of the differential flow $d\phi_t$ [3].

This problem is related to the asymptotic behavior of infinitesimal perturbations $\mathbf{y}(t)$ to a reference trajectory $\mathbf{x}_r(t)$, solution of equations (2.1) and (2.2).

As discussed in Section 2.3, the equation that describes the evolution of perturbations is given by

$$\dot{\mathbf{y}} = \mathbf{f}(\mathbf{x}_r + \mathbf{y}) - \mathbf{f}(\mathbf{x}_r) \tag{2.7}$$

The above equation can be linearized (since the perturbation considered is infinitesimal), resulting in the following equation for the evolution of the perturbations,

$$\dot{\mathbf{y}} = \left(\frac{\partial \mathbf{f}}{\partial \mathbf{x}}\right)_{\mathbf{x}=\mathbf{x}_r} \mathbf{y} \tag{2.8}$$

where $\partial \mathbf{f}/\partial \mathbf{x}$ is the Jacobian matrix of the vector function $\mathbf{f}(\mathbf{x})$. In what follows it is assumed, for simplicity, that Cartesian coordinates are employed and therefore matrices instead of tensors will be defined and used. Of course, the same concepts are applicable when other coordinate systems are considered.

A solution of equation (2.8) exists and is unique for every initial condition, $\mathbf{y}(t_0^*) = \mathbf{y}_0$, if the Jacobian matrix of the function $\mathbf{f}(\mathbf{x})$ evaluated at $\mathbf{x}_r$ satisfies the conditions of Theorem 1 at any time [3]. It can be shown that if $\mathbf{f}(\mathbf{x})$ is continuously differentiable the conditions are satisfied. In such a case, the perturbation can be expressed by

$$\mathbf{y}(t) = \mathbf{\Phi}(t, t_0^*)\ \mathbf{y}_0 \tag{2.9}$$

where the matrix $\mathbf{\Phi}(t, t_0^*)$ is the linearized flow matrix, a linear map of the tangent space of the vector function $\mathbf{f}(\mathbf{x}_r)$ at time t_0^*, E_0, onto the vector space associated with the tangent space of $\mathbf{f}(\mathbf{x}_r)$ at time t, E_t. The following relations, for the mapping $\mathbf{\Phi}$, are satisfied,

$$\begin{aligned} \mathbf{\Phi}(t_2, t_0^*) &= \mathbf{\Phi}(t_2, t_1)\ \mathbf{\Phi}(t_1, t_0^*) \\ \mathbf{\Phi}(t_n, t_n) &= \mathbf{I} \end{aligned} \tag{2.10}$$

where $t_2 > t_1 > t_0^*$, and $\mathbf{I}$ is the identity matrix. Note that, since the matrix $\mathbf{\Phi}$ is obtained from equation (2.8) and the Jacobian matrix changes as a function of time, $\mathbf{\Phi}$ depends on the specific times considered *and* on the reference trajectory chosen.

Assume that

$$\lim_{t\to\infty} \frac{1}{t} \ln \|\mathbf{\Phi}(t, t_0^*)\| < \infty \tag{2.11}$$

where the norm of the matrix $\mathbf{\Phi}$ is usually defined as $\|\mathbf{\Phi}\| = \max[\lambda(\sqrt{\mathbf{\Phi}^T\mathbf{\Phi}})]$ [30], and $\lambda(\mathbf{A})$ represents the eigenvalues of the matrix $\mathbf{A}$. Then, a *one-dimensional Lyapunov characteristic exponent* of the response of the nonlinear system (2.1), with initial conditions (2.2), is defined by

$$\chi(\mathbf{y}_0, \mathbf{x}_r) = \limsup_{t\to\infty} \frac{1}{t}\ ln\left(\frac{\|\mathbf{y}(t)\|}{\|\mathbf{y}_0\|}\right) \tag{2.12}$$

where the supremum is taken since otherwise the function can be oscillatory and the limit not defined.

From equation (2.12) the following properties can be derived,

[3] Note here that t_0^* , the initial time for the perturbation, is not necessarily equal to t_0, the initial time for the equations of motion.

- Given a constant number c

$$\chi(c\,\mathbf{y}_0, \mathbf{x}_r) = \chi(\mathbf{y}_0, \mathbf{x}_r) \tag{2.13}$$

Proof:

$\ln \| c\,\mathbf{y}\| = \ln \|c\| + \ln \|\mathbf{y}\|$

and therefore property (2.13) follows from equation (2.12). $\diamond$

- Given two perturbation vectors $\mathbf{y}_1$ and $\mathbf{y}_2$,

$$\chi(\mathbf{y}_{1_0} + \mathbf{y}_{2_0},\, \mathbf{x}_r) \leq \max\{\, \chi(\mathbf{y}_{1_0}, \mathbf{x}_r),\, \chi(\mathbf{y}_{2_0}, \mathbf{x}_r)\} \tag{2.14}$$

Proof:

Assume that $\|\mathbf{y}_1\| > \|\mathbf{y}_2\|$, at least for large values of t, then we have,

$$\begin{aligned} \ln \|\mathbf{y}_1 + \mathbf{y}_2\| &\leq \ln (\|\mathbf{y}_1\| + \|\mathbf{y}_2\|) \\ &\leq \ln [\ \|\mathbf{y}_1\|\ (1 + \|\mathbf{y}_2\| \,/\, \|\mathbf{y}_1\|)\ ] \\ &\leq \ln \|\mathbf{y}_1\| + \ln (1 + \|\mathbf{y}_2\| \,/\, \|\mathbf{y}_1\|) \end{aligned}$$

Since $\|\mathbf{y}_2\| \,/\, \|\mathbf{y}_1\| < 1$, it follows that $lim_{t\to\infty} ln(1 + \|\mathbf{y}_2\| \,/\, \|\mathbf{y}_1\|) = 0$,

and property (2.14) follows from equation (2.12). $\diamond$

Suppose that we have an n-dimensional unit sphere D in the tangent space of $\mathbf{f}(\mathbf{x})$ at $\mathbf{x}_r(t_0^*)$, E_0 (we can think of D as an n-dimensional unit sphere of perturbed initial conditions). The image of D in the tangent space E_t at $\mathbf{x}_r(t)$ is given by the the mapping $\mathbf{\Phi}(t, t_0^*)$ and is in general an ellipsoid, see Figure 2-2. It is possible to associate each ellipsoid semiaxis with a *coefficient of expansion* (also called a *Lyapunov characteristic number)*, λ_i, in the direction of the image vector of the semiaxis in the space E_0. Furthermore, we can associate each coefficient of expansion with a *Lyapunov characteristic exponent*, and therefore we have at most n Lyapunov characteristic exponents, where n is the dimension of the tangent space:

$$\chi_i = \limsup_{t\to\infty} \frac{1}{t}\ ln\lambda_i \quad with\ i = 1, 2, \ldots, n. \tag{2.15}$$

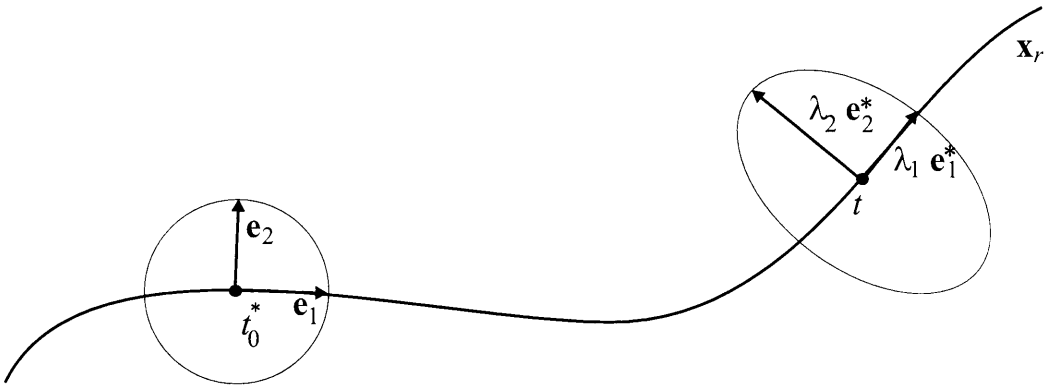

Figure 2-2: Graphical representation of the evolution of perturbations in all directions in a two-dimensional phase space. The vectors $\mathbf{e}_1$ and $\mathbf{e}_2$ change directions as the value of t increases. However, we are concerned with the basis vectors associated with $t \to \infty$.

The coefficients of expansion λ_i correspond to the eigenvalues of the matrix $\sqrt{(\mathbf{\Phi}^T\mathbf{\Phi})}$ (since the eigenvalues of $\mathbf{\Phi}$ might be imaginary numbers).

A basis $\mathbf{e}_1, \mathbf{e}_2, \ldots, \mathbf{e}_n$ in $\Re^n$, such that $\|\mathbf{e}_i\| = 1$ with $i = 1, 2, \ldots, n$, is called *normal* by Lyapunov if $\sum_{i=1}^{n} \chi(\mathbf{e}_i, \mathbf{x}_r)$ is a minimum for the basis, and therefore the basis $\{\mathbf{e}_i\}$ is formed by the eigenvectors of the matrix $\mathbf{\Phi}^T\ \mathbf{\Phi}(t, t_0^*)$ as time goes to infinity, or a set of independent basis vectors associated with repeated eigenvalues. Thus, if λ_i^2 represents the eigenvalue of the matrix $\mathbf{\Phi}^T\mathbf{\Phi}$ associated with the eigenvector $\mathbf{e}_i$,

$$\chi(\mathbf{e}_i, \mathbf{x}_r) = \limsup_{t\to\infty} \frac{1}{t}\ \ln(\lambda_i) \tag{2.16}$$

and therefore,

$$\sum_{i=1}^{n} \chi(\mathbf{e}_i, \mathbf{x}_r) = \limsup_{t\to\infty} \frac{1}{2t}\ \ln\det\left[\mathbf{\Phi}^T\mathbf{\Phi}(t, t_0^*)\right] \tag{2.17}$$

Then, $\chi_i = \chi(\mathbf{e}_i, \mathbf{x}_r)$, are the characteristic exponents associated with the basis vectors and they form the *spectrum* of Lyapunov characteristic exponents of first order (or one-dimensional). Arranging them in descending order,

$$\chi_1 \geq \chi_2 \geq \cdots \geq \chi_n \tag{2.18}$$

It can be shown that if the reference trajectory does not end in a fixed point, the Lyapunov characteristic exponent of a vector tangent to the orbit of the flow is zero [3] [11]. Therefore, except in the case of steady-state solutions, at least one of the Lyapunov characteristic exponents of first order is zero.

When a normal basis is considered, property (2.14) becomes,

$$\chi(\mathbf{e}_1 + \mathbf{e}_2 + \ldots + \mathbf{e}_n,\, \mathbf{x}_r) = \max\{\, \chi(\mathbf{e}_1, \mathbf{x}_r),\, \chi(\mathbf{e}_2, \mathbf{x}_r), \ldots, \chi(\mathbf{e}_n, \mathbf{x}_r)\} \tag{2.19}$$

since the vectors $\mathbf{e}_i$ are orthogonal.

Expressing the perturbation $\mathbf{y}$ as a linear combination of the normal basis defined above,

$$\mathbf{y} = c_1\mathbf{e}_1 + c_2\mathbf{e}_2 + \ldots + c_n\mathbf{e}_n \tag{2.20}$$

where $c_1, c_2, \ldots, c_n$ are constants. Using properties (2.13) and (2.19) it follows that

$$\chi(\mathbf{y}_0, \mathbf{x}_r) = \chi_1 \tag{2.21}$$

except in the case in which $\mathbf{y}_0$ has no components in the direction of the basis vector $\mathbf{e}_i$ associated with χ_1 (in a numerical calculation, however, round-off errors will always introduce a component in the mentioned direction). As a consequence, using equation (2.12), the *maximum Lyapunov characteristic exponent*, which will be denoted simply as the *Lyapunov characteristic exponent* or *LCE*, is in general obtained (it is always obtained in a numerical calculation). An alternative explanation is obtained by considering equation (2.9). At each time step, $\mathbf{y}$ tends to grow more in the direction of the eigenvector of $\mathbf{\Phi}$ that corresponds to the eigenvalue with largest real part. As a consequence, after a sufficient amount of time the vector $\mathbf{y}$ would be aligned with the direction associated with χ_1, so that χ_1 would be obtained from the calculation. Therefore, the value of the LCE does not depend, in general, on the initial perturbation vector selected, and thus $\chi(\mathbf{y}_0, \mathbf{x}_r) = \chi(\mathbf{x}_r)$.

Since the LCE is a measure of the asymptotic divergence of nearby trajectories in phase space, all trajectories that start in the basin of attraction of an attracting set

will have the same LCE, and hence $\chi(\mathbf{x}_r) = \chi_1 = \chi$ for all the trajectories considered that end in the same attracting set.

Let us also briefly consider here, for completeness, the so called k-dimensional Lyapunov characteristic exponents, although they are not used in this work.

Let $\mathbf{g}^k \subset \Re^n$ be a k-dimensional subspace generated by $\mathbf{e}_1, \mathbf{e}_2, \ldots, \mathbf{e}_k$ with $k \leq n$, and $V_k(t)$ the volume of the parallelotope determined by the vectors $\mathbf{\Phi}(t, t_0^*)\ \mathbf{e}_i$ with $i = 1, 2, ..., k$. A *k-dimensional Lyapunov characteristic exponent* is defined by

$$\chi^{(k)}(\mathbf{g}^k) = \limsup_{t\to\infty} \frac{1}{t} \ln V_k(t) \tag{2.22}$$

Using the definition of the LCEs of first order,

$$\chi^{(k)}(\mathbf{g}^k, \mathbf{x}_r) = \chi(\mathbf{e}_1, \mathbf{x}_r) + \chi(\mathbf{e}_2, \mathbf{x}_r) + ... + \chi(\mathbf{e}_k, \mathbf{x}_r) \tag{2.23}$$

Choosing arbitrary vectors that span a k-dimensional space (such as in a numerical calculation), from properties (2.13) and (2.19) the largest values of the Lyapunov characteristic exponents of first order will be obtained,

$$\chi^{(k)}(\mathbf{g}^k, \mathbf{x}_r) = \chi_1 + \chi_2 + ... + \chi_k \tag{2.24}$$

Therefore from the knowledge of the Lyapunov exponents of k-th order we can calculate the LCEs of first order. In fact, this property is used to calculate the complete spectrum of Lyapunov characteristic exponents of first order, see for example [3] [7].

A natural question that arises is whether the *exact* LCE exists, that is to say, whether the following number exists,

$$\chi = \lim_{t\to\infty} \frac{1}{t}\ ln\left(\frac{\|\mathbf{y}(t)\|}{\|\mathbf{y}_0\|}\right) \tag{2.25}$$

This question was addressed by Oseledec in [30].

Assume that M is a smooth compact manifold on which the dynamical system of equations (2.1) is defined. If the flow ϕ_t generated by the vector field $\mathbf{f}(\mathbf{x})$ is smooth,

at least one *normalized invariant measure* or *probabilistic measure* μ exists for the flow such that,

$$\begin{aligned} \mu(\phi(\mathbf{x},t)) &= \mu(\mathbf{x}) \\ \mu(M) &= 1 \end{aligned} \tag{2.26}$$

Then the Oseledec theorem [30] states:

Theorem 3: If a normalized measure $\mu(\mathbf{x})$ exists for the flow ϕ_t generated by the vector field of equation (2.1), such that $\mu(M) = 1$ the limit

$$\lim_{t\to\infty} \frac{1}{t} \ln \|\mathbf{\Phi}(t, t_0^*)\| \tag{2.27}$$

and therefore

$$\lim_{t\to\infty} \frac{1}{t}\, ln \left(\frac{\|\mathbf{y}(t)\|}{\|\mathbf{y}_0\|} \right) \tag{2.28}$$

exists for almost all $\mathbf{x}$ with respect to μ if

$$\sup_{-dt\leq\theta\leq dt} \int_M \ln^+ \|\mathbf{\Phi}(t_0^* + \theta, t_0^*)\|\ \mu(d\mathbf{x}) < +\infty \tag{2.29}$$

where $\ln^+(a) = \max\{\ln(a), 0\}$, with $a \in \Re$. $\diamond$

The Oseledec theorem is applicable to flows that are only almost everywhere differentiable. The fact that the limit exists for almost all $\mathbf{x}$ with respect to μ refers to the fact that there is a certain subset of the manifold M with measure zero, and then there exists a measurable set $M_1 \subset M$ such that $\mu(M_1) = 1$.

Furthermore, Benettin et al [3] showed that if the flow ϕ_t is of class C^1 and defined on a manifold N, not necessarily compact, which contains a compact differentiable manifold M invariant under ϕ_t (i.e. if $\mathbf{x} \in M$ then $\phi(\mathbf{x}, t) \in M$ for all t), then there exists a measurable subset $M_1 \subset M$ with $\mu(M_1) = 1$ such that for every $\mathbf{x} \in M_1$ LCEs of any order exist.

2.4.2 Numerical calculation of the maximum Lyapunov characteristic exponent

Let us consider again the nonlinear autonomous equations (2.1), with initial conditions (2.2), and the equations that describe the evolution of perturbations,

$$\begin{aligned} \dot{\mathbf{y}} &= \left(\frac{\partial \mathbf{f}}{\partial \mathbf{x}}\right)_{\mathbf{x}=\mathbf{x}_r} \mathbf{y} \\ \mathbf{y}(t_0^*) &= \mathbf{y}_0 \end{aligned} \tag{2.30}$$

where the initial times t_0 and t_0^* need not be the same, and in fact t_0^* is usually chosen so that the system transient effects have decayed, since in this case the convergence to the LCE value in a numerical calculation is faster.

The basis for the numerical calculation of LCEs has been described in references [4] [3]. Both equations (2.1) and (2.30) have to be numerically integrated to calculate the systems reference solution and evolution of perturbations from which successive approximations to the trajectory LCE as a function of time are obtained. In the calculation of the LCE it is assumed that the system reference trajectory is "correctly" obtained, i.e. the system behavior is properly captured by the numerical discretization of the equations. See a discussion about numerical errors in [3].

In what follows, the procedure employed to calculate the maximum LCE of discrete dynamical systems is briefly described, following [3]. The procedure has been mainly used with non-dimensional first-order ordinary differential equations in time, consisting of only a few degrees of freedom.

Without loss of generality, we chose a random initial perturbation $\mathbf{y}_0$ in equation (2.30), such that $\|\mathbf{y}_0\| = 1$, and a fixed time step Δt, so that $t_n = t_0^* + n\Delta t$.

The time steps employed to numerically integrate the equations of motion (2.1) and the equations for the evolution of perturbations (2.30) need not be the same. However, it is convenient to use the same time step because the linearized matrices needed to calculate the evolution of perturbations are usually also employed in the solution of the equations of motion (when linearization is used in the solution procedure). Then, the coefficient matrices obtained after discretizing the equations in time are the same, and they need to be factorized only once and use in both the calculation

of the perturbation evolution and the system response. It is then especially convenient to use the same time step when large systems of equations, as those obtained when using finite element methods, are solved.

The evolution of the perturbation vector at each time step, t_n, can be calculated by discretizing equation (2.30) in time and solving for $\mathbf{y}(t_n)$.

After n time steps the perturbation vector is [4]

$$\mathbf{y}_n = \mathbf{y}(t_n) = \mathbf{\Phi}(t_n, t_0^*)\ \mathbf{y}_0 = \mathbf{\Phi}(t_n, t_{n-1})\ \mathbf{\Phi}(t_{n-1}, t_{n-2})...\mathbf{\Phi}(t_1, t_0^*)\ \mathbf{y}_0 \tag{2.31}$$

The perturbation vector $\mathbf{y}_n$ may grow (exponentially fast) if the behavior of the trajectory considered is chaotic. In such a case, an overflow of the computed vector would soon occur in a numerical calculation. To avoid the overflow, the perturbation vector is normalized at every time step (or after a certain number of time steps).

Considering the n^{th} time step and $\hat{\mathbf{y}}_{n-1}$, the normalized perturbation vector obtained in the previous time step (i.e. $\|\hat{\mathbf{y}}_{n-1}\| = 1$), then

$$\mathbf{y}_n^* = \mathbf{\Phi}(t_n, t_{n-1})\ \hat{\mathbf{y}}_{n-1} \tag{2.32}$$

and

$$d_n = \|\mathbf{y}_n^*\| \tag{2.33}$$

The obtained perturbation vector, $\mathbf{y}_n^*$, is then normalized to be used in the calculation of the next time step,

$$\hat{\mathbf{y}}_n = \frac{\mathbf{y}_n^*}{d_n} \tag{2.34}$$

From equation (2.31), it is evident that following this procedure for n time steps,

$$\|\mathbf{y}_n\| = d_n\ d_{n-1}\ \cdots\ d_1 \tag{2.35}$$

[4] Here the matrices $\mathbf{\Phi}(t_n, t_{n-1})$ are approximated discretizing equation (2.30) in time at each time step.

and an approximation to the LCE can be calculated at each time step as follows,

$$k_n = \frac{1}{t_n} \ln \|\mathbf{y}_n\| = \frac{1}{t_n} \sum_{i=1}^{n} ln(d_i) \tag{2.36}$$

The value of the LCE is calculated as the limit,

$$\chi = \lim_{n \to \infty,\ \Delta t \to 0} k_n \tag{2.37}$$

In practice, a good approximation to the value of the LCE is obtained when it is observed that k_n reaches a constant value as n is increased. Convergence to this constant value usually implies that a large number of time steps need to be calculated and therefore the evaluation of the LCE of a trajectory can be a time consuming calculation.

In summary, to calculate the maximum LCE of the trajectory of a nonlinear system, we start with a unit but otherwise arbitrary perturbation vector $\mathbf{y}_0$, such that $\|\mathbf{y}_0\| = \|\hat{\mathbf{y}}_0\| = 1$. Then, the following procedure is performed at each time step,

- Discretize the perturbation evolution equations in time and obtain $\mathbf{y}_n^*$ from equation (2.32).
- Calculate the norm of the calculated vector $\mathbf{y}_n^*$, $d_n = \|\mathbf{y}_n^*\|$, which gives the growth/decay of the perturbation for the time step considered.
- Normalize the perturbation $\mathbf{y}_n^*$ to avoid overflow of the computed perturbation vector, equation (2.34).
- Calculate the approximation to the LCE, k_n, from equation (2.36), and repeat the procedure for the next time step.

Chapter 3

Governing equations of continuous media

The motion of continuous media is described by governing differential equations, which are derived from the laws of physics and constitutive equations.

Usually, the equations of motion of a solid medium are written using the *Lagrangian formulation*, i.e. the equations describe the position of particles as a function of time (with respect to a fixed frame), and therefore, particles are followed in their motion. In contrast, the fluid flow equations are usually written using the *Eulerian formulation*, i.e. the equations describe the fluid velocity and pressure at a fixed spatial position. For fluid flow-structural interaction problems, a combination of both formulations, an *arbitrary Lagrangian-Eulerian formulation*, is required to describe the fluid flow because the fluid domain changes as a function of time due to structural interactions.

In this chapter the Lagrangian, Eulerian and arbitrary Lagrangian-Eulerian formulations of motion are briefly discussed. The governing equations of Newtonian fluid flows and elastic isotropic solids are considered. In addition, the equilibrium and compatibility conditions that must be satisfied at the fluid flow-structural interface are given.

3.1 Kinematics of continuous media

Consider a body (or a part of it) that is moving through space. The space occupied by the body at time $t = 0$ is called the *reference configuration*, and the space occupied by the body at time t is called the *spatial configuration* (see figure 3-1).

At time $t = 0$ we can identify each particle of the body with a reference coordinate $\mathbf{x}$. At time t the particle will be at a different position $\mathbf{z}$. In other words, $\mathbf{z}$ is the position at time t of the particle that was at $\mathbf{x}$ at time $t = 0$.

There are different ways of describing the motion of the body (see, for example, [22]). Three of them will be considered here,

- Lagrangian formulation
- Eulerian formulation
- Arbitrary Lagrangian-Eulerian (ALE) formulation

Equations of motion are generally written in terms of *material* or *physical particles*. For example, when we say that a fluid is incompressible we mean that a particle cannot change its density with time, but different particles can have different densities. Newton's law of motion states that the rate of change of momentum of a body is equal to the sum of the external forces applied to that body, i.e. the law applies over a group of particles (that constitute the body) that are followed as a function of time.

In general, when solving a dynamic problem using finite element methods, any of the above descriptions can be employed (see [2], [29]).

3.1.1 Lagrangian formulation

In the Lagrangian formulation, the body particles are identified in the reference configuration, at time $t = 0$, and their movement followed as a function of time. The variables used to describe the equations of motion are then $\mathbf{x}$ and t. This description is usually employed to describe the motion of solids, for which the reference configuration is known.

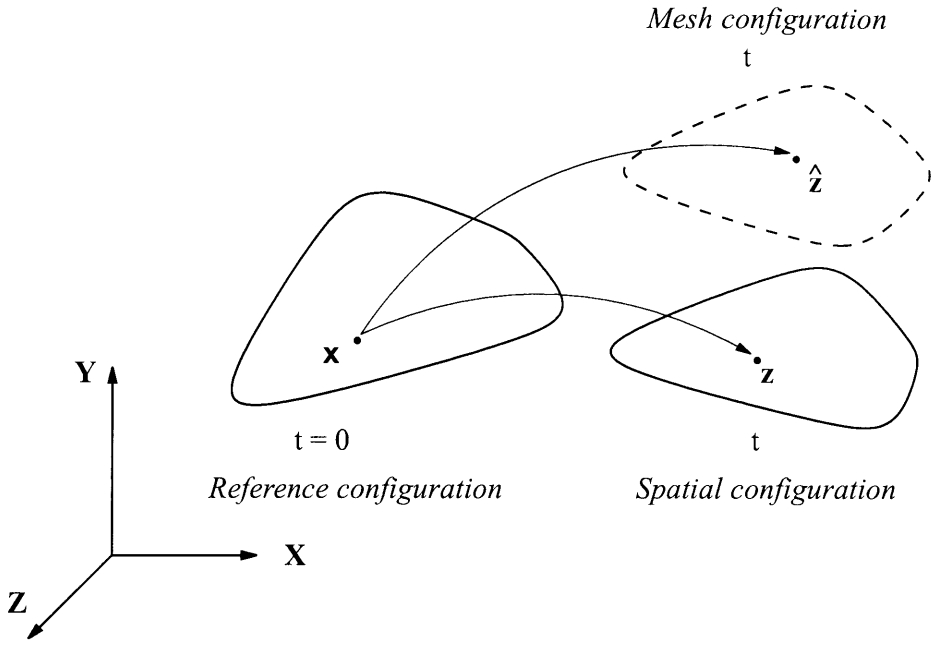

Figure 3-1: Reference, spatial and mesh configurations.

We are interested in deriving the Eulerian and ALE formulations from the Lagrangian formulation, for different equations of motion. In particular, the time derivatives that appear in the equations of motion need to be transformed, see for example [22].

3.1.2 Eulerian formulation

In the Eulerian formulation, the variables used in the description of the motion are $\mathbf{z}$ and t. The movement is described at a *fixed spatial position* $\mathbf{z}$. The position occupied at $t = 0$ by the particle that is at $\mathbf{z}$ at time t is not important and usually not known. This description is generally used to describe the motion of a fluid flow.

At time t the position of the *particles* can be expressed as a function of the particle position in the reference configuration

$$\mathbf{z} = \varphi(\mathbf{x}, t) \tag{3.1}$$

If equation (3.1) is known, then the velocity of a *particle* can be calculated by taking the partial derivative of (3.1) with $\mathbf{x}$ held constant

$$\mathbf{v} = \left(\frac{\partial \mathbf{z}}{\partial t}\right)_{\mathbf{x}} \tag{3.2}$$

likewise, the acceleration of the particle is

$$\mathbf{a} = \left(\frac{\partial \mathbf{v}}{\partial t}\right)_{\mathbf{x}} \tag{3.3}$$

However, when employing the Eulerian formulation equation (3.1) is generally not known. Physical quantities, f, are known as a function of a fixed spatial position $\mathbf{z}$, that is to say

$$f = g(\mathbf{z}, t) = G(\varphi(\mathbf{x}, t), t) \tag{3.4}$$

The time derivative of a physical quantity f with $\mathbf{x}$ held constant, is called the *material time derivative*, and is equal to the rate of change of f at the particle, i.e. as seen by an observer moving with a material particle (with respect to a fixed reference frame). The following notation is used from now on to refer to the material time derivative

$$\frac{Df}{Dt} \equiv \left(\frac{\partial f}{\partial t}\right)_{\mathbf{x}} \tag{3.5}$$

This expression is important since the equations of motion in the Lagrangian formulation are written using material derivatives, and therefore they have to be properly considered when converting one formulation of motion to another. For the Eulerian formulation we have,

$$\frac{Df}{Dt} = \left(\frac{\partial f}{\partial t}\right)_{\mathbf{z}} + \frac{\partial f}{\partial \mathbf{z}}\left(\frac{\partial \mathbf{z}}{\partial t}\right)_{\mathbf{x}} = \frac{\partial f}{\partial t} + \mathbf{v} \cdot \nabla f \tag{3.6}$$

3.1.3 Arbitrary Lagrangian-Eulerian formulation

The ALE formulation is a combination of the Lagrangian and Eulerian formulations. The movement of the body is described at an arbitrary position $\hat{\mathbf{z}}$ that can change as a function of time. In a finite element analysis, the position $\hat{\mathbf{z}}$ is associated with a mesh point, and the space occupied by the mesh at time t is called the *mesh*

configuration (see figure 3-1). The ALE formulation is used to describe the flow of a fluid whose domain is deforming as a function of time, as when considering fluid-structure interaction or free surface problems.

In the ALE formulation, the values of a physical quantity f are known as a function of the mesh positions, $\hat{\mathbf{z}}$.

. At time t each point $\hat{\mathbf{z}}$ can be associated with a material particle $\mathbf{x}$ using the mapping

$$\hat{\mathbf{z}} = \hat{\varphi}(\mathbf{x}, t) \tag{3.7}$$

And therefore, the physical quantity f can be expressed as

$$f = \hat{g}(\hat{\mathbf{z}}, t) = \hat{G}(\hat{\varphi}(\mathbf{x}, t), t) \tag{3.8}$$

The material derivative of $\hat{\mathbf{z}}$ is then the relative velocity of the particle with respect to the moving mesh referential (the field velocity as seen by an observer moving with the mesh),

$$\frac{D\hat{\mathbf{z}}}{Dt} = \mathbf{v} - \hat{\mathbf{v}} \tag{3.9}$$

where $\hat{\mathbf{v}}$ is the mesh velocity.

Then, in the ALE formulation we have,

$$\frac{Df}{Dt} = \left(\frac{\partial f}{\partial t}\right)_{\hat{\mathbf{z}}} + \frac{\partial f}{\partial \hat{\mathbf{z}}}\left(\frac{\partial \hat{\mathbf{z}}}{\partial t}\right)_{\mathbf{x}} = \frac{\partial f}{\partial t} + (\mathbf{v} - \hat{\mathbf{v}}) \cdot \nabla f \tag{3.10}$$

3.2 Conservation equations

Considerations in this work are restricted to isothermal processes of solids and almost incompressible fluids, and therefore the energy conservation equation is not needed in the description of motion.

3.2.1 Mass conservation

The principle of mass conservation states that mass cannot be created or destroyed within a (nonrelativistic) system. This means that the amount of mass enclosed in a *material volume* (one that is fixed to the physical particles) will not change in time. The simplest form of the mass conservation principle is then

$$\frac{Dm}{Dt} = \frac{D}{Dt}\int_{\Omega} \rho(\mathbf{x})\ d\Omega = 0 \tag{3.11}$$

where Ω is the body volume, m is the total mass enclosed in Ω and ρ is the body density. Equation (3.11) is the integral form of the mass conservation principle. The differential equation of mass conservation can be derived from (3.11), and it can be expressed in the Lagrangian formulation as

$$\frac{D\rho}{Dt} + \rho\ \nabla \cdot \mathbf{v} = 0 \tag{3.12}$$

where $\mathbf{v}$ is the body velocity (which is a function of $\mathbf{x}$). From equation (3.10), the ALE form of the mass conservation equation is

$$\frac{D\rho}{Dt} = \rho^{*} + (\mathbf{v} - \hat{\mathbf{v}}) \cdot \nabla\rho \tag{3.13}$$

where the superscript $*$ indicates time derivative with respect to a fixed mesh point, i.e. is the rate of change as seen by an observer that is moving with the mesh point; and $\hat{\mathbf{v}}$ is the velocity of the mesh referential. In the special case of no mesh movement, we have $\hat{\mathbf{v}} = \mathbf{0}$, and equation (3.13) corresponds to the Eulerian formulation of motion, similarly when $\hat{\mathbf{v}} = \mathbf{v}$, the mesh is moving with the physical particles and the Lagrangian formulation of motion is recovered.

3.2.2 Momentum conservation

Newton's law of motion can be expressed as

$$\frac{D\mathbf{P}}{Dt} = \sum \mathbf{F}_{ext} \tag{3.14}$$

where $\mathbf{P}$ is the momentum of the body, $\frac{D\mathbf{P}}{Dt}$ is the instantaneous rate of change of momentum at time t, and $\sum \mathbf{F}_{ext}$ is the sum of all external forces acting on the body at time t.

The equation of conservation of momentum in integral form can be written as

$$\frac{D}{Dt}\int_{\Omega(t)} \rho\ \mathbf{v}\ d\Omega = \sum \mathbf{F}_{ext}(t) \tag{3.15}$$

The differential equations of motion derived from (3.15) in the Lagrangian formulation are

$$\rho\ \frac{D\mathbf{v}}{Dt} = \mathbf{f}_{ext} \tag{3.16}$$

where $\mathbf{f}_{ext}$ is a vector of external forces per unit of volume. In the ALE formulation of motion we have,

$$\rho\ \frac{D\mathbf{v}}{Dt} = \rho\left[\mathbf{v}^* + (\mathbf{v} - \hat{\mathbf{v}}) \cdot \nabla\mathbf{v}\right] \tag{3.17}$$

where $\mathbf{v}^*$ is the rate of change of the fluid velocity as seen by an observer moving with the mesh referential, and $\hat{\mathbf{v}}$ is the mesh velocity.

3.3 Equations of motion

From the equation of momentum conservation (3.16) and the equation of mass conservation (3.12), the differential equations that describe the movement of continuous media can be obtained.

3.3.1 Structural equations

In general, structural equations are written using the Lagrangian formulation of motion. The equations of motion are derived from the momentum equations using appropriate constitutive relations.

Neglecting damping effects, the momentum equations for a structure in the Lagrangian formulation are

$$\rho \frac{D\mathbf{v}}{Dt} = \rho \frac{D^2\mathbf{u}}{Dt^2} = \nabla \cdot \boldsymbol{\tau}^S + \mathbf{f}^B \tag{3.18}$$

where $\mathbf{u}$ is the structural displacement field, $\boldsymbol{\tau}^S$ is the Cauchy stress tensor and $\mathbf{f}^B$ is the vector of body forces applied to the body.

The constitutive relations for a *linear elastic isotropic material* (in Cartesian coordinates) are

$$\tau_{ij}^S = \frac{E\nu}{(1+\nu)(1-2\nu)} \varepsilon_{kk} \delta_{ij} + \frac{E}{1+\nu} \varepsilon_{ij} \tag{3.19}$$

with

$$\varepsilon_{ij} = \frac{1}{2} (u_{i,j} + u_{j,i}) \tag{3.20}$$

where ρ is the density of the structure, E is the elastic or Young's modulus, ν is the Poisson's ratio, and the τ_{ij}^S and ε_{ij} are the *(ij)th* components of the Cauchy stress tensor $\boldsymbol{\tau}^S$ and the strain tensor $\boldsymbol{\varepsilon}$, respectively, and δ_{ij} is the Kronecker delta.

The boundary conditions needed to solve equation (3.18) are

$$\mathbf{u} = \mathbf{u}^s \quad \text{in } S_u^S \tag{3.21}$$

$$\boldsymbol{\tau}^S \mathbf{n}^S = \mathbf{t}^S \quad \text{in } S_f^S \tag{3.22}$$

and the initial conditions are

$$\mathbf{u}(t_0) = \mathbf{u}_0; \qquad \dot{\mathbf{u}}(t_0) = \dot{\mathbf{u}}_0 \tag{3.23}$$

where S_u^S is the part of the structural boundary with imposed displacements $\mathbf{u}^s$, S_f^S is the part of the boundary with imposed surface forces $\mathbf{t}^S$ and $\mathbf{n}^S$ is the unit outward vector normal to the structural boundary.

Since the equations of motion of the solid medium are written in the Lagrangian formulation, in which particles are followed in their movement, the mass conservation principle is already satisfied by the momentum equations and there is no need to impose it separately.

Equation (3.18) has to be satisfied for linear and nonlinear problems as well. It is important to notice that even when the material is linear (i.e. the constitutive equations are of the form of equation (3.19)), the equations of motion may be nonlinear if large displacements are present. The structural examples considered in Chapter 6 correspond to this situation.

In addition, nonlinearities in the equations may come from a nonlinear constitutive equation. This last case is not explicitly considered in this thesis, although the methods presented here are general and therefore applicable to this situation as well.

3.3.2 Fluid flow equations

The fluid flow equations of motion are derived from the momentum and mass conservation equations, (3.16) and (3.12), and appropriate constitutive laws. Since in a fluid flow-structural interaction problem, in general, the fluid domain changes as a function of time (due to the interaction with the structure), the equations of motion of the fluid are expressed using the ALE formulation. In what follows, some relevant fluid models are described.

Incompressible fluid flows

Using the ALE formulation, the Navier-Stokes equations for an incompressible fluid are

$$\rho \mathbf{v}^* + \rho \left[(\mathbf{v} - \hat{\mathbf{v}}) \cdot \nabla \right] \mathbf{v} = \nabla \cdot \boldsymbol{\tau}^F + \mathbf{f}^B \tag{3.24}$$

$$\nabla \cdot \mathbf{v} = 0 \tag{3.25}$$

where $\boldsymbol{\tau}^F$ is the fluid stress tensor and $\mathbf{f}^B$ here represents the vector of fluid body forces whereas ρ is the fluid density. Equation (3.24) is the momentum conservation and equation (3.25) is the continuity equation.

The constitutive relations for a Newtonian fluid (in Cartesian coordinates) are

$$\tau_{ij}^F = (-p)\ \delta_{ij} + 2\mu e_{ij} \tag{3.26}$$

with

$$e_{ij} = \frac{1}{2}\ (v_{i,j} + v_{j,i}) \tag{3.27}$$

In these relations, p is the pressure, μ is the dynamic viscosity coefficient, and e_{ij} is the *(i,j)th* component of the velocity strain tensor.

The boundary conditions required to solve equations (3.24) and (3.25) can be given as follows:

$$\mathbf{v} = \mathbf{v}^s \quad \text{in } S_v^F \tag{3.28}$$

$$\boldsymbol{\tau}^F\ \mathbf{n}^F = \mathbf{t}^F \quad \text{in } S_f^F \tag{3.29}$$

and initial condition

$$\mathbf{v}(t_0) = \mathbf{v}_0 \tag{3.30}$$

where S_v^F is the part of the fluid boundary with imposed velocities $\mathbf{v}^s$, S_f^F is the part of the boundary with imposed surface forces $\mathbf{t}^F$ and $\mathbf{n}^F$ is the unit outward vector normal to the fluid boundary.

Almost incompressible flow

For an almost incompressible fluid, the density can be expressed as $\rho = \rho_o + \Delta\rho$, and it is assumed that $\Delta\rho/\rho_o << 1$, such that $\rho \approx \rho_o$.

The bulk modulus of a fluid or solid, κ, is defined as

$$\kappa = \rho_o \left(\frac{\partial p}{\partial \rho}\right)_T \tag{3.31}$$

and therefore is a measure of the change of density due to a change of pressure at constant temperature, T. From equation (3.31) it follows that

$$\frac{1}{\rho_o}\frac{D\rho}{Dt} = \frac{1}{\rho_o}\left(\frac{\partial\rho}{\partial p}\right)_T \frac{Dp}{Dt} = \frac{1}{\kappa}\frac{Dp}{Dt} \tag{3.32}$$

Using equation (3.32) it can be shown that the continuity equation for an almost incompressible fluid in the ALE formulation becomes

$$\frac{1}{\kappa}\left[\, p^* + (\mathbf{v} - \hat{\mathbf{v}}) \cdot \nabla p \,\right] + \nabla \cdot \mathbf{v} = 0 \tag{3.33}$$

and the appropriate momentum equation to be considered is (3.24).

3.3.3 Fluid flow-structural interface conditions

We are interested in coupled systems in which fluid flows are interacting with structures. Hence, in addition to the fluid and structural equations, equilibrium and compatibility conditions must be satisfied at the fluid-structure interface.

The equilibrium conditions at the interface can be expressed as

$$\boldsymbol{\tau}^F \, \mathbf{n}^F + \boldsymbol{\tau}^S \, \mathbf{n}^S = 0 \quad \text{(at interface)} \tag{3.34}$$

where $\mathbf{n}^F$ and $\mathbf{n}^S$ are unit normal surface vectors pointing outward of the fluid and structural domains respectively. This condition ensures that forces are in equilibrium at the fluid-structure interface.

The compatibility condition at the interface requires that

$$\hat{\mathbf{u}}_f^I = \mathbf{u}_s^I \quad \text{(at interface)} \tag{3.35}$$

where $\hat{\mathbf{u}}_f^I$ is the vector of displacements of the fluid (domain) at the interface and $\mathbf{u}_s^I$ is the vector of displacements of the structure at the interface.

This condition ensures that the material will not overlap and no gaps will be formed at the interface.

Chapter 4

Finite element formulation

In a finite element formulation, the weak (or variational) form of the continuum governing equations of motion is considered, and the test functions correspond to the finite element interpolations (Galerkin procedure).

In what follows, some spaces needed in the formulation of the finite element method will be defined (see also [2], [9]).

Let us denote by Ω a bounded domain in $\Re^n$ (with $n = 2$ or 3) and by S its boundary.

$\mathrm{L}^2(\Omega)$ represents the space of functions that are square integrable over Ω,

$$L^2(\Omega) = \{q : \int_\Omega q^2 \, d\Omega < +\infty\}$$

Similarly, $\mathbf{L}^2(\Omega)$ is the space of vector functions that are square integrable over Ω,

$$\mathbf{L}^2(\Omega) = \{\mathbf{q} : \int_\Omega \sum_i q_i^2 \, d\Omega < +\infty\}$$

The *Sobolev space* is defined for any non-negative integer value k as the space of square integrable functions over Ω, whose derivatives up to order k are also square integrable over Ω

$$H^k(\Omega) = \{q \in L^2(\Omega) : \partial^n q \in L^2(\Omega) \qquad \forall\ 0 < n \leq k\}$$

For vector valued functions, we have

$$\mathbf{H}^k(\Omega) = \{\mathbf{v} : v_i \in H^k(\Omega)\}$$

4.1 Structural equations

The *weak form* of the transient structural equations (in Cartesian coordinates) can be stated as ([2]):

Given $\mathbf{f}^B$, find $\mathbf{u} \in \mathbf{H}^1(\Omega)$ with $\mathbf{u} = \mathbf{u}^s$ in S_u^S, such that

$$\int_\Omega \bar{u}_i \; \rho \; \ddot{u}_i \; d\Omega + \int_\Omega \; \bar{\varepsilon}_{ij} \; \tau_{ij}^S \; d\Omega = \int_\Omega \bar{u}_i \; f_i^B \; d\Omega + \int_{S_f^S} \bar{u}_i \; t_i^S \; dS \tag{4.1}$$

for all $\bar{\mathbf{u}} \in \mathbf{H}^1(\Omega)$ with $\bar{\mathbf{u}} = \mathbf{0}$ in S_u^S. $\diamond$

Where Ω is the body *material* volume, ρ is the structural density, $\mathbf{u}$ is the vector of body displacements, $\bar{\mathbf{u}}$ is the vector of *virtual displacements*, $\bar{\boldsymbol{\varepsilon}}$ is the virtual strain tensor, $\boldsymbol{\tau}^S$ is the Cauchy stress tensor and $\mathbf{f}^B$ is the vector of body forces; S_f^S is the part of the structural boundary with prescribed tractions of components t_i^S (which in the case of a fluid-structure interaction problem includes the interface, where tractions are exerted by the fluid onto the structure), and S_u^S is the part of the boundary with imposed displacements.

Finite element spaces for the structural equations of motion are defined as follows,

$$\mathbf{V}^h = \{\mathbf{u}^h \in \mathbf{H}^1(\Omega)\} \tag{4.2}$$

$$\bar{\mathbf{V}}^h = \{\bar{\mathbf{u}}^h \in \mathbf{H}^1(\Omega)\} \tag{4.3}$$

The finite element problem can be stated as:

Given $\mathbf{f}_B$, find $\mathbf{u}^h \in \mathbf{V}^h(\Omega)$ with $\mathbf{u}^h = \mathbf{u}^s$ in S_u^S, such that

$$\int_\Omega \bar{u}_i^h \; \rho \; \ddot{u}_i^h \; d\Omega + \int_\Omega \; \bar{\varepsilon}_{ij}^h \; (\tau_{ij}^h)^S \; d\Omega = \int_\Omega \bar{u}_i^h \; f_i^B \; d\Omega + \int_{S_f^S} \bar{u}_i^h \; t_i^S \; dS \tag{4.4}$$

for all $\bar{\mathbf{u}}^h \in \bar{\mathbf{V}}^h(\Omega)$ with $\bar{\mathbf{u}}^h = \mathbf{0}$ in S_u^S. $\diamond$

Equation (4.4) is the *displacement based finite element formulation* for structures.

In case nonlinearities are present in the system (either because the structural displacements are large or a nonlinear constitutive equation is appropriate), the equations (4.4) are linearized before solving them (using the Newton-Raphson procedure).

The dynamic equations of motion of a (nonlinear) structure can be written as,

$$^{t+\Delta t}\mathbf{W} = {}^{t+\Delta t}\mathbf{R}_s \tag{4.5}$$

where $^{t+\Delta t}\mathbf{W}$ and $^{t+\Delta t}\mathbf{R}_s$ represent the left and right hand sides of equation (4.4), respectively.

A careful description of the problem formulation and linearization process used when nonlinearities are present is given in [2], and will not be explicitly considered in this work.

The *linearized* finite element equations from (4.4), neglecting damping effects, can be written as

$$\mathbf{M}_u\ \ddot{\mathbf{u}} + \mathbf{K}_u\ \mathbf{u}\ =\ \mathbf{R}_s - \mathbf{F}_u \tag{4.6}$$

where $\mathbf{M}_u$ and $\mathbf{K}_u$ are the mass and tangent stiffness matrices, $\mathbf{u}$ and $\ddot{\mathbf{u}}$ are the vectors of *incremental* displacements and accelerations, $\mathbf{R}_s$ is the discretized load vector and $\mathbf{F}_u$ is obtained from the linearization process.

The finite element space $\mathbf{V}^h$ depends on the elements chosen to discretize the volume Ω. In a 2D space, we can choose, for example, quadrilateral bilinear or parabolic elements. In this thesis, the displacement-based 9-node elements [2] are used to calculate the structural response of the examples given in Chapter 6.

4.2 Fluid flow discretization

The variational formulation of an *almost incompressible fluid* modeled using the Navier-Stokes equations and expressed in the ALE description of motion (in Cartesian coordinates) can be stated as:

Given $\mathbf{f}^B$ and $\hat{\mathbf{v}}$, find $\mathbf{v} \in \mathbf{H}^1(\hat{V})$ with $\mathbf{v} = \mathbf{v}^{\mathbf{s}}$ in S_v^F and $p \in H^1(\hat{V})$ such that

$$\int_{\hat{V}} \bar{v}_i \; \rho \left[v_i^* + v_{i,j} \left(v_j - \hat{v}_j \right) \right] \; d\hat{V} + \int_{\hat{V}} \bar{e}_{ij} \; \tau_{ij}^F \; d\hat{V} = \int_{\hat{V}} \bar{v}_i \; f_i^B \; d\hat{V} + \int_{S_f^F} \bar{v}_i \; t_i^F \; dS \quad (4.7)$$

$$\int_{\hat{V}} \frac{\bar{p}}{\kappa} \; \left[\; p^* + p_{,i} \left(v_i - \hat{v}_i \right) \right] d\hat{V} + \int_{\hat{V}} \bar{p} \; v_{i,i} \; d\hat{V} = 0 \quad (4.8)$$

for all $\bar{\mathbf{v}} \in \mathbf{H}^1(\hat{V})$ with $\bar{\mathbf{v}} = \mathbf{0}$ in S_v^F and $\bar{p} \in H^1(\hat{V})$. $\diamond$

In the above expression $\bar{\mathbf{v}}$ and $\bar{p}$ are the *virtual* velocity and pressure, $\hat{V}$ is the volume of the fluid domain, ρ here is the fluid density, $\mathbf{v}$ and p are the fluid velocity and pressure, $\hat{\mathbf{v}}$ is the mesh velocity; $\boldsymbol{\tau}^F$ is the fluid stress tensor, $\bar{\mathbf{e}}$ is the virtual rate of strain tensor, κ is the fluid bulk modulus, S_v^F is the part of the fluid boundary with prescribed velocity $\mathbf{v}^S$, S_f^F is the part of the fluid boundary with prescribed tractions of components t_i^F (note that if the fluid is interacting with a structure, then the interface surface S_I, where tractions are exerted by the solid medium over the fluid, is included in S_f^F).

If the fluid is incompressible, the bulk modulus is such that $\kappa \to \infty$, and the term containing κ in equation (4.8) vanishes.

Equations (4.7) and (4.8) must be discretized in space in order to be solved numerically. The following finite element spaces are introduced for the velocity and pressure,

$$\mathbf{V}^h = \{ \mathbf{v}^h \in \mathbf{H}^1(\hat{V}) \} \quad (4.9)$$

$$\bar{\mathbf{V}}^h = \{ \bar{\mathbf{v}}^h \in \mathbf{H}^1(\hat{V}) \} \quad (4.10)$$

$$Q^h = \{ p^h \in H^1(\hat{V}) \} \quad (4.11)$$

$$\bar{Q}^h = \{ \bar{p}^h \in H^1(\hat{V}) \} \quad (4.12)$$

Then, the finite element problem can be stated as:

Given $\mathbf{f}_B$ and $\hat{\mathbf{v}}^h$, find $\mathbf{v}^h \in \mathbf{V}^h(\hat{V})$ with $\mathbf{v}^h = \mathbf{v}^s$ in S_v^F, and $p^h \in Q^h(\hat{V})$ such that

$$\int_{\hat{V}} \bar{v}_i^h \; \rho \left[(v_i^h)^* + v_{i,j}^h \left(v_j^h - \hat{v}_j^h \right) \right] \; d\hat{V} + \int_{\hat{V}} \bar{e}_{ij}^h \; \tau_{ij}^{h\ F} \; d\hat{V} = R^F \tag{4.13}$$

$$\int_{\hat{V}} \frac{\bar{p}^h}{\kappa} \; \left[\; (p^h)^* + p_{,i}^h \left(v_i^h - \hat{v}_i^h \right) \right] d\hat{V} + \int_{\hat{V}} \bar{p}^h \; v_{i,i}^h \; d\hat{V} = 0 \tag{4.14}$$

with

$$R^F = \int_{\hat{V}} \bar{v}_i^h \; f_i^B \; d\hat{V} + \int_{S_f} (\bar{v}_i^h)^{S_f} \; t_i^F \; dS \tag{4.15}$$

for all $\bar{\mathbf{v}}^h \in \bar{\mathbf{V}}^h(\hat{V})$ with $\bar{\mathbf{v}}^h = \mathbf{0}$ in S_v^F and $\bar{p}^h \in \bar{Q}^h(\hat{V})$. $\diamond$

In the finite element procedure, the space $\mathbf{V}^h$ depends on the elements chosen to discretize the volume $\hat{V}$. In a 2D space, we can choose, for example, quadrilateral bilinear or parabolic elements. The pressure interpolation, however, cannot be chosen arbitrarily (see for example [2], [9]), otherwise, the formulation may not be stable. In order to avoid this problem, the *inf-sup* condition must be satisfied. In this thesis, 9/3 elements, which satisfy the inf-sup condition, are used to calculate the fluid response of coupled systems. The 9/3 element is a quadrilateral 9 node element, in which the velocities are interpolated at the nodes and the pressure is taken to be a linear function inside the element (3 unknowns per element) and discontinuous across elements, see Figure (4-1).

For a fluid flow problem, the solution obtained using the discretized equations (4.13) and (4.14) is good for low Reynolds (Re) number flows corresponding to a *laminar* solution. However, if the Re is increased beyond a certain critical value that depends on the system considered, oscillations in the solution appear due to the presence of the convective terms $(\mathbf{v} - \hat{\mathbf{v}}) \cdot \nabla \mathbf{v}$ (here the Re number is based on the relative velocity $\mathbf{v}_r = \mathbf{v} - \hat{\mathbf{v}}$). To avoid oscillations, *upwinding* is introduced into the equations. Using upwinding, artificial diffusivity is introduced into the equations to stabilize the convective term, ideally without degrading the accuracy of the solution (see for example [5], [2], [13]). In this work, the following upwinding terms, proposed by Hendriana and Bathe [14], are used

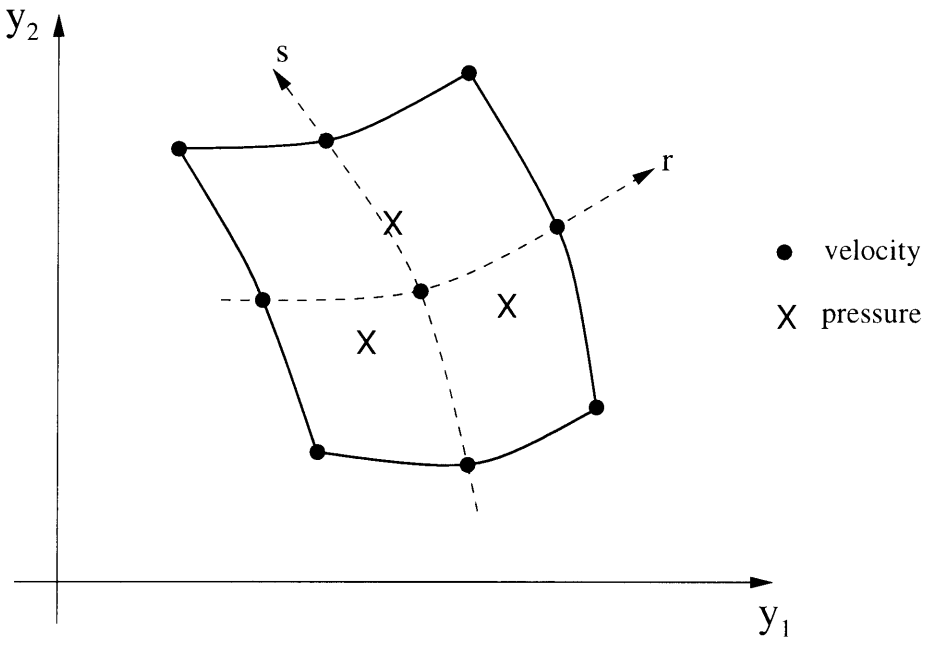

Figure 4-1: 9/3 element.

$$\sum_m \int_{\hat{V}^{(m)}} \frac{\partial^2 \bar{v}_i}{\partial y_j^2} \, \tau_j \, |v_j - \hat{v}_j| \, \frac{\partial^2 v_i}{\partial y_j^2} \, d\hat{V}^{(m)} \tag{4.16}$$

and

$$\tau_j = \frac{1}{9}\left[\left(\frac{\partial y_j}{\partial r}\right)^2 + \left(\frac{\partial y_j}{\partial s}\right)^2\right]^{3/2} \tag{4.17}$$

where $\hat{V}^{(m)}$ is the m^{th} element surface (2D), y_i are the coordinates of the body in a fixed Cartesian coordinate, and r, s are the isoparametric coordinates of the element (see Figure 4-1).

Note that a convective term is also present in the continuity equation, however, the term is divided by κ, which is usually a very large constant ($\sim 10^9$ Pa for water, for example), and therefore an upwinding term will not be necessary in the continuity equations.

The dynamic equations of the fluid flow, including the upwinding term can be represented as

$$^{t+\Delta t}\mathbf{W} \;=\; ^{t+\Delta t}\mathbf{W}_{NS} + \; ^{t+\Delta t}\mathbf{W}_{UP} \;=\; ^{t+\Delta t}\mathbf{R}_f \tag{4.18}$$

where ${}^{t+\Delta t}\mathbf{W}_{NS}$ and ${}^{t+\Delta t}\mathbf{W}_{UP}$ represent the terms from the standard Galerkin procedure and upwinding respectively, and ${}^{t+\Delta t}\mathbf{R}_f$ is the known load vector obtained from the boundary conditions.

Since equations (4.18) are nonlinear, an accurate solution is obtained by linearizing the equations and iterating at each time step (Newton-Raphson procedure).

Using a Taylor series expansion of (4.18) in time

$$ {}^{t+\Delta t}\mathbf{W} \simeq {}^{t}\mathbf{W} + {}^{t}\mathbf{W}^{*}\,\Delta t \tag{4.19} $$

and equation (4.18) can be expressed as

$$ {}^{t}\mathbf{W}^{*}\,\Delta t \simeq {}^{t+\Delta t}\mathbf{R}_f - {}^{t}\mathbf{W} \tag{4.20} $$

The details of the linearization process for a viscous fluid flow modeled using the ALE form of the Navier-Stokes equations, together with the final linearized matrices obtained can be found in [35].

The resulting linearized finite element equations can be expressed in matrix form as

$$ \begin{pmatrix} \mathbf{M}_{vv} & \mathbf{0} & \hat{\mathbf{M}}_v \\ \mathbf{0} & \mathbf{M}_{pp} & \hat{\mathbf{M}}_p \end{pmatrix} \begin{pmatrix} \dot{\mathbf{v}} \\ \dot{\mathbf{p}} \\ \hat{\mathbf{v}} \end{pmatrix} + \begin{pmatrix} \mathbf{K}_{vv} & \mathbf{K}_{vp} & \hat{\mathbf{K}}_v \\ \mathbf{K}_{pv} & \mathbf{K}_{pp} & \hat{\mathbf{K}}_p \end{pmatrix} \begin{pmatrix} \mathbf{v} \\ \mathbf{p} \\ \hat{\mathbf{u}} \end{pmatrix} = \begin{pmatrix} \mathbf{R}_f \\ \mathbf{0} \end{pmatrix} - \begin{pmatrix} \mathbf{F}_v \\ \mathbf{F}_p \end{pmatrix} \tag{4.21} $$

where the individual matrices are obtained from the expressions of ${}^{t}\mathbf{W}^{*}_{NS}$ and ${}^{t}\mathbf{W}^{*}_{UP}$; $\mathbf{v}$, $\mathbf{p}$, $\hat{\mathbf{u}}$, $\hat{\mathbf{v}}$, are the *increments* of velocity, pressure, mesh displacement and mesh velocity with respect to the last iteration; $\mathbf{R}_f$ is the discretized load vector, and $\mathbf{F}_v$, $\mathbf{F}_p$ contain terms from the linearization process. Because the mesh displacements and velocities inside the fluid domain are arbitrary, an algorithm must be provided to calculate them from the displacements and velocities of the fluid-structure interface and any other moving boundary.

4.3 Fluid flow-structural interaction problems

Consider a system composed of fluid and solid parts as shown in figure (4-2). We are interested in solving for the response of such a system. The first step is to choose an appropriate mathematical model to describe the behavior of the fluid and the structure. The next step is to couple the fluid and structural equations to obtain the response of the system.

In what follows, the coupling procedure employed to solve fluid-structure interaction problems in this thesis is presented [36]. The fluid flow is assumed to be modeled by the (almost) incompressible Navier-Stokes equations of motion (using the ALE formulation).

In the analysis considered here, the same layers of elements (number and type) are used along the interface in the discretization of the fluid and structural domains. Hence, the force equilibrium conditions at the fluid flow-structural interface are directly satisfied through the element assemblage process. However, the compatibility conditions at the fluid flow-structural interface must be enforced since the fluid flow and structural variables are velocities and displacements, respectively.

It is convenient to solve for the problem natural variables, displacements for structures and velocities for fluids, even in a fluid-structure interaction problem where the fluid is modeled using the Navier-Stokes equations. An advantage is that the same algorithm can be employed for both transient and steady state analysis. Furthermore, the functions describing the value of the natural variables in time are smoother than their time derivatives, and therefore convergence of the solution is easier to obtain.

At the fluid flow-structural interface the particles that correspond to the fluid and solid parts move together, i.e. they have the same displacements, velocities and accelerations. Therefore, in the ALE formulation the nodes at the interface should correspond to *Lagrangian nodes*. Assuming that no slip at the nodes of the fluid flow-structural interface is allowed, the *displacements* can be solved for *at the interface*, and these displacements can be used to calculate the velocities at the interface (and hence the velocities of the fluid particles at the interface).

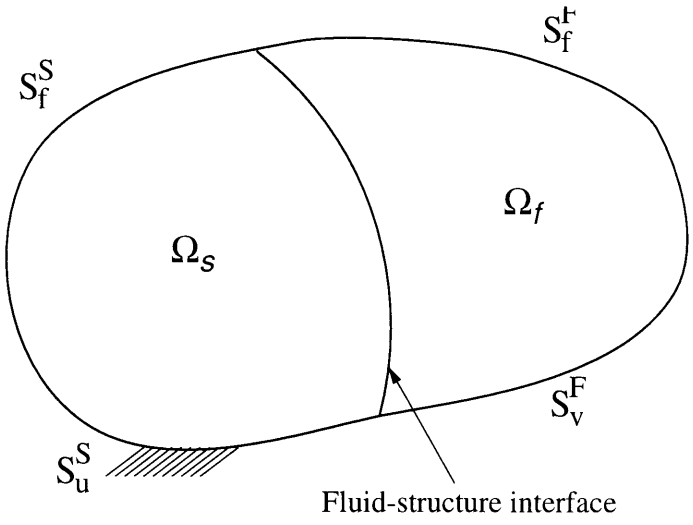

Figure 4-2: General fluid-structure interaction problem.

Since mesh displacements and velocities are calculated at the fluid-structure interface but can be arbitrarily specified otherwise, we can further assume that they are a linear function of fluid-structure interface displacements (and of the displacements of any other moving boundary or free surface),

$$\hat{\mathbf{u}} = \mathcal{L}(\mathbf{u}^I) \tag{4.22}$$

$$\hat{\mathbf{v}} = \mathcal{L}(\mathbf{v}^I) \tag{4.23}$$

where $\hat{\mathbf{u}}$ and $\hat{\mathbf{v}}$ are the mesh displacements and velocities respectively, $\mathbf{u}^I$ and $\mathbf{v}^I$ are the values of the displacements and velocities at the interface and $\mathcal{L}$ is a linear operator. These interpolations, although not general, allow the solution of the example problems to be presented in this work. In more general cases, it can be necessary to allow the mesh nodes to slip along the interface in order to preserve mesh regularity, and as a consequence, the above equations are no longer valid and an additional equation governing the slip movement of the mesh at the interface must be provided. In what follows, it is assumed that structural displacements coincide with nodal mesh displacements at the interface.

The *linearized* finite element matrix equations for the fluid, without including

pressure terms explicitly (they are assumed to be contained in the variable vector $\mathbf{v}$) and separating the degrees of freedom corresponding to the interface and "interior" nodes are,

$$\begin{pmatrix} \mathbf{M}_v^{II} & \mathbf{M}_v^{IF} \\ \mathbf{M}_v^{FI} & \mathbf{M}_v^{FF} \end{pmatrix} \begin{pmatrix} \dot{\mathbf{v}}^I \\ \dot{\mathbf{v}}^F \end{pmatrix} + \begin{pmatrix} \mathbf{K}_v^{II} + \hat{\mathbf{M}}_v^I \mathcal{L} & \mathbf{K}_v^{IF} \\ \mathbf{K}_v^{FI} + \hat{\mathbf{M}}_v^F \mathcal{L} & \mathbf{K}_v^{FF} \end{pmatrix} \begin{pmatrix} \mathbf{v}^I \\ \mathbf{v}^F \end{pmatrix} + \begin{pmatrix} \hat{\mathbf{K}}_v^I \mathcal{L} & \mathbf{0} \\ \hat{\mathbf{K}}_v^F \mathcal{L} & \mathbf{0} \end{pmatrix} \begin{pmatrix} \hat{\mathbf{u}}^I \\ \hat{\mathbf{u}}^F \end{pmatrix} = \begin{pmatrix} \mathbf{R}_f^I \\ \mathbf{R}_f^F \end{pmatrix} - \begin{pmatrix} \mathbf{F}_f^I \\ \mathbf{F}_f \end{pmatrix} \tag{4.24}$$

where the superscripts I and F refer to interface and interior fluid nodes respectively, $\mathbf{M}_v$ and $\mathbf{K}_v$ are coefficient matrices of the linearized fluid equations; $\hat{\mathbf{M}}_v$ and $\hat{\mathbf{K}}_v$ are linearized coefficient matrices from the ALE terms, $\mathbf{v}$ is the vector of velocity increments corresponding to the fluid flow, $\hat{\mathbf{u}}$ is the vector of mesh displacement increments, $\mathbf{R}_f$ is the load vector corresponding to the fluid without including body forces [1] and $\mathbf{F}_f$ comes from the constant terms of the linearization and contains also fluid body forces effects.

In what follows, for simplicity of notation, the linear operator $\mathcal{L}$ is omitted (it is assumed to be contained in the matrices $\hat{\mathbf{M}}_v$ and $\hat{\mathbf{K}}_v$).

The finite element matrix equations corresponding to the *linearized* behavior of a general (nonlinear) structure are (neglecting damping effects),

$$\begin{pmatrix} \mathbf{M}_u^{SS} & \mathbf{M}_u^{SI} \\ \mathbf{M}_u^{IS} & \mathbf{M}_u^{II} \end{pmatrix} \begin{pmatrix} \ddot{\mathbf{u}}^S \\ \ddot{\mathbf{u}}^I \end{pmatrix} + \begin{pmatrix} \mathbf{K}_u^{SS} & \mathbf{K}_u^{SI} \\ \mathbf{K}_u^{IS} & \mathbf{K}_u^{II} \end{pmatrix} \begin{pmatrix} \mathbf{u}^S \\ \mathbf{u}^I \end{pmatrix} = \begin{pmatrix} \mathbf{R}_s^S \\ \mathbf{R}_s^I \end{pmatrix} - \begin{pmatrix} \mathbf{F}_s^S \\ \mathbf{F}_s^I \end{pmatrix} \tag{4.25}$$

where the superscripts I and S refer to interface and interior structural nodes respectively, $\mathbf{M}_u$ and $\mathbf{K}_u$ are the mass and stiffness matrices corresponding to the structure, $\mathbf{u}$ is the vector of displacement increments, $\mathbf{R}_s$ is the structure load vector without including body forces [2] and $\mathbf{F}_s$ is obtained from the linearization process and body forces applied to the structure.

[1] Note that $\mathbf{R}_f$ is different from the $\mathbf{R}_f$ of equation (4.21), which includes body forces.

[2] Here $\mathbf{R}_s$ is different from the one in equation (4.6), which contains body forces effects.

Assuming that no slip of nodes is allowed at the fluid-structure interface, $\mathbf{v}^I = \dot{\mathbf{u}}^I$ and $\dot{\mathbf{v}}^I = \ddot{\mathbf{u}}^I$ (continuity condition) [3] and $\mathbf{R}_s^I + \mathbf{R}_f^I = \mathbf{0}$ (compatibility condition). Then, the *linearized* coupled fluid flow-structural equations can be expressed as

$$\mathbf{A}\ddot{\mathbf{U}} + \mathbf{B}\dot{\mathbf{U}} + \mathbf{C}\mathbf{U} = \mathbf{G} \tag{4.26}$$

where

$$\mathbf{A} = \begin{pmatrix} \mathbf{M}_u^{SS} & \mathbf{M}_u^{SI} & \mathbf{0} \\ \mathbf{M}_u^{IS} & \mathbf{M}_u^{II} + \mathbf{M}_v^{II} & \mathbf{M}_v^{IF} \\ \mathbf{0} & \mathbf{M}_v^{FI} & \mathbf{M}_v^{FF} \end{pmatrix} \tag{4.27}$$

$$\mathbf{B} = \begin{pmatrix} \mathbf{0} & \mathbf{0} & \mathbf{0} \\ \mathbf{0} & \mathbf{K}_v^{II} + \hat{\mathbf{M}}_v^I & \mathbf{K}_v^{IF} \\ \mathbf{0} & \mathbf{K}_v^{FI} + \hat{\mathbf{M}}_v^F & \mathbf{K}_v^{FF} \end{pmatrix} \tag{4.28}$$

$$\mathbf{C} = \begin{pmatrix} \mathbf{K}_u^{SS} & \mathbf{K}_u^{SI} & \mathbf{0} \\ \mathbf{K}_u^{IS} & \mathbf{K}_u^{II} + \hat{\mathbf{K}}_v^I & \mathbf{0} \\ \mathbf{0} & \hat{\mathbf{K}}_v^F & \mathbf{0} \end{pmatrix} \tag{4.29}$$

$$\mathbf{G} = \begin{pmatrix} \mathbf{R}_s^S - \mathbf{F}_s^S \\ -\mathbf{F}_f^I - \mathbf{F}_s^I \\ \mathbf{R}_f^F - \mathbf{F}_f^F \end{pmatrix} \tag{4.30}$$

and

$$\mathbf{u} = \begin{pmatrix} \mathbf{u}^S & \mathbf{u}^I & \mathbf{u}^F \end{pmatrix}^T \tag{4.31}$$

here $\mathbf{u}^F$ are the displacement increments of the interior fluid particles, which are not calculated (see matrix $\mathbf{C}$), but instead, the fluid velocity increments are calculated (see matrix $\mathbf{B}$).

Solving for displacements at the interface, the coupling between fluid and structure becomes easy to perform.

[3] Note however that equation $\dot{\mathbf{v}}^I = \ddot{\mathbf{u}}^I$ is usually not satisfied, since different time integration schemes are used for the fluid and structure.

Consider first the steady state case,

$$\ddot{\mathbf{u}}^S = \ddot{\mathbf{u}}^I = \ddot{\mathbf{u}}^F = \mathbf{0} \tag{4.32}$$

and

$$\dot{\mathbf{u}}^S = \dot{\mathbf{u}}^I = \mathbf{0} \tag{4.33}$$

Then, the steady state coupled fluid flow-structural equation (4.26) become,

$$\begin{pmatrix} \mathbf{K}_u^{SS} & \mathbf{K}_u^{SI} & \mathbf{0} \\ \mathbf{K}_u^{IS} & \mathbf{K}_u^{II}+\hat{\mathbf{K}}_v^I & \mathbf{K}_v^{IF} \\ \mathbf{0} & \hat{\mathbf{K}}_v^F & \mathbf{K}_v^{FF} \end{pmatrix} \begin{pmatrix} \mathbf{u}^S \\ \mathbf{u}^I \\ \mathbf{v}^F \end{pmatrix} = \begin{pmatrix} \mathbf{R}_s^S - \mathbf{F}_s^S \\ -\mathbf{F}_f^I - \mathbf{F}_s^I \\ \mathbf{R}_f^F - \mathbf{F}_f^F \end{pmatrix} \tag{4.34}$$

where $\mathbf{v}^F$ is the vector of internal fluid velocity increments.

To solve for the transient fully coupled fluid flow-structural interaction response, time integration schemes need to be chosen. In this work, implicit time integration is used, and hence the time discretization can be written as follows (using a linear multistep method)

- Fluid (first order differential equation in time)

  The time integration scheme has the form:

$$^{t+\Delta t}\dot{v} = \alpha\ ^{t+\Delta t}v + f\ (\ ^{t}v, ^{t}\dot{v}, ...) \tag{4.35}$$

  where α is a constant that depends on the specific time integration scheme employed and f is a linear function of the known velocities and accelerations at times t, $t - \Delta t$, $t - 2\Delta t$, ... With the equilibrium equations to be satisfied at time $t + \Delta t$ (for an implicit method), the linearized fluid flow equations can be written as

$$\mathbf{M}_v\ ^{t+\Delta t}\dot{\mathbf{v}} + \mathbf{K}_v\ ^{t+\Delta t}\mathbf{v} = \ ^{t+\Delta t}\tilde{\mathbf{R}}_f \tag{4.36}$$

  Solving for $^{t+\Delta t}\mathbf{v}$ gives

$$(\alpha\ \mathbf{M}_v + \ \mathbf{K}_v)\ {}^{t+\Delta t}\mathbf{v} = {}^{t+\Delta t}\tilde{\mathbf{R}}_f - \mathbf{M}_v\ \mathbf{f}\ (\ {}^{t}\mathbf{v}, {}^{t}\dot{\mathbf{v}}, ...) \tag{4.37}$$

where ${}^{t+\Delta t}\tilde{\mathbf{R}}_f$ contains the load vector and the constant terms of the linearization.

- Structure (second order differential equation in time)

  The time integration scheme has the form:

$${}^{t+\Delta t}\ddot{u} = \beta\ {}^{t+\Delta t}u + g\ ({}^{t}u, {}^{t}\dot{u}, {}^{t}\ddot{u}, ...) \tag{4.38}$$

$${}^{t+\Delta t}\dot{u} = \gamma\ {}^{t+\Delta t}u + h\ ({}^{t}u, {}^{t}\dot{u}, {}^{t}\ddot{u}, ...) \tag{4.39}$$

  where β and γ are constants that depend on the actual integration time scheme employed and g and h are linear functions of the known displacements, velocities and accelerations at time t, $t - \Delta t$, $t - 2\Delta t$, ... Satisfying the equilibrium equations at time $t + \Delta t$ gives

$$\mathbf{M}_u\ {}^{t+\Delta t}\ddot{\mathbf{u}} + \mathbf{K}_u\ {}^{t+\Delta t}\mathbf{u} = {}^{t+\Delta t}\tilde{\mathbf{R}}_s \tag{4.40}$$

  Solving for ${}^{t+\Delta t}\mathbf{u}$ results in

$$(\beta\ \mathbf{M}_u + \mathbf{K}_u)\ \ {}^{t+\Delta t}\mathbf{u} = \ {}^{t+\Delta t}\tilde{\mathbf{R}}_s - \mathbf{M}_u\ \mathbf{g}\ ({}^{t}\mathbf{u}, {}^{t}\dot{\mathbf{u}}, {}^{t}\ddot{\mathbf{u}}, ...) \tag{4.41}$$

  where ${}^{t+\Delta t}\tilde{\mathbf{R}}_s$ contains known terms.

- Fluid flow-structural interface

  The time integration scheme has the form:

$${}^{t+\Delta t}v^I = \gamma\ {}^{t+\Delta t}u^I + h\ ({}^{t}u^I, {}^{t}v^I, {}^{t}\dot{v}^I, ...) \tag{4.42}$$

  Note that here the same scheme is used as for the time integration of the displacements of the structure, see equation (4.39).

Introducing equation (4.42) into equation (4.37) we obtain

$$\begin{pmatrix} \gamma(\alpha\mathbf{M}_v^{II} + \mathbf{K}_v^{II}) & \alpha\mathbf{M}_v^{IF} + \mathbf{K}_v^{IF} \\ \gamma(\alpha\mathbf{M}_v^{FI} + \mathbf{K}_v^{FI}) & \alpha\mathbf{M}_v^{FF} + \mathbf{K}_v^{FF} \end{pmatrix} \begin{pmatrix} \mathbf{u}^I \\ \mathbf{v}^F \end{pmatrix} = \begin{pmatrix} \check{\mathbf{R}}_f^I \\ \check{\mathbf{R}}_f^F \end{pmatrix} \tag{4.43}$$

where the load vector $\check{\mathbf{R}}_f$ contain the known terms of the linearization and time integration. The contributions of the mesh movement to the fluid coefficient matrix are not shown explicitly [4].

Note here that by using equations (4.35) and (4.42) for the interface degrees of freedom, the compatibility condition $\ddot{\mathbf{u}}^I = \dot{\mathbf{v}}^I$ is not satisfied. This condition can however be relaxed provided that $\dot{\mathbf{u}}^I = \mathbf{v}^I$ and the obtained system of fluid-structure equations results in an unconditionally stable scheme in time. This issue is investigated in [36] [35].

The fluid flow and structural equations can now be coupled using equations (4.41) and (4.43), and the linearized fully coupled incremental fluid flow-structural interaction equation becomes

$$\begin{pmatrix} \bar{\mathbf{K}}_u^{SS} & \bar{\mathbf{K}}_u^{SI} & \mathbf{0} \\ \bar{\mathbf{K}}_u^{IS} & \bar{\mathbf{K}}_u^{II} + \bar{\mathbf{K}}_v^{II} & \bar{\mathbf{K}}_v^{IF} \\ \mathbf{0} & \bar{\mathbf{K}}_v^{FI} & \bar{\mathbf{K}}_v^{FF} \end{pmatrix} \begin{pmatrix} \mathbf{u}^S \\ \mathbf{u}^I \\ \mathbf{v}^F \end{pmatrix} = \begin{pmatrix} \check{\mathbf{R}}_s^S \\ \check{\mathbf{R}}^I \\ \check{\mathbf{R}}_f^F \end{pmatrix} \tag{4.44}$$

where from equation (4.41)

$$\begin{aligned} \bar{\mathbf{K}}_u^{SS} &= \beta\mathbf{M}_u^{SS} + \mathbf{K}_u^{SS} \\ \bar{\mathbf{K}}_u^{SI} &= \beta\mathbf{M}_u^{SI} + \mathbf{K}_u^{SI} \\ \bar{\mathbf{K}}_u^{IS} &= \beta\mathbf{M}_u^{IS} + \mathbf{K}_u^{IS} \\ \bar{\mathbf{K}}_u^{II} &= \beta\mathbf{M}_u^{II} + \mathbf{K}_u^{II} \end{aligned} \tag{4.45}$$

and from equation (4.43)

[4] Alternatively, Lagrange multipliers could have been used to enforced the satisfaction of the continuity condition at the fluid-structure interface, but in such a case the unknowns to solve for increase.

$$\begin{aligned}
\bar{\mathbf{K}}_v^{II} &= \gamma(\alpha \mathbf{M}_v^{II} + \mathbf{K}_v^{II}) \\
\bar{\mathbf{K}}_v^{IF} &= \alpha \mathbf{M}_v^{IF} + \mathbf{K}_v^{IF} \\
\bar{\mathbf{K}}_v^{FI} &= \gamma(\alpha \mathbf{M}_v^{FI} + \mathbf{K}_v^{FI}) \\
\bar{\mathbf{K}}_v^{FF} &= \alpha \mathbf{M}_v^{FF} + \mathbf{K}_v^{FF}
\end{aligned} \tag{4.46}$$

The variables corresponding to the fluid and interface were defined above; $\check{\mathbf{R}}_s^S$ corresponds to the load vector of the internal structural degrees of freedom (including the known terms).

Equation (4.44) contains the coupling procedure proposed in [36], for fluid flows interacting with structures.

The solution of coupled problems can be obtained by employing one of two main approaches,

- *Simultaneous* or *direct solution*: the equations are coupled and solved together;
- *Partitioned* or *iterative solution*: the system is divided into subsystems (corresponding to the fluid and structure domains), and each subsystem is solved separately. "Boundary conditions" at the fluid-structure interface act as coupling terms between the two subsystems.

The two main approaches that can be used to solve equation (4.44) are discussed in [35] and references therein. In this work, we used a simultaneous (also refer to as monolithic or direct) solution procedure with *condensation* of structural degrees of freedom [36] to solve the problem of fluid flows interacting with structures presented.

This approach is more efficient than the partitioned procedure in cases in which the coupling between fluid and structure is strong, resulting in a large deformation of the structure, as will be the case in the examples analyzed in Chapter 6.

Note that by using the Navier-Stokes equations of motion to model the fluid flow, a non-symmetric coefficient matrix results when the problem is discretized using finite element methods. This significantly increases the amount of computations to be performed at each time step as compared with the calculation of a system with the same number of degrees of freedom but with a symmetric coefficient matrix. When the

fluid and structural equations are coupled, the whole fluid-structure coefficient matrix is non-symmetric, and has to be treated as such in the calculations, although the structural portion of it is symmetric. By using condensation of the structural degrees of freedom, in equation (4.44), advantage is taken of the symmetry of the structural equations, and this results in a faster algorithm. In addition, by using condensation of the structural degrees of freedom, the equations are not solved all together and larger problems can be solved without being concerned about the computer capacity. A more detailed description of the coupling and condensation procedures used in this work can be found in [36] [35].

Chapter 5

Lyapunov characteristic exponents of continuous systems

Small motions of a solid (or fluid-structure interaction) problem about a certain state can be analyzed using the linear undamped natural modes of the problem. In this case, the system displacements can be written as

$$\mathbf{w}(\mathbf{r},t) = \sum_{p=1}^{\infty} a_p(t)\,\boldsymbol{\vartheta}_p(\mathbf{r}) \tag{5.1}$$

where $\mathbf{w}(\mathbf{r},t)$ represents the displacement field of the solid medium, $\mathbf{r}$ is the position vector of the solid particles, t the time, and $\boldsymbol{\vartheta}_p$ are the linear undamped natural modes of the system. Therefore, an infinite number of modes contribute to the response of the system. Usually, however, only a few modes are excited, and it is reasonable to approximate the response of the system by a finite series. In such a case, using the orthogonality property of the natural modes $\boldsymbol{\vartheta}_p$, a structural continuous problem can be reduced to a finite number of coupled [1] second order ordinary differential equations in time, in which the unknowns are the amplitudes of oscillation of each mode $a_p(t)$.

The preceding procedure, called the modal decomposition technique, can be used to assess the conditions under which one or more of the modal responses may become

[1] For a nonlinear problem in which nonlinearities are carried over through the decomposition, a coupled system of equations is obtained. If nonlinearities are neglected, then the linearized system is decomposed into a system of uncoupled equations.

unstable. This is done by applying a perturbation to the modes and analyzing whether those perturbations decay/grow in time. Such studies were carried out analytically (taking only a few modes) for some structure and fluid-structure interaction problems, see for example [6] [16] [31].

However, it is usually difficult to assess how many modes to include and the procedure becomes more complex as more modes are included in the series representation (5.1). Furthermore, the modal decomposition technique is not applicable in the case in which strong nonlinearities have to be considered, since in such a case the linearized modes of the system cannot accurately represent its dynamic behavior. Alternatively, nonlinear modes could be used, but it is very difficult to obtain them.

In essence, the finite element discretization of a continuous medium is just a way of cutting the infinite series (5.1) into a finite one, by projecting the natural modes of the system into the finite element space in which it is discretized. Therefore, using finite element methods, a perturbation can be applied to all of the (discretized) modes at the same time, and the stability of their motion can thus be studied. Furthermore, when the system contains strong nonlinearities, the finite element procedure can still be employed. At each time step linearized modes can be obtained that describe small motions of the body about the system current state. Those modes, however, change as a function of time as the system moves, and this change is taken into account by the finite element discretization.

The concept of Lyapunov exponents, described before for discrete systems, can then be employed in the analysis of continuous systems. In fact, in this case, the stability and divergence/convergence of trajectories can be thought of as the one corresponding to the nonlinear modes representing the system response. The perturbation of modes that are stable would decay in a relatively small number of time steps, whereas the unstable modes would contribute to the growth of the LCE approximations, k_n. Of course this calculation can be done, using a finite element discretization (or other discretization) of the continuous equations of motion, without explicitly finding the system modes.

Some assumptions need to be made in what follows for the development of the

procedure to calculate the LCE of continuous systems.

It is assumed that the numerical discretization chosen in space and time accurately captures the nature of the system dynamic behavior. For the time discretization, this means that a stable time integration scheme has been chosen (usually and unconditional stable scheme is preferred). In other words, the system response will not grow without bounds (because of the time integration scheme) if the mathematical model of the system does not predict such grow. In addition, the time step chosen should be small enough to capture the essence of the behavior. For the space discretization, it is not only necessary to make sure that the number of elements employed in the discretization is enough to accurately captured the body behavior, but also that the appropriate elements are used. For example, in the two-dimensional analysis of almost incompressible media in which a plane strain analysis is assumed, a mixed formulation that satisfies the inf-sup condition must be used. For a detailed description on how to choose appropriate discretizations in space and time for fluid flows and structures see [2].

Another assumption is regarding the solution of the mathematical model of the continuous systems employed. In Chapter 2 we define the Lyapunov characteristic exponent of the response of a system defined in a differential manifold. Therefore, we assumed that given an initial condition to the dynamic system of equations, a unique reference solution exists. This assumption is also made for the dynamic solution of continuous systems. For fluid flows modeled using the Navier-Stokes equations, existence and uniqueness theorems can be found in [17] [34] among others. For structural equations, some theorems can be found in [12] and references therein.

Given this assumptions, from now on, when we refer to a stable or unstable dynamic behavior, we refer to the stability of the motion (assuming that the finite element discretization is "stable").

In Chapter 2, the approach presented by Benettin et al [4] [3], for calculating the LCE of non-dimensional discrete systems of coupled first order differential equations in time, was briefly described. This procedure is used as a basis to develop a numerical technique to evaluate the LCE of solid and fluid-structure interaction continua

discretized using finite element methods. The proposed method is discussed below.

Before discussing the implementation of the procedure, it is worth to mention here that the approach proposed by Benettin is not directly applicable to finite element discretized continuous media. The main reason is that different time scales are present in the system of equations obtained by a finite element discretization and usually the smallest scales, which correspond to high-frequency modes, are not accurately captured by the time integration scheme employed.

5.1 Structural problems

Let us first consider the case of a structure/solid medium.

The displacements and velocities of the structural nodal degrees of freedom form the finite element discretized phase space of the problem in consideration (assuming that forcing terms and material properties are time independent, and therefore an autonomous system is considered [2]).

The finite element equations that represent the motion of the solid can be written as,

$$^{t}\mathbf{W} = ^{t}\mathbf{R}_s \tag{5.2}$$

where $^{t}\mathbf{W}$ is the vector of nodal point forces corresponding to the internal element stresses and inertial forces and $^{t}\mathbf{R}_s$ is the vector of discretized loads applied to the body at time t (see also Chapter 4).

If $\tilde{\mathbf{u}}$ corresponds to perturbations in the displacements, the linearized equations that describe the evolution of perturbations, neglecting dissipative terms, can be written as

$$\mathbf{M}_u \, \ddot{\tilde{\mathbf{u}}} + \mathbf{K}_u(\mathbf{u}) \, \tilde{\mathbf{u}} = \mathbf{0} \tag{5.3}$$

with initial conditions,

[2] If forcing terms or material properties are a function of time then a change of variables can be performed (as discussed in Chapter 2) and the time included in the system phase space.

$$\begin{aligned} \tilde{\mathbf{u}}(t_0^*) &= \tilde{\mathbf{u}}_0 \\ \dot{\tilde{\mathbf{u}}}(t_0^*) &= \dot{\tilde{\mathbf{u}}}_0 \end{aligned} \tag{5.4}$$

where $\mathbf{M}_u$ and $\mathbf{K}_u$ are the same matrices as in equation (4.6) but it is emphasized here that the tangent stiffness matrix $\mathbf{K}_u$ changes as a function of time with the body displacements $\mathbf{u}$, since nonlinear equations of motion are considered.

An important difference with the discrete system, equation (2.1), is that for a continuum model the perturbations must be compatible with the problem's boundary conditions at all times. Thus, the boundary conditions for the perturbations are specified as,

$$\begin{aligned} \tilde{\mathbf{u}} &= \mathbf{0} \quad \text{in } S_u^S \\ \tilde{\boldsymbol{\tau}}\,\mathbf{n}^S &= \mathbf{0} \quad \text{in } S_f^S \end{aligned} \tag{5.5}$$

where S_u^S and S_f^S are the parts of the boundary with prescribed displacements and tractions respectively, $\mathbf{n}^S$ is a unit outward normal vector to the structural boundary, and $\tilde{\boldsymbol{\tau}} = \boldsymbol{\tau}^S(\mathbf{u}+\tilde{\mathbf{u}}) - \boldsymbol{\tau}^S(\mathbf{u})$ is equal to the difference between the stress tensor of the perturbed problem, $\boldsymbol{\tau}^S(\mathbf{u}+\tilde{\mathbf{u}})$, and the stress tensor of the reference problem, $\boldsymbol{\tau}^S(\mathbf{u})$. These boundary conditions are already included in equation (5.3), but it is important that the initial perturbations of the system satisfy equations (5.5).

Equation (5.3) could be easily re-written in the form of equation (2.1) with $\mathbf{y}^T = (\tilde{\mathbf{u}}\ \dot{\tilde{\mathbf{u}}})$, where the superscript T indicates transpose. However, it is more convenient (from a numerical point of view) to solve directly the second order differential equations in time using, for instance, the Newmark method of time integration, see [2]. Otherwise, the number of equations to solve increases from N to $2\,N$, where N is the number of degrees of freedom for the problem considered, and this increase is computationally very expensive for large systems of equations, which are usually encountered in the finite element discretization of structures.

Note that the nonlinear equations of motion of the structure (5.2) must be solved in order to obtain the stiffness matrix $\mathbf{K}_u(\mathbf{u})$ necessary to calculate the linearized evolution of perturbations (the mass matrix $\mathbf{M}_u$ is independent of the state of the

system). Furthermore, since the structural equations of motion are discretized in time, the same time discretization can be used to calculate the evolution of perturbations, although this is not necessary (for example, we could use $\Delta t^* = 2\,\Delta t$, where Δt^* is the time step used for perturbations and Δt the time step used to discretize the equations of motion). The advantage of using the same time step is that exactly the same (left-hand) matrices are used in the calculation of the first iteration of the nonlinear problem (when using for instance the Newton-Raphson scheme) and in the calculation of the perturbation evolution at each time step. Then, the coefficient matrix obtained after discretizing the equations in time has to be factorized only once, and used for both the system response and perturbation calculation.

Recall from Chapter 2 that the one-dimensional LCE of a trajectory is defined as

$$\chi = \lim_{t\to\infty} \frac{1}{t} \ln\left[\frac{d(t)}{d(t_0^*)}\right] \tag{5.6}$$

where $d(t)$ is defined as $d(t) = \|\mathbf{y}(t)\|$, the norm of the perturbation vector. In addition, using a time discretization with time step Δt, such that $t_n = t_0^* + n\,\Delta t$, and assuming that $d(t_0^*) = d_0 = 1$, the norm of the perturbation vector can be expressed by $d(t_n) = d_n\, d_{n-1} \cdots d_1$. An approximation to the LCE, k_n, can then be calculated at each time step,

$$k_n = \frac{1}{t_n} \sum_{i=1}^{n} \ln d_i \tag{5.7}$$

such that the trajectory LCE can be calculated as

$$\chi = \lim_{n\to\infty,\Delta t\to 0} k_n \tag{5.8}$$

For a structural discretized problem, the relevant perturbed variables in phase space are the system nodal point displacements and velocities, and therefore the discretized phase space belongs to $\Re^{2N}$ (N is the number of degrees of freedom of the system considered). However, displacements and velocities have different units, and a non-dimensionalization must be performed before the calculation of the norm of the perturbation vector. We use a characteristic length L, and a characteristic velocity

V to nondimensionalize the perturbations [3],

$$d(t) = \sqrt{\frac{\|\tilde{\mathbf{u}}\|^2}{L^2} + \frac{\left\|\dot{\tilde{\mathbf{u}}}\right\|^2}{V^2}} \tag{5.9}$$

Let us assume, without loss of generality, that the initial perturbation (5.4) is such that $d_0 = 1$. Then, we can calculate the initial perturbed accelerations from equation (5.3), discretize the equation in time, and calculate the perturbed displacements and velocities, $\tilde{\mathbf{u}}_1^*$ and $\dot{\tilde{\mathbf{u}}}_1^*$, at time t_1.

When the system behavior is chaotic, the norm of the perturbation (5.9) grows as a function of time. Thus, if the perturbation vectors are not normalized after a certain number of time steps, overflow might occur. If the normalization process is carried out at each time step, then we have that the normalized perturbations at t_1 are

$$\hat{\mathbf{u}}_1 = \frac{\tilde{\mathbf{u}}_1^*}{d_1}; \quad \dot{\hat{\mathbf{u}}}_1 = \frac{\dot{\tilde{\mathbf{u}}}_1^*}{d_1} \tag{5.10}$$

where

$$d_1 = \sqrt{\frac{\|\tilde{\mathbf{u}}_1^*\|^2}{L^2} + \frac{\left\|\dot{\tilde{\mathbf{u}}}_1^*\right\|^2}{V^2}} \tag{5.11}$$

An approximation of the LCE can be calculated as $k_1 = t_1^{-1} \ln d_1$.

The same procedure is repeated for the successive time steps, ideally until a *flat* value of k_n as a function of time (t_n) is obtained, that is to say, until the value of k_n remains constant as n is further increased. This constant value of k_n should be the system LCE.

However, when using the described procedure for the calculation of the structural response LCE, the obtained values of k_n grow as a function of time, t_n, even when a

[3]Note that it might seem that an energy norm would also solve the normalization problem without the necessity of introducing a characteristic length and velocity. However, such norm is not appropriate for the calculation of the LCE since *conservative* systems, characterized by a constant energy, can become chaotic.

dynamically stable problem is considered. A more detailed analysis of the procedure is presented below to establish why the values of k_n grow.

A key point in the described procedure is the determination of the proper values of the problem characteristic length and velocity, L and V, to use in equation (5.11), or equation (5.9).

It seems natural to express the characteristic velocity in terms of some characteristic frequency of the system, $\hat{\omega}$, such that $V = \hat{\omega}\, L$. In such a case, it is evident from equation (5.9) that the characteristic length L plays only the role of a scaling constant. However, the determination of the correct value of the frequency $\hat{\omega}$ is fundamental in the evaluation of the system LCE. Alternatively, we could use $V = c$, the characteristic speed of propagation of waves in the solid medium (that is the characteristic velocity resulting from nondimensionalizing the continuum equations of motion). Since it is always possible to express $V = c = \hat{\omega} L$, $V = c$ can be considered as a special case of $V = \hat{\omega} L$.

To elucidate how to choose the correct value of $\hat{\omega}$ let us first consider a simple problem: a single degree of freedom (linear) harmonic oscillator (which cannot become chaotic or unstable),

$$\ddot{x} + \omega^2 x = 0 \tag{5.12}$$

with initial conditions

$$\begin{aligned} x(t_0) &= x_0 \\ \dot{x}(t_0) &= \dot{x}_0 \end{aligned} \tag{5.13}$$

where x represents the oscillator displacement and ω its frequency of oscillation.

Solutions of equation (5.12) are of the form,

$$x = A \sin(\omega\, t + \theta) \tag{5.14}$$

where A and θ are constants determined by initial conditions.

Similarly, the equation for the evolution of the perturbation, $\tilde{x}$, is

$$\ddot{\tilde{x}} + \omega^2 \tilde{x} = 0 \tag{5.15}$$

with initial conditions

$$\begin{aligned} \tilde{x}(t_0^*) &= \tilde{x}_0 \\ \dot{\tilde{x}}(t_0^*) &= \dot{\tilde{x}}_0 \end{aligned} \tag{5.16}$$

And its solution is of the form,

$$\tilde{x} = \tilde{A} \sin(\omega t + \tilde{\theta}) \tag{5.17}$$

where $\tilde{A}$ and $\tilde{\theta}$ are constants.

Let us calculate the LCE of the response of the harmonic oscillator. The perturbation vector is,

$$\mathbf{y} = \begin{bmatrix} \tilde{x} \\ \dot{\tilde{x}} \end{bmatrix} \tag{5.18}$$

and therefore,

$$d(t) = \sqrt{\frac{\tilde{x}^2}{L^2} + \frac{\dot{\tilde{x}}^2}{\omega^2 L^2}} = \frac{\tilde{A}}{L} = 1 \tag{5.19}$$

assuming that $d(t_0^*) = 1$. Then the response LCE can be calculated as,

$$\chi = \lim_{t \to \infty} \frac{1}{t} \ln d(t) = 0 \tag{5.20}$$

The obtained LCE is zero, which is the correct value of the LCE for this case (since the harmonic oscillator describes a regular oscillatory behavior, in which trajectories do not converge nor diverge from each other). Note that to calculate the norm of the perturbation, the system frequency was used for the velocity nondimensionalization (i.e. $\hat{\omega} = \omega$) in equation (5.9).

If instead of using the correct frequency of oscillation of the system, ω, another frequency $\hat{\omega}$ is used, the norm of the perturbation would be

$$d(t) = \frac{\tilde{A}}{L}\sqrt{\sin^2(\omega\, t + \tilde{\theta}) + \frac{\omega^2}{\hat{\omega}^2}\cos^2(\omega\, t + \tilde{\theta})} \tag{5.21}$$

Although in this case the norm $d(t)$ has an oscillatory behavior in time the limit of $t \to \infty$ of $1/t \ln d(t)$ is zero (except when $\omega/\hat{\omega} = 0$ since then the limit does not exist), which is the correct value of the LCE for this case.

Consider now the finite element discretized equations of a solid continuum medium. At each time step, the *linearized* system of equations that describe the evolution of perturbations (5.3) can be decoupled into N equations of the form of equation (5.15), the linearized system normal modes. It becomes evident that if the characteristic frequency $\hat{\omega}$, used to non-dimensionalize the velocity components, is relatively small (for instance we choose the first natural frequency of the system) then $\omega/\hat{\omega} >> 1$ for high-frequency modes and therefore the velocity contribution of the high-frequency modes becomes the dominant component of the norm. Considering expression (5.21), and the limiting value as time goes to infinity of the natural logarithm of the norm over time, this is not really a problem (at least analytically in the case of a linear system) since those contributions oscillate very fast and therefore in the calculation of the LCE the limiting value of zero is once again obtained. However, for a general nonlinear system it would be desirable to put a stronger weight on the modes that determine the behavior of the system (which are usually the low-frequency modes).

When solving a continuous problem using finite element methods, time is discretized in such a way that usually only low frequencies are accurately represented by the time step chosen (when using unconditionally stable time integration schemes). Thus, high-frequency modes are not properly discretized in time. This characteristic does not pose a difficulty for the computation of the system response, since usually the contribution of high-frequency modes can be neglected. Unfortunately, it is decisive in the perturbation norm calculation since the approximations to the LCE, k_n, are governed by the high frequency velocity terms.

Let us consider here the effect of the time discretization employed in the calculation of the square of the norm of the perturbation, d^2. As mentioned above, in a finite element discretization the fast response associated with high-frequency modes is not

in general captured by the time discretization. Consider then only one equation of the form (5.15) for the perturbation, i.e. the contribution of one mode of the finite element discretization of a *linear system* (which cannot be chaotic or unstable) to the norm of the perturbation.

Furthermore, assume that the chosen characteristic frequency is $\hat{\omega} = 1$, the characteristic length is $L = 1$, and the time step employed is $\Delta t = 0.3 \simeq \frac{2\pi}{20}$ (small enough to capture an oscillation with frequency $\omega = 1$).

Now, consider the numerical calculation of three cases, shown in figure 5-1, with different frequencies of oscillation ω of the harmonic oscillator,

- $\omega = 1$, figure 5-1a shows that in this case $d^2 = 1$ is obtained for every time step, which is the value of the norm expected for the linear problem considered.

- $\omega = 100$, figure 5-1b shows that the calculated value of d^2 is oscillatory, but nevertheless the amplitude of the oscillations remains constant as a function of time (or time step) and therefore in the limit of $t \to \infty$, $\frac{ln(d)}{t}$ is zero (numerically).

- $\omega = 5000$, in this case, shown in figure 5-1c the norm of the perturbation, as calculated using equation (5.9) grows as a function of the time step. Eventually, it is expected that the behavior would be as when $\omega = 100$ but this would only occur after a huge amount of time steps. The observed behavior is due to the time discretization considered, which cannot capture the fast oscillations of the equation, and *not* the physics of the problem.

In the case of a finite element discretization, the cumulative effect of the high-frequency modes makes the value of k_n grow as a function of time, even when the problem considered is stable, giving the wrong impression that the system response is unstable.

In this work we found that a solution to this problem is to use the *maximum frequency* of the discretized finite element model as the characteristic problem frequency, such that $\hat{\omega} = \omega_{\max}$, and the contribution to the perturbation norm of each mode i becomes,

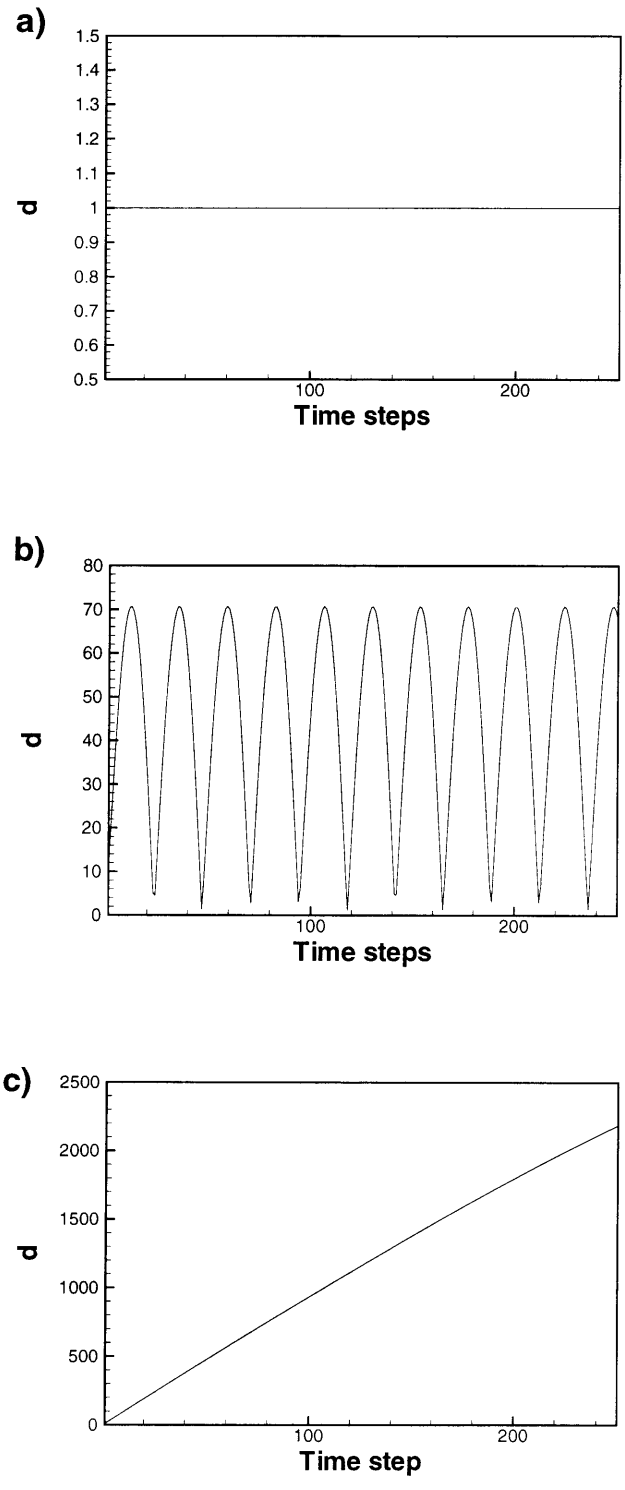

Figure 5-1: Numerical calculation of norm of the perturbation for the harmonic oscillator equation. The time step used in all three cases is $\Delta t = 0.3$. a) $\omega = 1$, b) $\omega = 100$, c) $\omega = 5000$.

$$\left(\frac{\tilde{A}_i}{L}\right)^2 \left[\sin^2(\omega_i\, t + \tilde{\theta}_i) + \frac{\omega_i^2}{\omega_{\max}^2}\cos^2(\omega_i\, t + \tilde{\theta}_i)\right] \tag{5.22}$$

Then, the high-frequency modes do not have such an important role. However, the contribution to the norm of perturbed velocity components of low-frequency modes becomes negligible, since $\omega_{\max}$ is usually a very large number. In fact, most of the velocity terms become negligible. Furthermore, it is very difficult to exactly calculate the maximum frequency of the finite element model, and therefore some approximation to it must be used. A simpler solution would be to *neglect* the velocity contributions in the calculation of the perturbation norm. Then, we assume that,

$$d(t) \simeq \sqrt{\sum_{i=1}^{N} \frac{\tilde{x}_i^2}{L^2}} \tag{5.23}$$

The natural question that then arises is: Would the *true* value of the LCE be obtained when using equation (5.23) given that the LCE measures exponential divergence of trajectories in the phase space (i.e. the space of discretized displacements *and* velocities)? To answer this fundamental question let us first go back to the simple case of the harmonic oscillator.

The norm of the perturbation vector of equation (5.15) resulting from applying equation (5.23) is

$$d = \sqrt{\frac{\tilde{x}^2}{L^2}} = \frac{\tilde{A}}{L}\left|\sin(\omega\, t + \tilde{\theta})\right| \geq 0 \tag{5.24}$$

Of course in this case, it could be a problem to numerically calculate the LCE using the given value of d when $d = 0$ since $\lim_{d\to 0} \ln(d) = -\infty$. This problem does not occur when considering many equations of the form of the harmonic oscillator, since it is almost impossible to have all the contributions equal to zero at the same time. However, the maximum value of the norm d corresponds indeed to the true value of the perturbation norm, i.e. $d = A/L$. In fact, the *average* value of the norm in time is constant, and thus a zero LCE is obtained in the asymptotic limit.

Even when more degrees of freedom are considered, d presents oscillations but the behavior of its local maximums contain information about the stability of the system.

Thus, when calculating the LCE of a solid continuous system discretized using finite element methods, the following equations should be used,

$$d(t) = \frac{\|\tilde{\mathbf{u}}\|}{L} \tag{5.25}$$

$$\chi = \limsup_{t\to\infty} \frac{1}{t} \ln[d(t)] \tag{5.26}$$

Furthermore, in the case of a solid medium, displacements and velocities are not independent, but related by a time derivative. Therefore, we expect that information would not be lost by considering only displacements in the calculation of the perturbation norm. Let us look to this problem in more detail.

Consider equation (5.3), and make the following change of variables,

$$\tilde{\mathbf{v}} = \dot{\tilde{\mathbf{u}}} \tag{5.27}$$

Then, expressing equation (5.3) as a system of first order differential equations in time,

$$\begin{bmatrix} \dot{\tilde{\mathbf{u}}} \\ \dot{\tilde{\mathbf{v}}} \end{bmatrix} = \begin{bmatrix} \mathbf{0} & \mathbf{I} \\ -\mathbf{M}_u^{-1}\mathbf{K}_u & \mathbf{0} \end{bmatrix} \begin{bmatrix} \tilde{\mathbf{u}} \\ \tilde{\mathbf{v}} \end{bmatrix} \tag{5.28}$$

or simply

$$\dot{\mathbf{y}} = \mathbf{A}\ \mathbf{y} \tag{5.29}$$

where the perturbation $\mathbf{y}^T = (\tilde{\mathbf{u}}\ \ \tilde{\mathbf{v}})$, and $\mathbf{I}$ is the identity matrix.

The solution of the equations that describe the evolution of perturbations (5.28) can be assumed to be (at each time step) of the form,

$$\mathbf{y} = e^{\lambda\ t}\tilde{\boldsymbol{\phi}} \tag{5.30}$$

Replacing equation (5.30) into (5.29), the following eigenvalue problem is obtained,

$$\lambda\tilde{\boldsymbol{\phi}} = \mathbf{A}\tilde{\boldsymbol{\phi}} \tag{5.31}$$

The dynamic stability of the problem can then be assessed by looking at the evolution of the eigenvalues λ as a function of time. Whenever the maximum real part of λ is less that zero, perturbations to the reference trajectory will decay with time. In contrast, a positive value of the real part of λ implies that perturbations grow as a function of time. Then by considering successive time steps, the average growth of perturbation can be computed.

In addition, the solution of the equations that describe the evolution of perturbations (5.3) can be assumed to be (at each time step) of the form,

$$\tilde{\mathbf{u}} = e^{i\ \omega\ t}\boldsymbol{\phi} \tag{5.32}$$

and as a consequence the velocity terms are

$$\dot{\tilde{\mathbf{u}}} = e^{i\ \omega\ t}\boldsymbol{\phi}' \tag{5.33}$$

Substituting equation (5.32) into (5.3), the following eigenvalue problem is obtained,

$$\omega^2\ \mathbf{M}_u\boldsymbol{\phi} = \mathbf{K}_u\boldsymbol{\phi} \tag{5.34}$$

Note that for the problems considered the matrix $\mathbf{K}_u$ can be indefinite.

It is evident that the two eigenvalue problems are equivalent (they describe exactly the same equations, in a different form), and therefore comparing equations (5.30) and (5.32) we have,

$$i\omega = \lambda \tag{5.35}$$

and

$$-i\omega = \bar{\lambda} \tag{5.36}$$

where $\bar{\lambda}$ is the complex conjugate of λ.

The growth or decay of perturbations will be captured considering only displacements or by considering displacements and velocities in the eigenvalue problem. Since

the velocities are related to the displacements by a time derivative, the growth of displacements will be passed to the velocities (and vice-versa), and as a consequence there is no real need to consider both variables to capture the nature of the system dynamic behavior (i.e. whether the response is stable or unstable).

Of course, the conclusions reached for a structural problem are no longer true in the case of a general system of first order ordinary differential equations, since the variables are no longer related to each other by a time derivative.

In summary, to calculate the successive approximations of the LCE, k_n, for each time step n, the following procedure is proposed:

- Given the (normalized) "initial" conditions $\hat{\mathbf{u}}_n$ and $\dot{\hat{\mathbf{u}}}_n$ at each time step, calculate the accelerations $\ddot{\hat{\mathbf{u}}}_n$ that satisfy equation (5.3).

- Discretize equation (5.3) in time, and solve for $\tilde{\mathbf{u}}^*_{n+1}$ and $\dot{\tilde{\mathbf{u}}}^*_{n+1}$, which are the nodal point displacements and velocities, for the time t_{n+1}, obtained from the linear equation (5.3).

- Obtain the norm of the perturbation as

$$d_{n+1} = \frac{\left\| \tilde{\mathbf{u}}^*_{n+1} \right\|}{L} \tag{5.37}$$

  where L is a characteristic length of the problem.

- Normalize the perturbation,

$$\hat{\mathbf{u}}_{n+1} = \frac{\tilde{\mathbf{u}}^*_{n+1}}{d_{n+1}}; \quad \dot{\hat{\mathbf{u}}}_{n+1} = \frac{\dot{\tilde{\mathbf{u}}}^*_{n+1}}{d_{n+1}} \tag{5.38}$$

- Calculate k_{n+1} and advance to the next time step,

$$k_{n+1} = \frac{1}{t_{n+1}} \sum_{i=1}^{n+1} \ln d_i \tag{5.39}$$

5.2 Fluid problems

The turbulent behavior of fluid flows is probably one of the better known examples of chaotic behavior, and yet it is not completely understood. It is extremely difficult to numerically calculate the behavior of turbulent fluid flows due to the small length scales characteristic of the eddy formation and the statistical space-time patterns of eddies [23]. In order to represent small length scales more and more elements have to be added to the analysis, which makes the calculation time unaffordable for most engineering problems. For this reason, different ways of approximately dealing with turbulent flows have been proposed, such as the $k-\varepsilon$ model. Such methods were designed to represent only the *average* behavior of the fluid flow and not to solve for the details of eddy patterns.

Let us consider the case of an (almost) incompressible fluid flow in the Eulerian formulation. The (complete) linearized equations for the perturbations are

$$\begin{bmatrix} \mathbf{M}_{vv} & \mathbf{0} \\ \mathbf{0} & \mathbf{M}_{pp} \end{bmatrix} \begin{bmatrix} \dot{\tilde{\mathbf{v}}} \\ \dot{\tilde{\mathbf{p}}} \end{bmatrix} + \begin{bmatrix} \mathbf{K}_{vv} & \mathbf{K}_{vp} \\ \mathbf{K}_{pv} & \mathbf{K}_{pp} \end{bmatrix} \begin{bmatrix} \tilde{\mathbf{v}} \\ \tilde{\mathbf{p}} \end{bmatrix} = \begin{bmatrix} \mathbf{0} \\ \mathbf{0} \end{bmatrix} \tag{5.40}$$

where $\mathbf{M}$ and $\mathbf{K}$ are the mass and tangent coefficient matrices for the fluid flow and $\tilde{\mathbf{v}}$ and $\tilde{\mathbf{p}}$ are the vectors of velocity and pressure perturbations. For an incompressible fluid, $\mathbf{M}_{pp} = \mathbf{0}$ and $\mathbf{K}_{pp} = \mathbf{0}$.

When the fluid flow is modeled using the Eulerian formulation of motion, the fluid velocities are calculated at certain fixed points in space and therefore instabilities in space (such as turbulence) will affect the value of the calculated k_n and LCE.

Equation (5.40) can be separated into two equations,

$$\begin{aligned} \mathbf{M}_{vv}\,\dot{\tilde{\mathbf{v}}} + \mathbf{K}_{vv}\,\tilde{\mathbf{v}} + \mathbf{K}_{vp}\,\tilde{\mathbf{p}} &= \mathbf{0} \\ \mathbf{M}_{pp}\,\dot{\tilde{\mathbf{p}}} + \mathbf{K}_{pv}\,\tilde{\mathbf{v}} + \mathbf{K}_{pp}\,\tilde{\mathbf{p}} &= \mathbf{0} \end{aligned} \tag{5.41}$$

where the first equation corresponds to the perturbed momentum equations and the second one to the continuity condition for the perturbation. It follows that perturbations in velocity and pressure are not completely arbitrary but are constrained by the continuity equation and boundary conditions of the perturbation. For example,

considering specifically the case of an incompressible fluid flow, the velocity perturbation must satisfy $\mathbf{K}_{pv}\tilde{\mathbf{v}} = \mathbf{0}$ at all times. The boundary conditions, on the other hand, prevent the pressure perturbation from growing arbitrarily.

The procedure to calculate the successive approximations to the LCE, k_n, would be analogous to the one described for the structural equations, taking $\mathbf{y}^T = (\tilde{\mathbf{v}} \quad \tilde{\mathbf{p}})$, and using an appropriate non-dimensionalization in the calculation of the norm of the perturbation $d = \|\mathbf{y}\|$. However, good approximations of the chaotic behavior would have to be used in order to calculate the LCE (average methods would not be useful when the interest lies in capturing the fluid chaotic behavior).

When the fluid flow is modeled using the ALE formulation of motion, i.e. when the fluid domain changes as a function of time, the situation is more complex. Some of the difficulties are mentioned below.

Since the fluid mesh is moving and the fluid flow velocities are calculated at the mesh nodal points, the obtained velocities do not correspond to fixed points in space nor can they be associated with specific fluid particles. A similar situation occurs with the pressure degrees of freedom. The immediate consequence is that if the mesh points are moving arbitrarily, spurious growth of the perturbations may be included in k_n.

Another difficulty is that in addition to perturbations in velocity and pressure, perturbations in the displacement of certain moving boundaries (such as free surfaces and fluid-structure interfaces) must be considered.

We have not investigated the calculation of the LCE of fluid flows further in this work and concentrated on the calculation of the LCE for structures and fluid-structure interaction systems in which the behavior of the structure is of primary interest (and for which the Re number of the fluid flow is low). Usually, the turbulent behavior of a fluid flow is not avoided in engineering applications and it is actually desired in many situations. Then, although it is important to determine the system behavior (i.e. whether it is turbulent or not) the details of the fluid flow (i.e. eddy patterns) that would be required to calculate the system response LCE are usually not important.

In addition, it is still not clear whether the Navier-Stokes equations are mathe-

matically self-consistent for the description of the high Reynolds turbulent behavior of flows, for which the eddy scales to be analyzed are frequently too small to fit in a continuous description of the medium [34].

5.3 Fluid-structure interaction problems

In fluid-structure interaction (FSI) problems, usually the details of the flow behavior are not the focus of the analysis, but rather the structural behavior is of main importance. Therefore, it is not important whether the fluid is turbulent or not, but the dynamic stability of the structure, resulting from the interaction with the fluid flow, is essential to the analysis. In such cases, only the behavior of the structure needs to be analyzed, and the evolution of structural perturbations followed.

For the structure, the fluid interaction is nothing else but a forcing term at the FSI surface, which depends on the fluid pressure, velocity and displacement of the fluid-structure interface,

$$ {}^{t}\mathbf{W} = {}^{t}\mathbf{R}_s^S + {}^{t}\mathbf{R}_s^I(\mathbf{u}^I, \mathbf{v}, \mathbf{p}) \tag{5.42} $$

where ${}^{t}\mathbf{R}_s^S$ and ${}^{t}\mathbf{R}_s^I$ represent the forcing terms applied to the structural boundary that is not in contact with the fluid and to the fluid-structure interface, respectively. It is assumed here that ${}^{t}\mathbf{R}_s^S$ does not depend on the structural displacement $\mathbf{u}$.

From equation (5.42), the equation for the evolution of structural perturbations in the system can be obtained as follows

$$ \mathbf{M}_u\ \ddot{\tilde{\mathbf{u}}} + \mathbf{K}_u(\tilde{\mathbf{u}}) - \frac{\partial \mathbf{R}_s^I}{\partial \mathbf{u}^I}\ \tilde{\mathbf{u}} - \frac{\partial \mathbf{R}_s^I}{\partial \mathbf{v}}\ \tilde{\mathbf{v}} - \frac{\partial \mathbf{R}_s^I}{\partial \mathbf{p}}\ \tilde{\mathbf{p}} = \mathbf{0} \tag{5.43} $$

Thus it is important to identify and take into account, at each time step, the forces exerted from the fluid to the structure in the calculation of the evolution of the perturbations.

Alternatively, the complete linearized equations for the fluid flow coupled with the structure can be considered to evaluate the evolution of perturbations. However, since the main interest lies in the analysis of the behavior of the structural/solid part of the

problem, the evolution of the complete vector of perturbations might be calculated but only the displacements of the structural degrees of freedom used in the calculation of the norm of the perturbation vector, d, as described in the section corresponding to the behavior of structures (using the proposed procedure). In this way, while only the growth/decay of structural perturbations are considered and specifically followed, the effects of these perturbations in both the structural and fluid domains are taken into account. The difficulties associated with the arbitrary motion of the mesh are then circumvented, since the structural equations are only affected by forces exerted at the interface that are independent of the choice of mesh movement selected. This approach was used in the calculations of the LCE of FSI systems presented in the next Chapter.

5.4 Local stability

It is frequently important to know the *local* dynamic stability of the system, and the moment at which the system dynamic behavior loses stability. This information is not contained in the response LCE, which is a measure of the asymptotic divergence of nearby trajectories in phase space. However, it is possible to use the value of $ln(d) = k_n\ t_n$, to assess the local stability of the system response. Since $d(t_n) = d_n d_{n-1} \cdots d_1$ measures the divergence or convergence of trajectories in the phase space, and d_n is calculated at each time step, and instability can be captured by $ln(d)$ shortly after it occurs. Note however that the "instant" values of d_n alone do not provide information about the response local stability since the values of $ln(d)$ present oscillations (see the discussion above). The overall system stability behavior is nevertheless captured by a progressive growth/decay of the maximum values of $ln(d)$. Then, by looking at the average slope of $ln(d)$ as a function of time, the local stability of the response can be obtained.

However, one must be careful when assessing the local stability using $ln(d)$ since at the beginning of the LCE calculations a grow/decay in the values of $ln(d)$ might only indicate a transient response in the perturbation evolution not related to the

stability of the continuous problem in consideration.

Chapter 6

Numerical examples

In this Chapter, the algorithm proposed in Chapter 5 to calculate the LCE of structural and fluid-structure interaction problems is numerically investigated. The algorithm is first tested in a low dimensional order system and then examples of continuous systems are considered.

6.1 Discrete nondimensional equation of motion: the Duffing equation

Let us first consider the Duffing equation, a nonlinear non-dimensional single degree of freedom equation with sinusoidal forcing, to gain insight into the kind of behavior and problems that can be encountered when analyzing a nonlinear dynamic problem. The equation has been analyzed in various publications, see for example [1] [26].

The Duffing equation is

$$\ddot{x} + c\,\dot{x} - b\,x + a\,x^3 = g\,\cos(\bar{\omega}\,t) \tag{6.1}$$

with initial conditions,

$$\begin{aligned} x(t_0) &= x_0 \\ \dot{x}(t_0) &= \dot{x}_0 \end{aligned} \tag{6.2}$$

where a, b, c, g and $\bar{\omega}$ are the equation parameters. The equation can exhibit different behaviors depending on the value of the parameters considered. Of course, the algorithm employed in the calculation of the LCE must properly capture the different types of behavior encountered (thus, if the system becomes chaotic the LCE should be greater than zero, otherwise it should be less than or equal to zero). Usually, a, b and c are chosen to be positive values, and therefore the Duffing equation is a two-well potential problem with dissipation and

$$V(x) = -\frac{b}{2}x^2 + \frac{a}{4}x^4 \tag{6.3}$$

where $V(x)$ is the potential function. A generic graphical representation of the potential as a function of x is shown in Figure 6-1.

Consider first the case in which $g = 0$ (and a, b, and c are positive numbers). In this case, the problem has three fixed points in phase space, corresponding to each potential well, x_1^* and x_2^*, and the local maximum of the potential, $x = 0$. Depending on the initial conditions, the system long-term response is a steady state in which the value of x is either x_1^* or x_2^*. However, there are also values of the initial conditions for which the system steady state response corresponds to $x = 0$, which is an unstable equilibrium point. In practice, it is extremely difficult to obtain a response in which the system steady state is $x = 0$: experimentally, small errors in the initial conditions and random inputs will affect the system response; numerically, even if the initial conditions are the exact ones, numerical errors will deviate the trajectories from the theoretical one. For this reason, the trajectories that finish in an unstable fixed point are usually called *irregular* [1]. The presence of irregular trajectories gives rise, in this case, to the concept of *transient chaos*. Infinitesimal differences in the initial conditions, near the irregular trajectory, may correspond to a completely different outcome of the system long-term response. That is to say, the asymptotic behavior is a steady-state in which x is equal to either x_1^* or x_2^*, depending on infinitesimal differences in the initial conditions. The irregular trajectory then separates the basin

[1] Note that the trajectories that are called *irregular* here are not related to the irregular trajectories mentioned in Chapter 1, which correspond to chaotic trajectories.

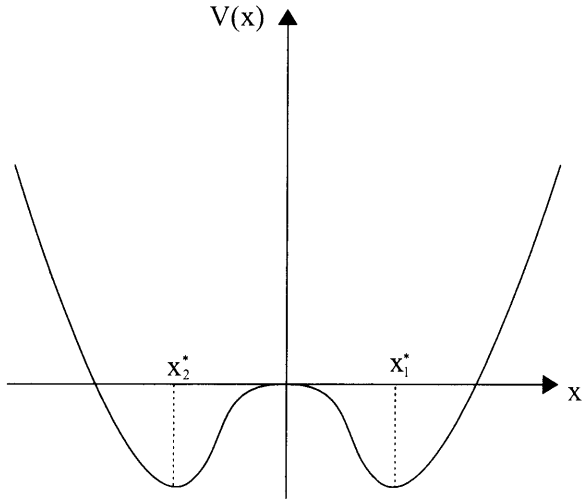

Figure 6-1: Sketch of the potential function of the Duffing equation without forcing and when all the parameters are positive numbers.

of attraction of one of the well points from the basin of attraction corresponding to the other. The representation of the system phase portrait is shown in Figure 6-2, in which the irregular trajectory is shown as a dotted line. Note however, that the term transient chaos refers only to the fact that the system long-term response cannot be predicted, but it does not mean that the asymptotic system behavior is chaotic (in fact in this case, the asymptotic behavior corresponds to a steady-state solution).

Now, consider the case in which $g \neq 0$. Energy is periodically supplied and taken out from the system, and when the parameter g is small the system asymptotic behavior corresponds to an oscillatory response. Oscillations about either x_1^* or x_2^* can occur, and transient chaos is again a possibility. For certain choices of the values of g and $\bar{\omega}$, a chaotic behavior may also develop; the trajectories oscillate about one of the potential wells for certain time and then go to the other, and so forth. However, the exact moment in which the "jump" from one potential well to the other takes place is unpredictable, and of course the number of oscillations about each of the potential wells varies in an unpredictable manner. The chaotic behavior can be explained by considering a small ball moving in the potential of Figure 6-1, while the potential itself is oscillating (due to the forcing term). In this situation, it is easy to imagine that for certain choices of the forcing term parameters the ball can reach the relative

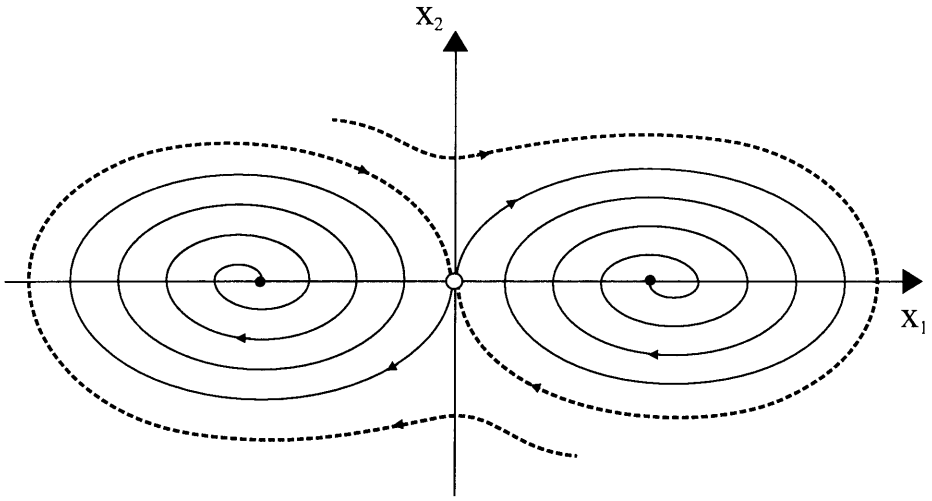

Figure 6-2: Sketch of the phase portrait for the Duffing equation without forcing. The black dots correspond to stable fixed points for the system, whereas the white dot (at the plot origin) corresponds to the unstable fixed point.

maximum of the potential with a relative velocity close to zero, and an infinitesimal perturbation may induce the ball to go to one of the potential wells or to the other, making the system behavior unpredictable.

To calculate the system's response LCE, we need to derive the equations corresponding to the evolution of perturbations. Since the system is non-autonomous, a change of variables is first performed to transform the equations into autonomous form (see Chapter 2). In addition, the equations will be expressed as a system of first order differential equations in time (so that the procedure described in [3] for discrete systems can be directly applied). The following change of variables is performed,

$$\begin{aligned} x_1 &= x \\ x_2 &= \dot{x} \\ x_3 &= t \end{aligned} \tag{6.4}$$

and equation (6.1) can be expressed as,

$$\begin{aligned} \dot{x}_1 &= x_2 \\ \dot{x}_2 &= b\,x_1 - a\,x_1^3 - c\,x_2 + g\,\cos(\bar{\omega}\,x_3) \\ \dot{x}_3 &= 1 \end{aligned} \tag{6.5}$$

The linearized equations that describe the time evolution of perturbations are

$$\begin{aligned} \dot{\tilde{x}}_1 &= \tilde{x}_2 \\ \dot{\tilde{x}}_2 &= (b\,-\,3\,a\,x_1^2)\;\tilde{x}_1 - c\,\tilde{x}_2 - g\,\bar{\omega}\,\sin(\bar{\omega}\,x_3)\,\tilde{x}_3 \\ \dot{\tilde{x}}_3 &= 0 \end{aligned} \tag{6.6}$$

where $\tilde{x}_1$, $\tilde{x}_2$ and $\tilde{x}_3$ are the perturbations to the system variables x_1, x_2 and x_3, respectively. From equations (6.6), it follows that $\tilde{x}_3$ = constant. In particular, we can choose $\tilde{x}_3 = 0$, which corresponds to the case in which the time is not perturbed, the case to be taking into account from physical considerations. Thus, equations (6.6) are reduced to

$$\begin{aligned} \dot{\tilde{x}}_1 &= \tilde{x}_2 \\ \dot{\tilde{x}}_2 &= (b\,-\,3\,a\,x_1^2)\;\tilde{x}_1 - c\,\tilde{x}_2 \end{aligned} \tag{6.7}$$

and hence the behavior of infinitesimal perturbations to the system depend on the specific trajectory analyzed.

Let us numerically analyze different behaviors of equation (6.1). In all the cases considered below, the following parameter values are used: $a = 0.53$, $b = 0.2$, $c = 0.04$, and $\bar{\omega} = 0.16$, whereas the value of g is changed as indicated. The initial conditions considered in all cases are $x_0 = 1$ and $\dot{x}_0 = 0$.

- $g = 0$: For this particular choice of parameters, the asymptotic behavior of the system corresponds to a steady state. Figure 6-3a shows a phase portrait of the system response, and the LCE calculated for this system. Since the system response is regular, the LCE obtained cannot be positive. The calculated LCE value, which is negative in this case, can be seen in the Figure as the value for which k_n remains constant as a function of time.

- $g = 0.01$: In this case, a small forcing term is considered, and the system behavior is shown in Figure 6-3b. The behavior is regular, although oscillatory, and the value of k_n in the limit of time going to infinity is negative. Note however, that this is *not* the maximum LCE of the system. Considering equations (6.6), the maximum LCE is equal to zero, associated with the equation $\dot{\tilde{x}}_3 = 0$ (this is consistent with the fact that at least one Lyapunov characteristic exponent must be zero).

- $g = 0.4$: This case is shown in Figure 6-3c. The system behavior for this case is chaotic, as can be seen from either the phase plot or the value of the LCE obtained, which is positive and approximately equal to 0.035.

Note that in all the cases considered above, the convergence to the LCE value (obtained when the number k_n, from equation (2.36), remains constant as a function of time) is very slow. However, the divergence (convergence) of trajectories in phase space, characterized by growing (decreasing) values of $ln(d) = k_n\, t_n$ are obtained after only a few time step calculations, see Figure 6-4. Therefore, trends in the behavior of the values of $ln(d)$ can be used to characterize the *local stability* of the system behavior, although the exact value of the LCE is not calculated. As can be observed from Figure 6-4, even for a chaotic behavior the perturbations grow and decrease as a function of time, and only the *average* behavior becomes important.

One might expect that the values of the LCEs obtained for different time steps would converge to the correct LCE as the time step is decreased. Since it can be difficult to compare the system responses obtained with different time steps when the behavior is chaotic (due to the exponential divergence of trajectories in phase space) the values of the LCE (or in general trends in the behavior of $ln(d)$) can be compared to guarantee that the chaotic behavior is properly captured (a behavior might seem chaotic when the time step used to calculate the system response is not small enough). Figure 6-5 shows the values of k_n obtained as a function of time when the response is calculated using different time steps. Note that even though a final value of the LCE (constant k_n) has not been obtained in the cases considered, all the

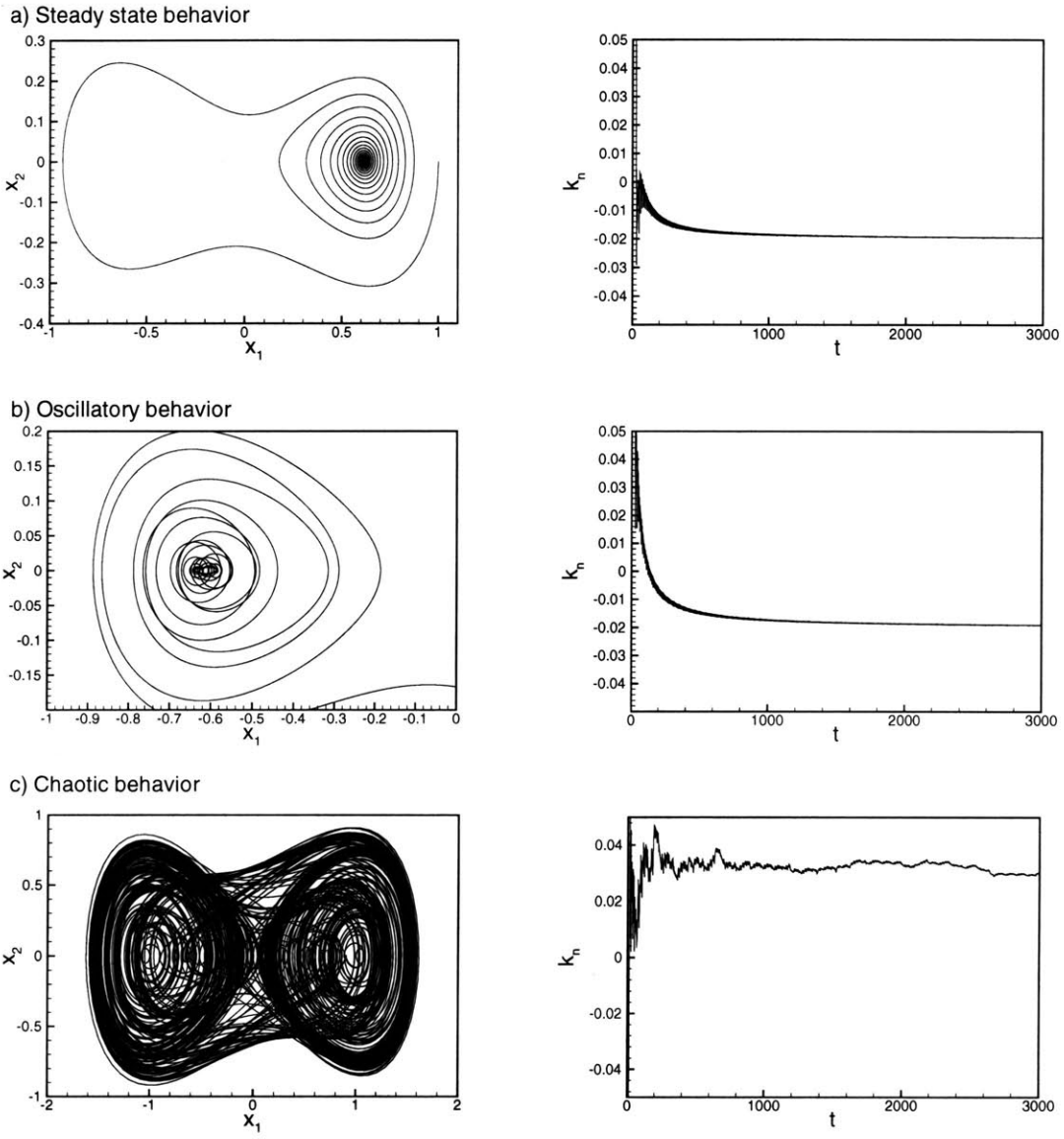

Figure 6-3: Different behaviors exhibit by the Duffing equation and the values of the LCEs associated with them. a) Steady-state response. b) Oscillatory behavior. c) Chaotic response.

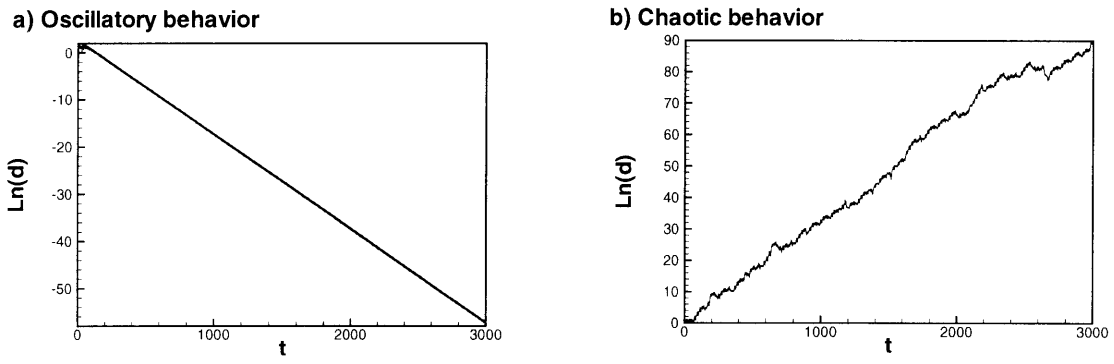

Figure 6-4: Values of $ln(d)$ as a function of time for two responses of the Duffing equation. a) Oscillatory behavior. b) Chaotic response.

curves captured the chaotic nature of the system, and the values of k_n are closed to each other during all the calculation.

One question remains to be analyzed: what happens, in this case, if instead of calculating the LCE using the norm of the perturbations considering both $\tilde{x}$ and $\dot{\tilde{x}}$, only the contribution due to $\tilde{x}$ is employed, as proposed in this work for the LCE calculation of structural systems discretized using finite element methods? From theoretical considerations (see Chapter 5), we expect both approaches to be equivalent for a discrete system of few degrees of freedom (it was already discussed that the procedure proposed by Benettin et al [3] cannot be used in the case of discretized continuous structural systems). The proposed procedure was then applied to the case in which the response of the Duffing equation is chaotic. A comparison of the two results for a small period of time, so that differences can be appreciated, is shown in Figure 6-6. Note that, if the LCE, calculated using the values of k_n described in the proposed procedure, is evaluated as

$$\chi = \limsup_{n \to \infty} k_n \tag{6.8}$$

both procedures give the same results (the trends in the behavior of both calculations are the same). Indeed the same results were obtained, except that using the proposed procedure, the values of k_n present stronger oscillations, as expected.

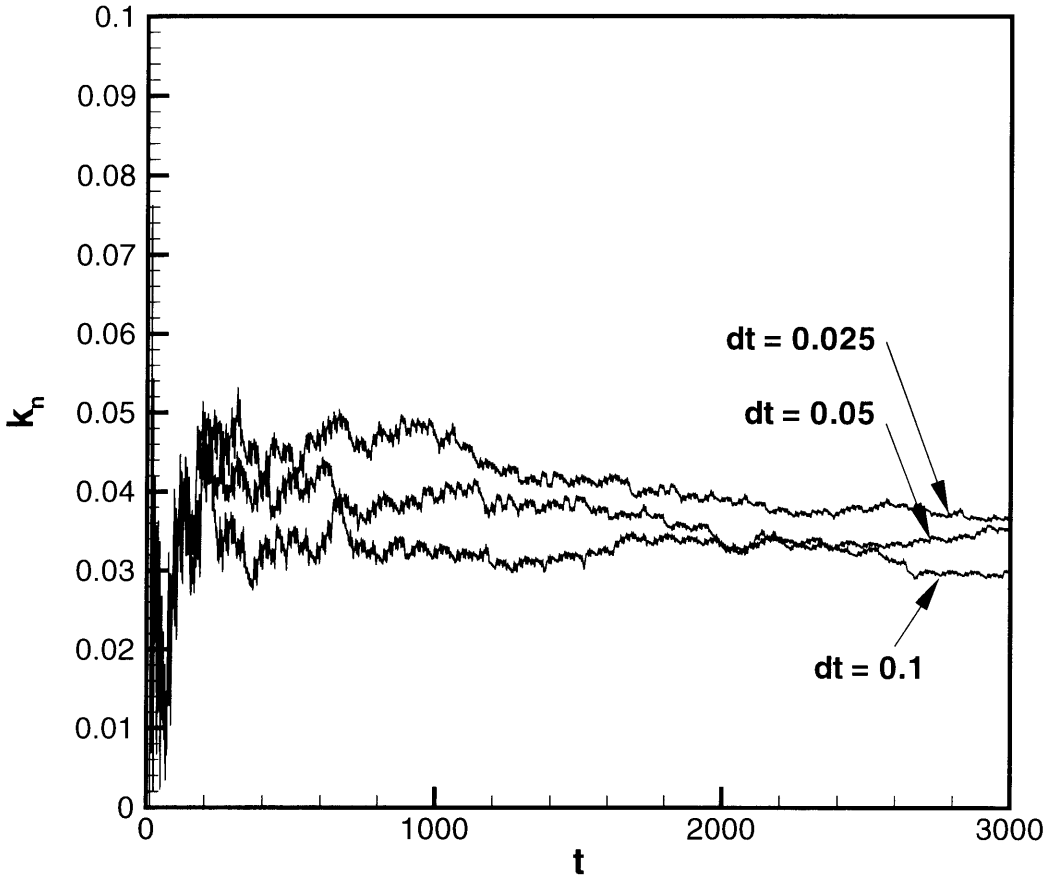

Figure 6-5: Values of k_n obtained when the Duffing equation presents the chaotic behavior considered above, and for different values of the time step used to discretize the equations in time.

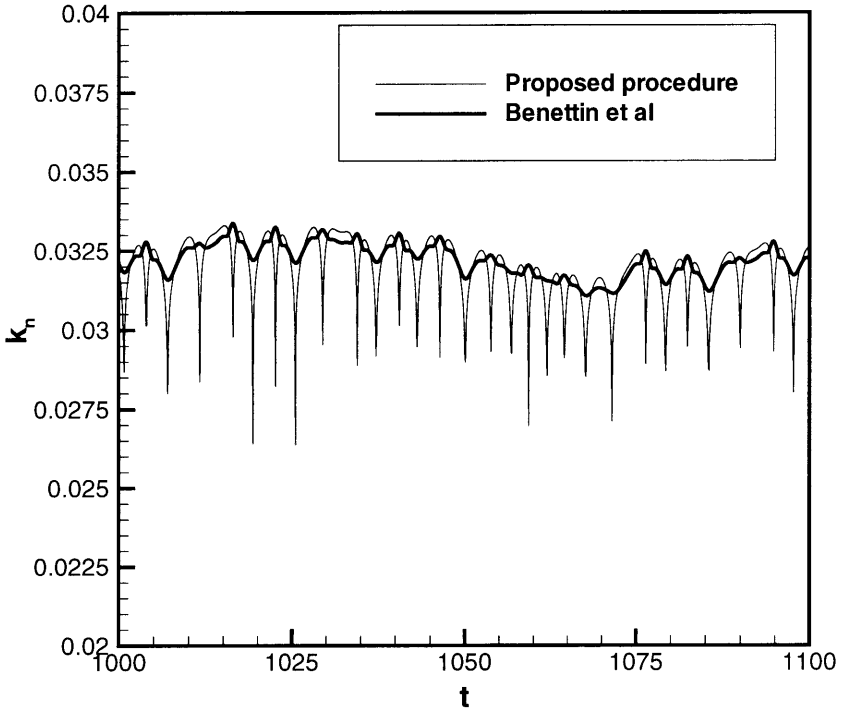

Figure 6-6: Comparison of the values of k_n obtained for the chaotic response of the Duffing equation considered above, using the method proposed by Benettin et al. and the proposed procedure.

6.2 Structural systems

In this section the analysis of structural continuous systems, discretized using finite element methods is considered. In all the cases, the successive approximations to the LCE, k_n, are calculated using the proposed procedure. In addition, a Fourier analysis of a sample point of the response is performed for validation purposes.

The system response and LCE calculation was performed using a code developed specifically for this work by the author. Validation of some code results with the finite element software program ADINA was done, to ensure that the behavior captured is the correct one.

6.2.1 Analysis of steady-state behavior

This example is included as a validation of the procedure proposed in this work for the calculation of the Lyapunov characteristic exponent of the response of structural continuous systems. The two-dimensional cantilever beam problem shown in Figure 6-7 is considered, assuming a plane stress analysis. The beam is discretized with a mesh of 100 by 1, using 9-node displacement-based elements.

The beam is initially at rest. Since no loading or imposed displacement boundary conditions (other than the zero displacement conditions at the clamped-end) are applied to the body, the beam remains at rest. This situation is equivalent to a stable steady state behavior. Applying an arbitrary initial perturbation to the system, the evolution of the perturbations can be computed and the results tested. For this

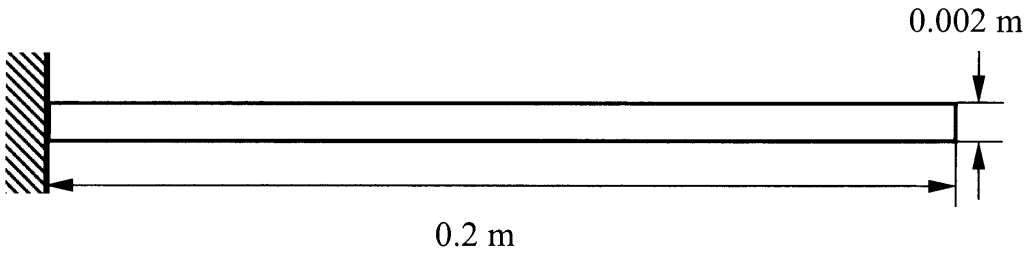

Figure 6-7: Cantilever beam used in the analysis of the perturbation evolution of a steady-state behavior.

case, we expect that perturbations would decay as a function of time if dissipation is included in the model, or they would remain the same (no decay in the norm of the perturbations) if no dissipation were included. Of course, many time integration methods include some artificial dissipation in the system response. In this example, however, the trapezoidal rule, which does not include dissipation in the system response, is employed in the calculations [2].

The case in which no dissipation is included in the model, and a homogeneous perturbation in velocity is applied to the system is considered. That is to say, we impose a constant velocity for all the degrees of freedom (both velocity directions), and thus the perturbation satisfies the required boundary conditions. Using these initial perturbed velocities, perturbed displacements are calculated and non-dimensionalized. The obtained displacements and velocities are then used as the perturbation initial conditions (such that $d_0 = 1$).

Figure 6-8 shows the calculated successive approximations of the value of the response LCE, k_n, when the time step employed is $\Delta t = 0.002s$. For this example, a value of zero is expected for the response LCE, and a zero slope is expected in the curve of $ln(d) = k_n\ t_n$ as a function of time. Looking at Figure 6-8 the correct value seems to be obtained. However, using linear regression analysis to fit the curve of $ln(d)$ as a function of time, we find that the slope of the curve is equal to $0.0024s^{-1}$. Since this value is very small, we consider that this is due to the numerical error in the calculations.

In the next case considered, dissipation was once more not included in the structural model. This time, a random initial perturbed velocity was assigned to each degree of freedom, so that all the structural modes are perturbed, and the proposed algorithm can be tested in a more general situation. The time step employed in the calculations is $\Delta t = 0.002s$. The results obtained looked like those in Figure 6-8. By performing a linear regression analysis of the curve $ln(d)$ as a function of time, a slope equal to $0.0022s^{-1}$ is obtained, which can be attributed to numerical errors in the calculation.

The same calculation was repeated for $\Delta t = 0.001s$, and this time the slope of

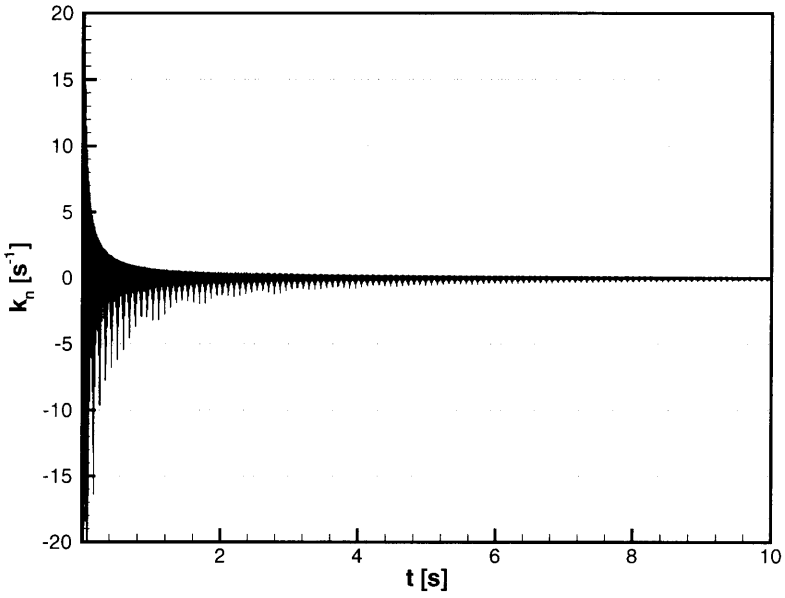

Figure 6-8: LCE calculation of a steady-state solution of the cantilever beam. Oscillation of the values of k_n are typical when using the proposed procedure (since the norm of the perturbation is calculated using only displacements).

the curve of $ln(d)$ as a function of time was $-0.00073s^{-1}$. Refining the time step even more, with $\Delta t = 5 \cdot 10^{-5}s$ a slope equal to $-0.0008s^{-1}$ is obtained, and with $\Delta t = 2.5 \cdot 10^{-5}s$ the slope is $2 \cdot 10^{-5}s^{-1}$. These results confirm the hypothesis that the small slope obtained is only due to numerical errors, and therefore it is related to the sensitivity of the numerical algorithm.

6.2.2 Buckled beam analysis

The system shown in Figure 6-9 is considered. It consists of an initially buckled beam under equilibrium, that for time $t \geq 0$ is excited with a sinusoidal pressure applied to one of its sides. A two-dimensional plane stress analysis, in which large displacements but small strains are considered, was used in the calculation of the system behavior. The continuous body was discretized using displacement-based 9-node elements. The system properties and forcing parameters used in the analysis are as follows,

- Young's modulus, $E = 206.85 \cdot 10^9$ Pa
- Poisson's ration, $\nu = 0.3$
- Density, $\rho = 7805.86$ kg/m^3
- Excitation amplitude, $p = 45$ Pa
- Excitation frequency, $\omega^* = 90$ Hz

The two-dimensional analysis of the described buckled beam problem is a two-well potential problem, where the potential wells correspond to the beam bending to the right or left side. As in the case of the Duffing equation considered above, by choosing the appropriate amplitude and frequency of the forcing term, a chaotic behavior can be obtained. This type of problem is extensively analyzed experimentally in the literature, see for example [15] and [16], and the Duffing equation is frequently used as a simplified model to analyze the behavior of a buckled beam simply supported at both ends. In the mentioned works, it is shown that indeed the system behavior can become chaotic under certain values of the forcing amplitude and frequency.

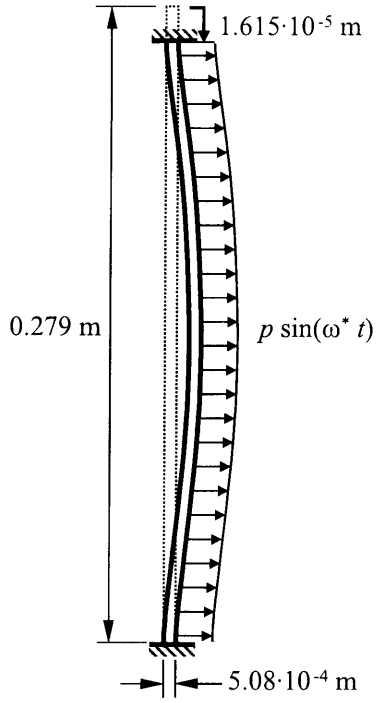

Figure 6-9: Buckled beam problem considered.

The system response and the calculated values of k_n, which in the limit of $t \to \infty$ gives the response LCE, are shown in Figure 6-10. The beam mid-point displacement seems rather stochastic, since there are no apparent patterns in its behavior and the time for which the mid-point displacement changes from positive to negative seems unpredictable. The chaotic nature of the system is confirmed by a positive value of the LCE. Furthermore, a chaotic behavior is non-periodic and therefore characterized by a response that contains a broad spectrum of frequencies (that is to say that there are no dominant frequencies but rather all the frequencies, in a certain range, are present in the behavior). The response frequency contents can be extracted by performing a Fourier analysis, as shown in Figure 6-11. Note that the spectrum presents a relatively small spike at 90Hz (the excitation frequency). Nevertheless a continuous spectrum of frequencies (in which each frequency has approximately the same importance) is otherwise obtained.

Note, from Figure 6-10, that in order to obtain a good approximation of the beam response LCE, obtained when the value of k_n remains constant as a function of

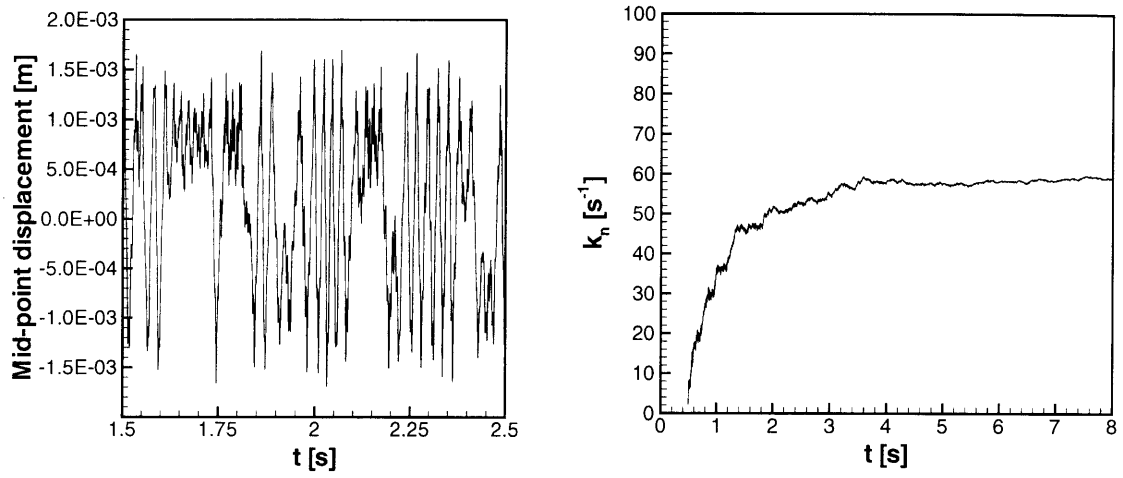

Figure 6-10: Mid-point displacement of buckled beam problem and LCE calculation.

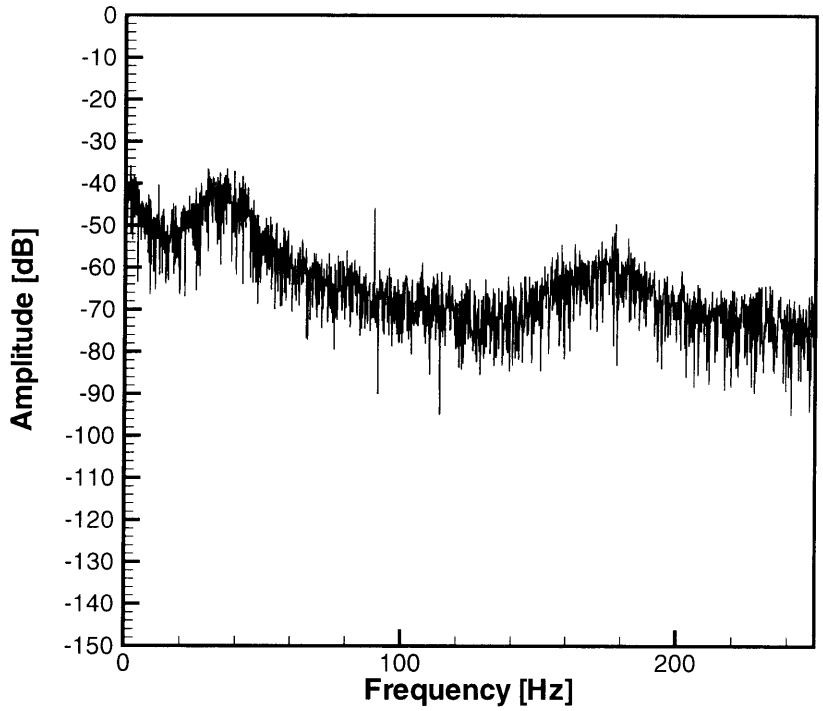

Figure 6-11: Fourier spectrum of the buckled beam response obtained for the mid-point displacement.

time, the behavior of the perturbations over many time steps needs to be calculated. However, the values of $ln(d)$, where d is the accumulated norm of the perturbations, provide information about the local stability behavior (in time) of the system. The values of $ln(d)$ as a function of time for the beam response considered are shown in Figure 6-12, and it can be observed that the slope of the curve is positive, indicating an unstable behavior (associated with growth of perturbations) for the period of time considered.

Convergence of the system's response LCE is expected as the time step considered is decreased and as the mesh used in the discretization is finer (i.e. more finite elements are used). A convergence analysis for the system is shown in Figure 6-13. It can be observed that for some values of the time step Δt, the final value of the LCE was not yet obtained (since k_n has not converged to a constant value). Nevertheless, in all the cases a chaotic behavior, characterized by a positive value of the LCE, is detected and the values of k_n obtained are all relatively closed to each other.

6.2.3 Beam subjected to nonlinear boundary condition

The system depicted in Figure 6-14 was analyzed using a two-dimensional plane stress analysis in which large displacements and small strains are assumed. From the Figure, it can be seen that the beam free-end cannot displace arbitrarily, since a nonlinear (cubic) spring is attached to it. This case is considered to simulate situations in which nonlinear boundary conditions are present, an important factor that can contribute to a chaotic system response in engineering systems. In this case, for instance, a contact condition, in which stops are located near the free-end of the beam to restrict its movement, can be idealized by a cubic spring attached to the beam free-end. Some analysis on the behavior of beam systems subject to nonlinear boundary conditions are considered in [25] and [27] and it was experimentally observed that the systems may develop a chaotic behavior under certain conditions.

The beam properties are the same as for the buckled beam problem, and the system parameters are,

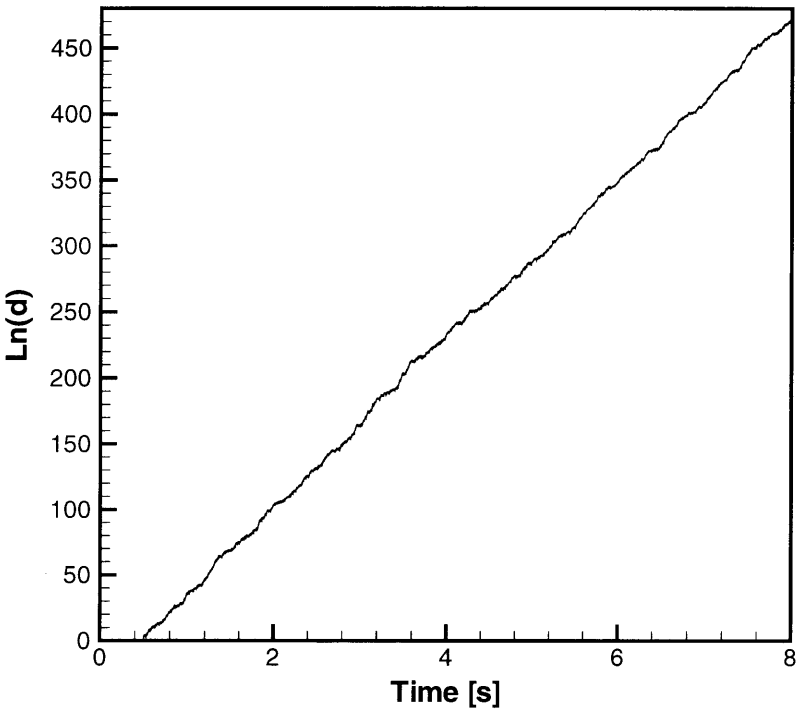

Figure 6-12: Plot of $ln(d)$ as a function of time for the buckled beam problem. Note that the local stability of the system is captured by this graph, without explicitly calculating the system LCE (which defines only the system long-term stability).

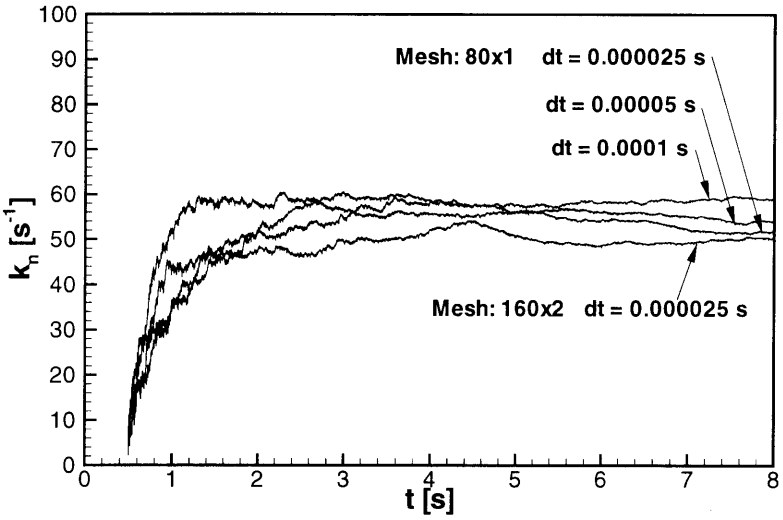

Figure 6-13: Convergence analysis for the LCE value obtained in the case of the buckled beam.

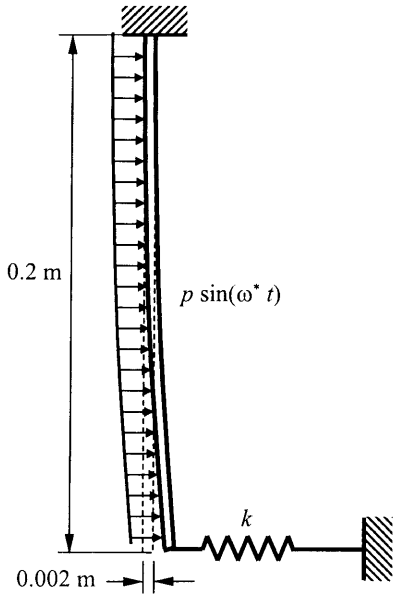

Figure 6-14: Beam subject to nonlinear boundary conditions. Sketch of system considered.

- Excitation amplitude, $p = 6000$ Pa
- Excitation frequency, $\omega^* = 90$ Hz
- Cubic spring constant, $k = 5 \cdot 10^{10}$ kg/s^2

The displacement of the beam end that has the spring attached to it, which is referred to as the beam "free-end" (although this is not a precise description of it), is shown in Figure 6-15 together with the calculated response LCE. It can be seen that the beam "free-end" displacement seems to be non-periodic, a characteristic of a chaotic behavior. This is confirmed by examining the power spectrum of the response shown in Figure 6-16. A spike corresponding to a frequency of 90Hz, the excitation frequency, is present but a continuous spectrum of frequencies of similar importance is also present. Furthermore, from Figure 6-15, the value of the LCE is positive confirming the unstable nature of the system long-term response.

Looking at the plot of the $ln(d)$ as a function of time, Figure 6-17, it can be seen that the dynamic local stability behavior of the system is captured, since the average slope of the curve is positive. It is clear from this example that for different parts of the $ln(d)$ curve the average slope is different. Of course, at the beginning of the calculation this may indicate that transient effects have not yet decayed (i.e. the trajectory is not yet in the chaotic attractor). However, it is also possible that the magnitude of the divergence of nearby trajectories in phase space changes from one part of the attractor to the other. The value of the LCE will then be an *average* measure of the divergence of nearby trajectories in phase space in different parts of the attractor.

6.3 Fluid-structure interaction

In this section, the analysis of fluid flows interacting with solid media is considered. In the two cases analyzed here, the system response was obtained employing a code developed by the author, in which the coupling and condensation procedure described

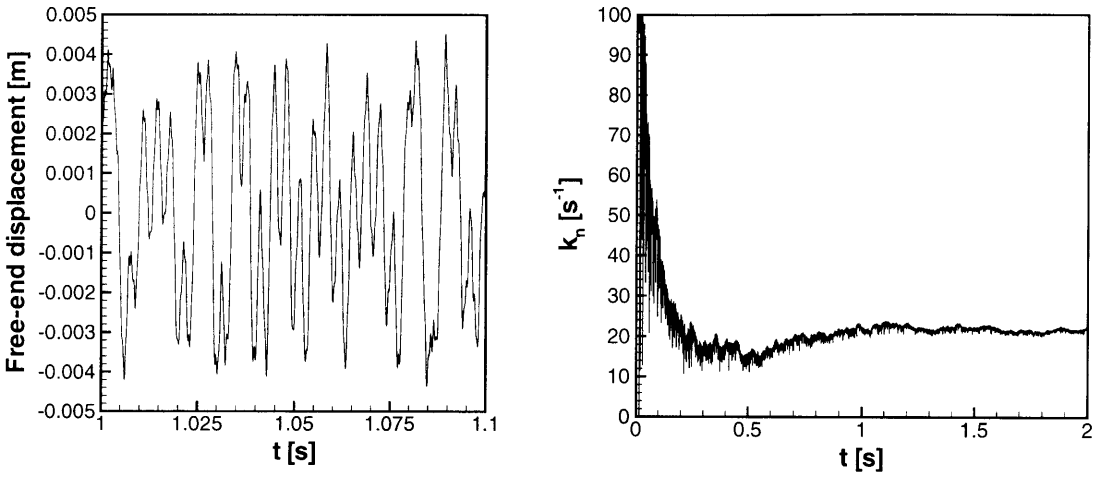

Figure 6-15: Displacement of the end of the beam with an attached cubic spring (the "free-end") as a function of time; and the calculated values of k_n, which give the response LCE in the limit for time going to infinity.

in [36] [35] was implemented. In addition, the problems to be presented were calculated using the developed code and the program ADINA, and similar results were obtained using both programs.

6.3.1 Collapsible channel

The first fluid-structure interaction problem considered is shown in Figure 6-18. It consists of a two-dimensional channel initially filled with a viscous fluid with a Poiseuille velocity profile. Part of the channel upper wall was replaced by a thin structure that can displace in the vertical direction (the collapsible segment), and another structure, which is stiffer, and that can only displace in the horizontal direction. The fluid is modeled using the ALE form of the almost incompressible Navier-Stokes equations; and the structure is modeled using a linear plane stress analysis (which can be transformed into a plane strain analysis). This kind of model is used to qualitatively describe the flow of blood inside a blood vessel, to study certain phenomena observed in this type of systems, see for example [33] [19] [20]. The fluid domain was discretized using the mixed 9/3 element formulation, whereas the structure was

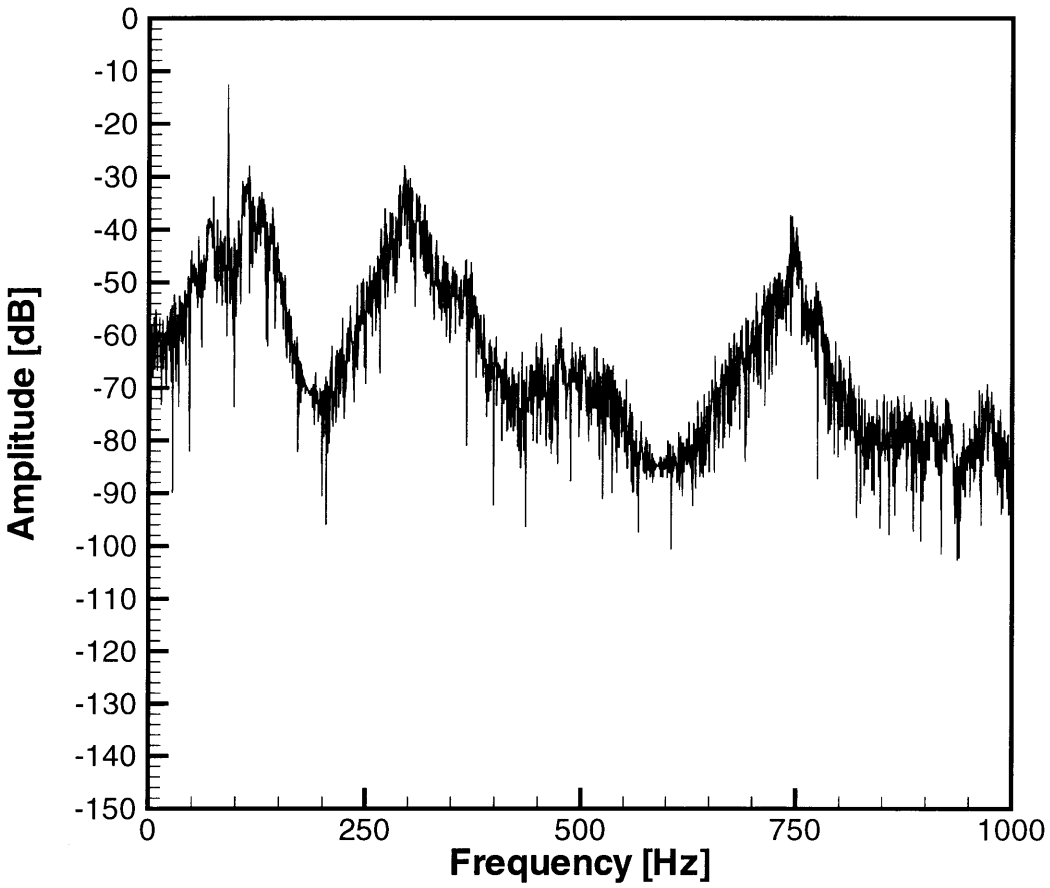

Figure 6-16: Fourier spectrum of the response obtained for the beam with an attached cubic spring, shown in Figure 6-15.

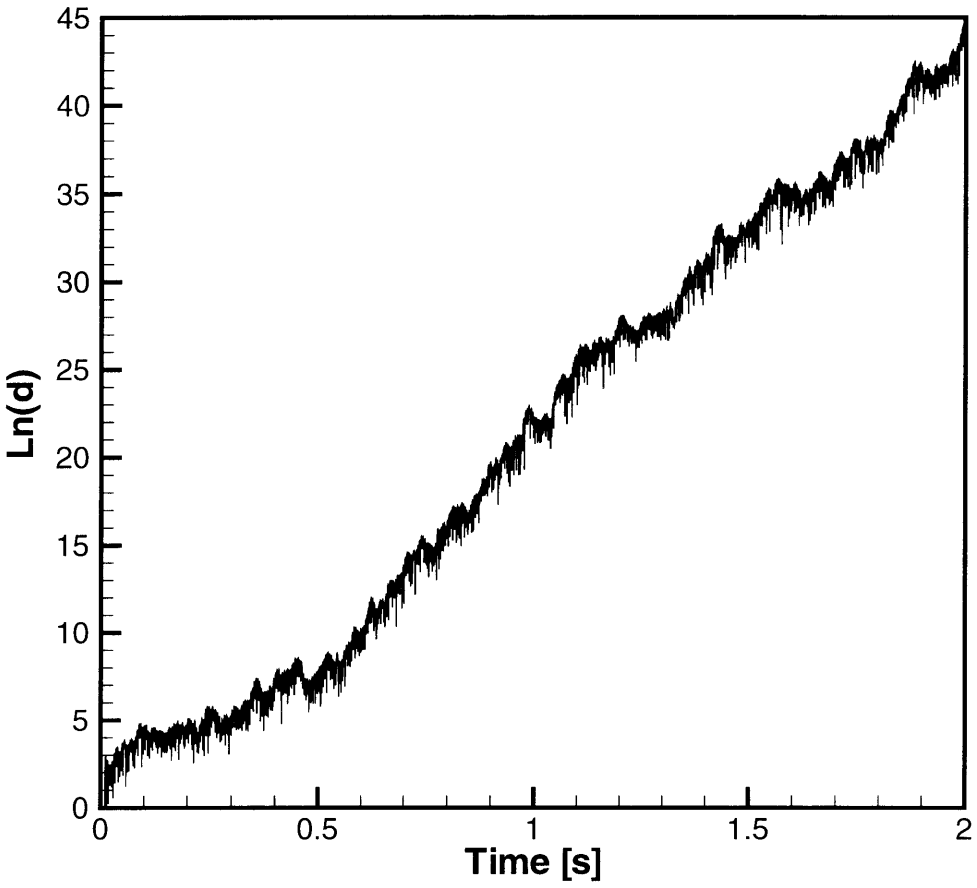

Figure 6-17: Calculated $ln(d)$ as a function of time, for the beam problem with nonlinear boundary conditions.

discretized employing displacement-based 9-node elements [2].

The properties of the system considered are as follows,

- Fluid:

  Viscosity, $\mu = 0.002$ kg/m s,

  Density, $\rho = 1000$ kg/m^3,

  Bulk modulus, $\kappa = 2.1 \cdot 10^9$ Pa

  Pressure difference, $p_0 - p = 3.255$ Pa

- Collapsible segment:

  $E = 2 \cdot 10^5$ Pa

  $\nu = 0.2$

  $\rho = 1000$ kg/m^3

- Segment that can displace only in the horizontal direction:

  $E = 2 \cdot 10^8$ Pa

  $\nu = 0.3$

  $\rho = 1$ kg/m^3

Figure 6-19 shows the obtained collapsible segment mid-point displacement as a function of time as well as the calculated values of k_n. The system presents an instability for values of time about $t = 10s$ after which a limit cycle behavior develops. The instability, however, is only *local* and the long-term system behavior (a limit cycle) corresponds to a stable response. The system stability is also reflected in the calculated values of k_n. When the system first develops the instability before the limit cycle, the values of k_n jump to positive values, indicating that the system is unstable. However, as soon as the oscillations stop growing at a fast pace, the values of k_n start to decrease, indicating that the system is stabilizing. When the values of $ln(d)$ are analyzed, as shown in Figure 6-20, it is observed that at approximately $t = 10s$ the slope of the $ln(d)$ curve is very steep, and then it changes to a curve which still grows, but with a much smaller slope (the slope is about $0.31s^{-1}$ when using $\Delta t = 0.0025s$ and $\Delta t = 0.005s$). This suggests that the system is not yet

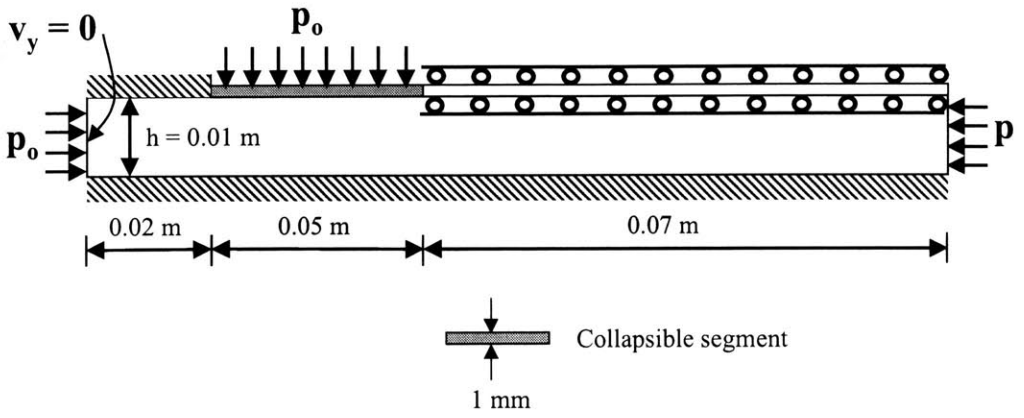

Figure 6-18: Collapsible channel problem considered.

stable, and that the amplitude of the limit cycle is still growing. This is of course a small effect, and that is why it cannot be appreciated by looking at Figure 6-20. Nevertheless, a more detailed analysis would be needed in this case to determine the errors of the calculation (to make sure that slope in $ln(d)$ is not due to numerical errors), and to assess whether other physical phenomena could be contributing to the growth of $ln(d)$.

A Fourier analysis of the response obtained after $t = 20s$ is shown in Figure 6-21. It can be seen that in this case there are only two important peaks in the response frequency spectrum, and then some smaller ones (that actually correspond to super-harmonic frequencies). The fact that the system does not present a continuous spectrum of frequencies (the "tail" of the plot is attributed to numerical errors, and not real system frequencies) confirms the fact that the response is not chaotic, although it is probably not yet completely stable.

6.3.2 Modified collapsible channel model

The collapsible channel problem considered in the last section was slightly modified, as shown in Figure 6-22. A linear spring of constant k was included in the model to avoid the complexity associated with contact conditions between the collapsible segment and the downward channel wall. The spring, shown in the figure as a truss

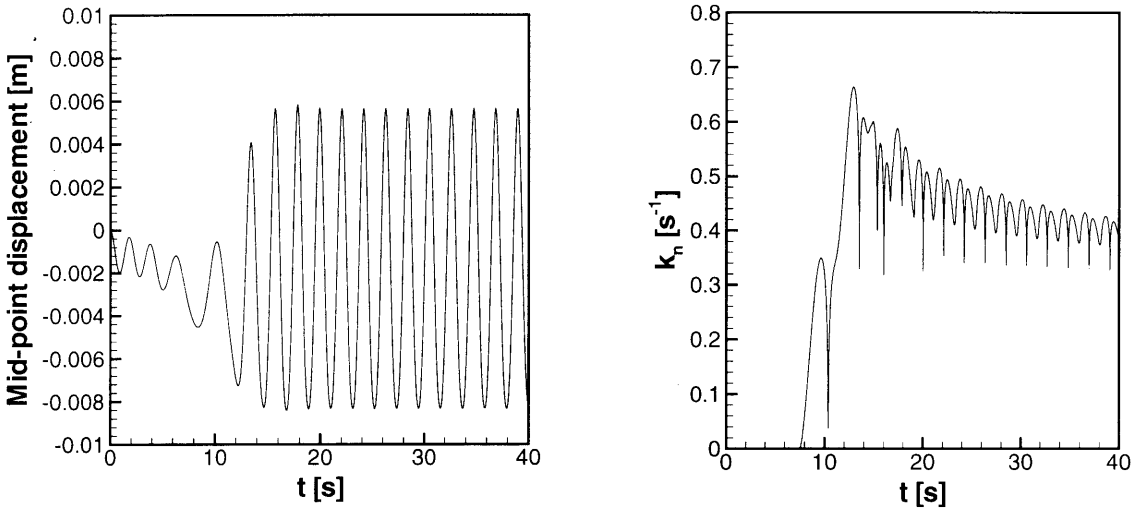

Figure 6-19: Mid-point displacement of the collapsible segment for the collapsible channel problem depicted in figure 6-18, and the calculated LCE.

element, allows the fluid to flow through it without any restriction, and it starts to act only when the lower point of the collapsible segment that is originally at $0.05m$ from the channel entrance, has displaced $0.009m$ inside the channel (90% of the channel height). The spring acts only if the point displacement is greater or equal than $0.009m$ inside the channel. Thus, a nonlinear boundary condition is imposed at one point of the collapsible segment. The system properties are the same as in the problem considered in the previous section, except that in this case the pressure difference is $p_0 - p = 15.942$ Pa, and the spring constant is $k = 1000$ kg/s^2.

Luo et al. [21] investigated numerically the problem of the collapsible channel imposing a velocity profile at the channel entrance. Although in their work a chaotic behavior was not explicitly found, it was argued that it is possible for the system to develop a chaotic behavior.

The obtained system response is shown in Figure 6-23, together with the calculated LCE. It is observed that the segment mid-point response is not periodic, as expected in a chaotic behavior, and the obtained value of the LCE is positive. In addition, by looking at the power spectrum of the response, Figure 6-24, it can be seen that many frequencies are excited, confirming the chaotic nature of the behavior. Furthermore,

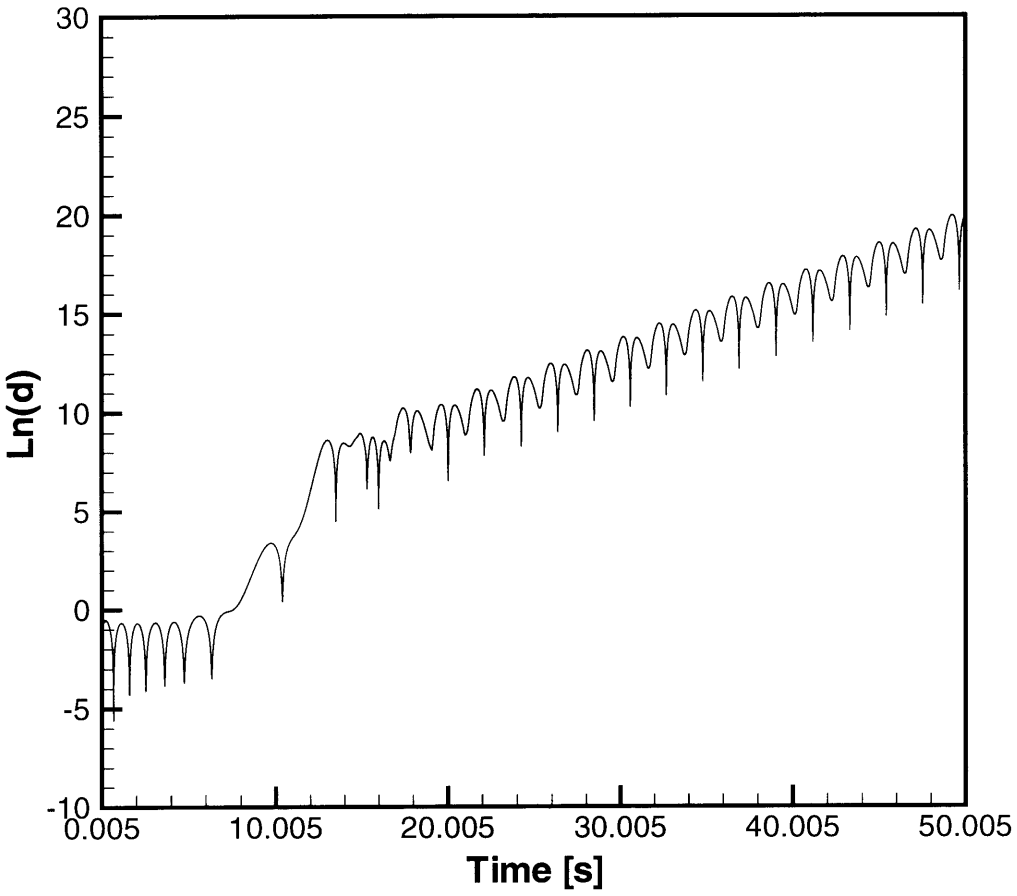

Figure 6-20: Plot of the $ln(d)$ as a function of time for the collapsible channel problem.

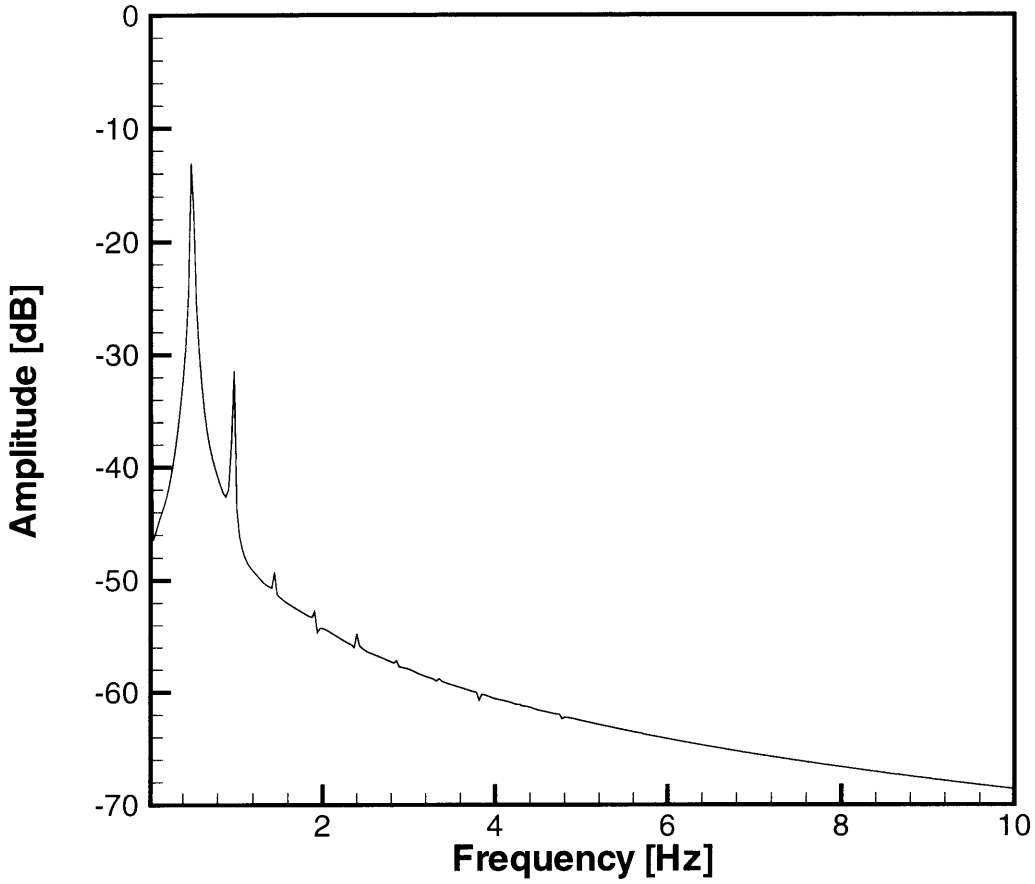

Figure 6-21: Power spectrum of the mid-point collapsible segment displacement obtained for the channel problem.

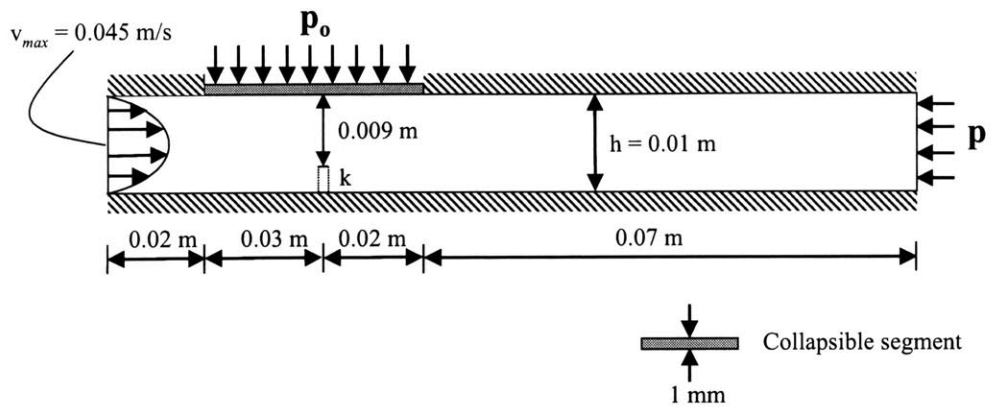

Figure 6-22: Modified collapsible channel problem considered. A parabolic velocity profile, constant in time, is imposed at the tube inlet. The linear truss of constant $k = \frac{EA}{L}$, acts over one point of the membrane when it reaches a vertical displacement of 0.009m or more inside the channel, and it does not interfere with the fluid flow inside the channel.

the plot of $ln(d)$ as a function of time, Figure 6-25, shows a positive slope for all times considered.

It can also be noticed that the value of the LCE obtained is much smaller than in the cases of the chaotic behavior of the beams discussed above. This fact can be justified by comparing the obtained displacements for the beams and the collapsible segment of this example. In the case of the beams the behavior is highly non-periodic and there is absolutely no pattern, indicating that the divergence of nearby trajectories in phase space is rather strong. However, in the case considered here, even though the displacement is not periodic, it is more "regular" than in the beam case. This behavior is a consequence of the fact that nearby trajectories in phase space diverge from each other exponentially fast but at a much slower rate than in the case of the beam problems. This is also consistent with the lower values of the LCE obtained for this collapsible channel example as compared to the value obtained for the beam problems considered before.

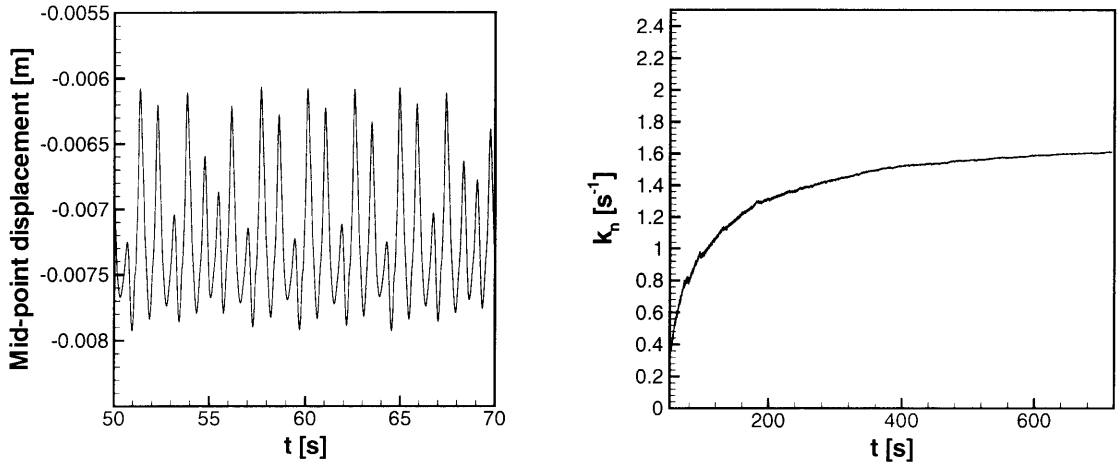

Figure 6-23: Collapsible segment mid-point displacement for the channel problem depicted in Figure 6-22, together with the calculated values of k_n.

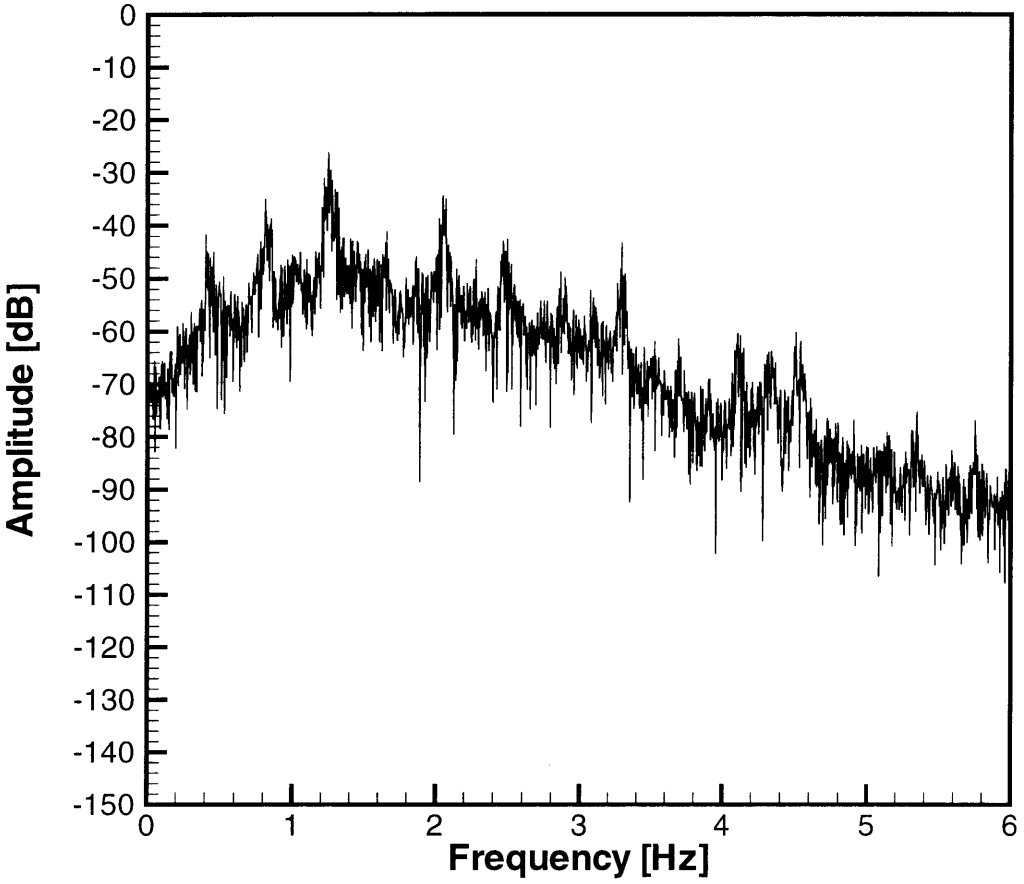

Figure 6-24: Power spectrum of the mid-point collapsible segment displcement obtained for the modified channel problem.

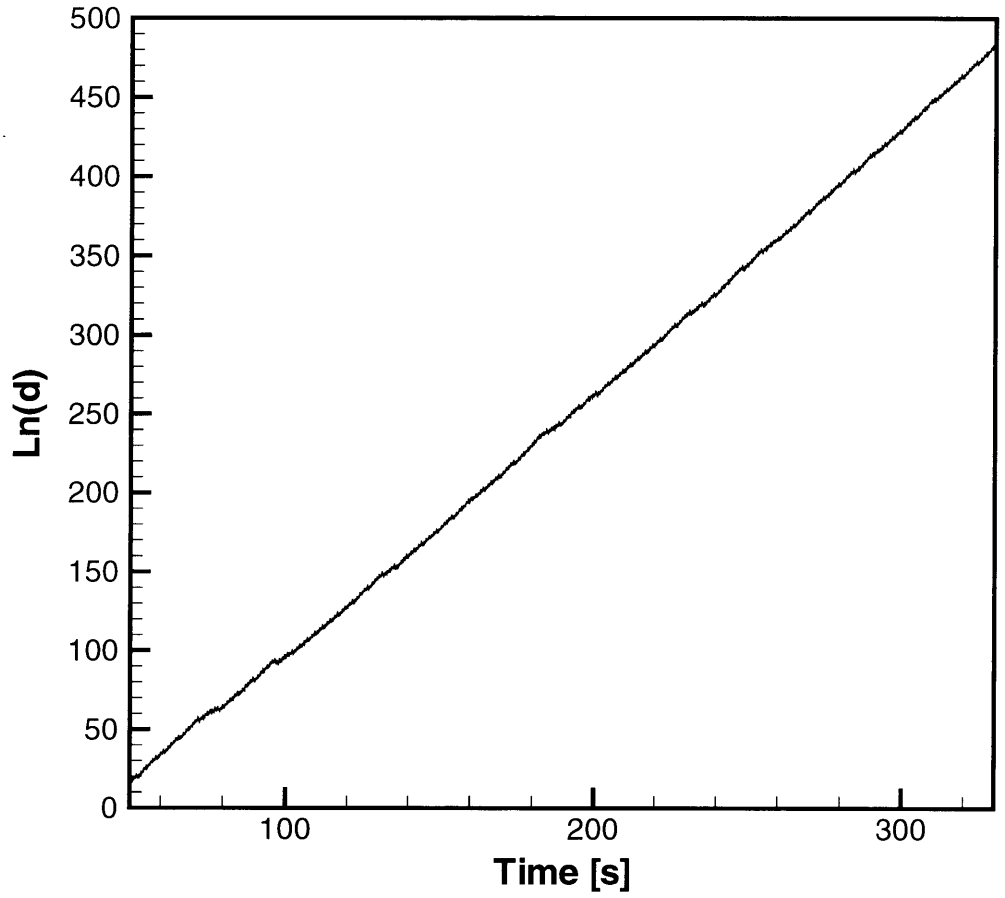

Figure 6-25: Plot of $ln(d)$ as a function of time for the modified channel problem.

Chapter 7

Conclusions and future work

Finite element methods have been successfully used in the analysis of complex structural, fluid and fluid-structure interaction problems, which in many cases present strong nonlinearities. The response of a nonlinear dynamic system of equations can exhibit a large and rich variety of behaviors that might be stable or unstable. If the system asymptotic behavior is unstable, then the response is chaotic and unpredictable. It can also happen that the system dynamic behavior becomes unstable at some point in time and then stabilizes, or vice-versa. Since an unstable behavior is usually not desirable in engineering practice, it becomes important not only to calculate the response of the system but also to characterize its dynamic stability. In most cases, the stability characterization of the system response is not a simple task, especially when the behavior of continuous systems is considered.

In this thesis, the calculation of the system Lyapunov characteristic exponent (LCE), was investigated. The LCE is a measure of the asymptotic divergence of nearby trajectories in phase space, thus the asymptotic dynamic stability of the system response can be assessed by calculating its LCE. Previous works on the calculation of the LCE were mostly focused on the analysis of nondimensional discrete systems that consist of a few first order ordinary differential equations in time, and iterative maps. A relatively small number of works were published on the calculation of the LCE of the response of continuous systems, and the mentioned publications either included experimental investigations or reduced order models. Therefore, a

more general method to calculate the LCE of continuous systems was needed. In this work, a numerical procedure to calculate the LCE of structural and fluid-structure interaction problems discretized using finite element methods is proposed. The proposed procedure is based on the computation of the evolution of perturbations of all the discretized finite element degrees of freedom. By calculating the LCE of complex systems, it is no longer necessary to monitor the behavior of many system sample points to detect an irregular or unstable behavior, since an instability on any part of the system will be captured by the LCE.

Some example problems, in which continuous systems were discretized using finite element methods, were considered. For all the examples, approximations to the LCE, k_n, were calculated at each discretized time step using the proposed procedure. Fourier analyses of sample points of the system responses were also performed to confirm the types of behavior predicted by the LCE calculation in the simple cases considered in this thesis.

The calculation of the LCE, as proposed in this work, requires typically between 20 to 25 % of extra computations at each time step for the example problems considered, and therefore the procedure is computationally inexpensive. Efficiency in the calculations is achieved because the matrices used in the computation of the system response can also be utilized in the calculation of the perturbation evolution, saving an important amount of computations per time step. In addition, the second order ordinary differential equations in time, which result from the linearized finite element discretization of the structural continuous system, are integrated in time directly (without converting them into first order differential equations, procedure that would double the number of degrees of freedom to be solved at each time step).

The calculation of an accurate value of the response LCE may take a large number of time steps, since the LCE is a measure of the *asymptotic* divergence of trajectories in phase space. Computer speed then becomes a constraint in the LCE evaluation procedure. Fortunately, it is not necessary to converge to the value of the LCE if the interest of the analysis lies in the *local stability* of the response. In this work, it is proposed to assess the local divergence/convergence of trajectories in phase space

(which in turn will give the local instability/stability of the system) by looking at the average slope of the plot of $ln(d) = k_n\ t_n$ versus time. The advantage of using $ln(d)$ is that instabilities would be detected shortly after they occur in the system response. However, since at the beginning of the LCE calculation a random initial perturbation vector is selected, it would be necessary to wait until transient effects in the perturbation calculation decay before using $ln(d)$ to assert the local response stability. Plots of the value of $ln(d)$ as a function of time, and a discussion of the results, were presented for the example problems considered.

In the following, some suggested topics of research, that would complement and enhance this work, are briefly discussed.

First of all, it would be neccessary to perform an error analysis of the LCE calculations. The aim of the study is to assess the error bound of the calculation, to be used especially in "limit cases" in which the theoretical value of the LCE is zero. As shown in Chapter 6, for those "limit cases", the calculated value of the LCE is not actually zero, but a positive or negative value, which is a function of the discretization employed. It can then be important to characterize the error bound to determine whether a system for which the calculated LCE is closed to zero is stable.

In the field of structural mechanics, it would also be useful to investigate algorithms to predict the necessary changes to be implemented in the original system such that an unstable response can be stopped or avoided. The changes might be in the properties of the system (i.e. a change of material) or in the forcing terms considered. This same ideas are of course applicable to fluid-structure interaction problems, in which the focus of the analysis is on the structural part of the system (as was considered in this work).

In the field of fluid mechanics, there is still a need to investigate algorithms to calculate the system LCE. However, in order to calculate the correct value of the LCE, the finite element formulation used should not include terms that incorporate artificial viscosity in the model. Otherwise, the "true" fluid behavior would not be captured. The procedures employed in the calculation of the system LCE for fluid-flow systems can later be used, for example, to predict the onset of turbulence.

In addition, the procedure proposed to characterize the stability of the dynamic behavior of systems can also be extended to other continuous problems, in which for example heat transfer or electro-magnetic effects are important.

In summary, the calculation of the response LCE of continuous systems opens a broad and almost unexplored field in mechanics. This work represents only a first step in the characterization of the dynamic behavior of continuous systems, since it provides a procedure to calculate the LCE of structural continuous systems discretized using finite element methods and to assess the local stability of the system response.

Appendix A

Exponential divergence of trajectories in phase space

The Duffing equation, a nonlinear discrete non-dimensional equation of motion, was considered as the first example in Chapter 6. The equation represents a two-well potential problem with dissipation with a periodic forcing term, and can be written as,

$$\ddot{x} + c\,\dot{x} - b\,x + a\,x^3 = g\,\cos(\bar{\omega}\,t) \tag{A.1}$$

where a, b, c, g and $\bar{\omega}$ are the equation parameters, which are assumed to be positive real numbers.

As discussed in Chapter 6, the divergence/convergence of trajectories of the system response is obtained, from equation (6.7), by solving a linearized equation of motion (that is by solving the equation that describes the evolution of infinitesimal perturbations to the system response). In this way approximations to the response LCE can be calculated at each time step. However, this procedure does not necessarily coincide with the physical intuition that the Lyapunov characteristic exponent measures the *average* exponential divergence of trajectories in phase space. In other words, for a chaotic behavior the following approximation is usually assumed,

$$\|\mathbf{y}\| \simeq e^{\chi(t-t_0)} \|\mathbf{y}_0\| \tag{A.2}$$

where $\mathbf{y}_0$ and $\mathbf{y}$ are the initial perturbation vector and the perturbation vector at time t, respectively, and χ is the response LCE.

It is possible to calculate the distance between originally nearby trajectories in phase space by computing two different trajectories whose initial conditions are very close to each other. The result of such a calculation, for the chaotic behavior of the Duffing equation analyzed in Chapter 6, is shown in Figure A-1. Note that for small times, the trajectories diverge from each other at a fast pace, but after some time (approximately $t = 200$), the natural logarithm of the distance between trajectories stops growing. This behavior occurs since the asymptotic trajectories (or the strange attractor) only occupy a bounded region of the phase space (see Figure 6-3c), and therefore after some time the distance between trajectories cannot grow any more. Using linear regression analysis to compute the slope of the curve shown in Figure A-1 for $t \leq 200$ (the time at which the distance between trajectories is growing) we found that $\chi \cong 0.42$. In contrast, the approximate value of the LCE from Figure 6-3c is $\chi \cong 0.35$.

Therefore, each of these two ways of *approximating* the value of the system response LCE seems to give the same result and captures the correct nature of the behavior. This is in general true for trajectories that remain inside the *same* strange attractor for all times.

However, if a good approximation of the value of the LCE is sought, or if the use of a fast algorithm is important, then the linearized equations of motion (6.7) should be used.

The Lyapunov characteristic exponent is defined by computing the growth of an initial perturbation by applying a mapping from the tangent space of $\mathbf{f}(\mathbf{x})$ at time t_0^* to the tangent space at time t to the initial perturbation (see Chapter 2). Thus, from the definition of LCE, the linearized equations of motion (6.7) are the appropriate equations to use in the calculation.

Furthermore, in the case of *transient chaos*, calculating the distance between two

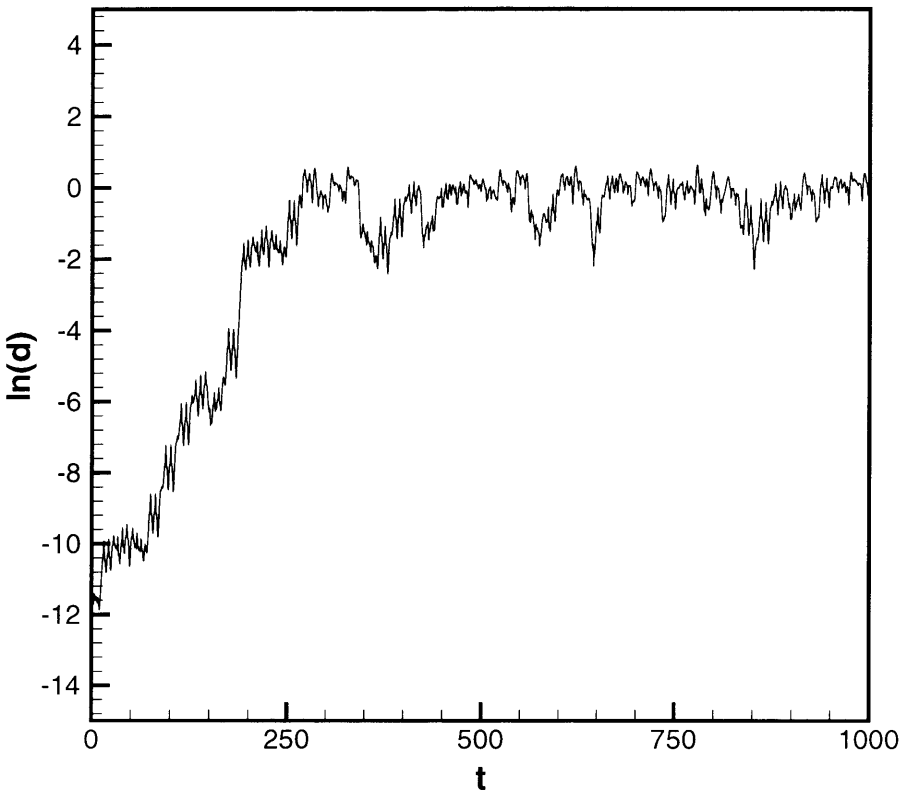

Figure A-1: Natural logarithm of the distance between two trajectories that were originally very close to each other. The trajectories were calculated using the Duffing equation and for the value of parameters analyzed in Chapter 6 that result in a chaotic behavior.

trajectories will not give the correct value of the response LCE. Consider for example the case in which the forcing term in equation (A.1) is zero. The long term response of the system is a steady state, in which the value of the variable x corresponds to one of the equation potential wells, see Figure 6-1 and the discussion in Chapter 6. However, there are some initial conditions such that the trajectory corresponds to a steady-state solution associated with one of the potential wells, and by slightly perturbing those initial conditions, a steady-state behavior associated with the other potential well is obtained. Of course in this case we can calculate the response LCE which is zero (since the steady state behavior is stable), using equation (6.7). However, if two different trajectories are followed and their distance as a function of time calculated, then the plot of the natural logarithm of the distance would look like Figure A-1, although the asymptotic system response is *not chaotic* (i.e. the algorithm would capture only the potential instability due to transient chaos and *not* the asymptotic stability of the system).

Bibliography

[1] J. Argyris, G. Faust, and M. Haase. *An Exploration of Chaos*, volume 7 of *Texts on Computational Mechanics*. North-Holland, 1994.

[2] K. J. Bathe. *Finite Element Procedures*. Prentice Hall, 1996.

[3] G. Benettin, L. Galgani, A. Giorgilli, and J.M. Strelcyn. Lyapunov characteristic exponents for smooth dynamical systems and for Hamiltonian systems; a method for computing all of them. Part 1: Theory. Part 2: Numerical applications. *Meccanica*, 15:9–30, 1980.

[4] G. Benettin, L. Galgani, and J.M. Strelcyn. Kolmogorov entropy and numerical experiments. *Physical Review A*, 14:2338–2345, 1976.

[5] A.N. Brooks and T.J.R. Hughes. Streamline upwind/Petrov-Galerkin formulations for convection dominated flows with particular emphasis on the incompressible Navier-Stokes equations. *Computer Methods in Applied Mechanics and Engineering*, 32:199–259, 1982.

[6] E.H. Dowell. Flutter of a buckled plate as an example of chaotic motion of a deterministic autonomous system. *Journal of Sound and Vibration*, 85:333–344, 1982.

[7] K. Geist, U. Parlitz, and W. Lauterborn. Comparison of different methods of computing Lyapunov characteristic exponents. *Progress of Theoretical Physics*, 83:875–893, 1990.

[8] J. Guckenheimer and P. Holmes. *Nonlinear Oscillations, Dynamical Systems, and Bifurcations of Vector Fields*, volume 42 of *Applied Mathematical Sciences*. Springer, 1983.

[9] M.D. Gunzburger. *Finite Element Methods for Viscous Incompressible Flows. A Guide to Theory, Practice and Algorithms.* Academic Press, Inc., 1989.

[10] W. Hahn. *Theory and Applications of Liapunov's Direct Method.* Prentice Hall, 1963.

[11] H. Haken. At least one Lyapunov exponent vanishes if the trajectory of an attractor does not contain a fixed point. *Physical Review Letters A*, 94:71–72, 1983.

[12] A. Haraux. Two remarks on hyperbolic dissipative problems. In H. Brezis and J.L. Lions, editors, *Nonlinear Partial Differential Equations and their Applications*, number VII in Research Notes in Mathematics. Pitman Publishing Inc., 1985.

[13] D. Hendriana. *A parabolic quadrilateral finite element for compressible and incompressible flows.* PhD thesis, MIT, 1998.

[14] D. Hendriana and K.J. Bathe. On a parabolic quadrilateral finite element for compressible flows. *Computer Methods in Applied Mechanics and Engineering*, 186:1–22, 1998.

[15] W. Kreider and A.H. Nayfeh. Experimental investigation of single-mode response in a fixed-fixed buckled beam. *Nonlinear Dynamics*, 15:155–177, 1998.

[16] W. Lacarbonara and A.H. Nayfeh. Experimental validation of reduction methods for nonlinear vibrations of distributed-parameter systems: analysis of a buckled beam. *Nonlinear Dynamics*, 17:95–117, 1998.

[17] O.A. Ladyzhenskaya. *The Mathematical Theory of Viscous Incompressible Flows.* Gordon and Breach Science Publishers, Second English edition, 1969.

[18] E.N. Lorenz. Deterministic non-periodic flow. *Journal of the Atmospheric Sciences*, 20:130–141, 1963.

[19] T.W. Lowe and T.J. Pedley. Computation of Stokes flow in a channel with a collapsible segment. *Journal of Fluids and Structures*, 9:885–905, 1995.

[20] X.Y. Luo and T.J. Pedley. A numerical simulation of steady flow in a 2-D collapsible channel. *Journal of Fluids and Structures*, 9:149–174, 1995.

[21] X.Y. Luo and T.J. Pedley. A numerical simulation of unsteady flow in a two-dimensional collapsible channel. *Journal of Fluid Mechanics*, 314:191–225, 1996.

[22] L.E. Malvern. *Introduction to the Mechanics of a Continuous Medium.* Prentice-Hall, 1969.

[23] J. L. McCauley. *Chaos, Dynamics and Fractals an Algorithmic Approach to Deterministic Chaos*, volume 2 of *Cambridge Nonlinear Science Series.* Cambridge University Press, 1993.

[24] F. C. Moon. *Chaotic Vibrations.* John Wiley and Sons, 1987.

[25] F.C. Moon. Experimental measurement of chaotic attractors in solid media. *Chaos*, 1:31–41, 1991.

[26] F.C. Moon and G.X. Li. The fractal dimension of the two-well potential strange attractor. *Physica D*, 17:99–108, 1985.

[27] F.C. Moon and S.W. Shaw. Chaotic vibrations of a beam with non-linear boundary conditions. *International Journal of Non-Linear Mechanics*, 18:465–477, 1983.

[28] A. H. Nayfeh and D. T. Mook. *Nonlinear Oscillations.* John Wiley and Sons, 1995.

[29] C. Nitikitpaiboon and K.J. Bathe. An arbitrary Lagrangian-Eulerian velocity potential formulation for fluid-structure interaction. *Computers and Structures*, 47:871–891, 1993.

[30] V.I. Oseledec. *A multiplicative ergodic theorem. Ljapunov characteristic numbers for dynamical systems*, volume 19 of *Transactions of the Moscow Mathematical Society*, pages 197–231. 1968.

[31] M.P. Paidoussis, G.X. Li, and F.C. Moon. Chaotic oscillations of the autonomous system of a constrained pipe conveying fluid. *Journal of Sound and Vibration*, 135:1–19, 1989.

[32] M.P. Paidoussis and F.C. Moon. Nonlinear and chaotic fluidelastic vibrations of a flexible pipe conveying fluid. *Journal of Fluids and Structures*, 2:567–591, 1988.

[33] T.J. Pedley. *The Fluid Mechanics of Large Blood Vessels.* Cambridge University Press, 1980.

[34] A. Rauh. Remarks on unsolved basic problems of the Navier-Stokes equations. *Nonlinear Phenomena in Complex Systems*, 2:32–37, 1999.

[35] S. Rugonyi. A simultaneous solution procedure for fully coupled fluid flows with structural interactions. Master's thesis, MIT, 1999.

[36] S. Rugonyi and K.J. Bathe. On the analysis of fully-coupled fluid flows with structural interactions – a coupling and condensation procedure. *International Journal for Computational Civil and Structural Engineering*, 1:29–41, 2000.

[37] S. H. Strogatz. *Nonlinear Dynamics and Chaos.* Addison-Wesley, 1994.

[38] A. Wolf, J.B. Swift, H.L. Swinney, and J.A. Vastano. Determining Lyapunov exponents from a time series. *Physica D*, 16:285–317, 1985.